MARTIN MARIETTA ENERGY SYSTEMS LIBRARIES
3 4456 0364314 5

CENTRAL RESEARCH LIBRARY
DOCUMENT COLLECTION

ORNL-3114
UC-34 – Physics
TID-4500 (17th ed.)

2

OPTICAL EMISSION FROM IRRADIATED THIN METALLIC FOILS

A. L. Frank
E. T. Arakawa
R. D. Birkhoff
R. H. Ritchie
H. B. Eldridge

CENTRAL RESEARCH LIBRARY
DOCUMENT COLLECTION
LIBRARY LOAN COPY
DO NOT TRANSFER TO ANOTHER PERSON
If you wish someone else to see this document, send in name with document and the library will arrange a loan.

OAK RIDGE NATIONAL LABORATORY
operated by
UNION CARBIDE CORPORATION
for the
U.S. ATOMIC ENERGY COMMISSION

LEGAL NOTICE

This report was prepared as an account of Government sponsored work. Neither the United States, nor the Commission, nor any person acting on behalf of the Commission:

A. Makes any warranty or representation, expressed or implied, with respect to the accuracy, completeness, or usefulness of the information contained in this report, or that the use of any information, apparatus, method, or process disclosed in this report may not infringe privately owned rights; or

B. Assumes any liabilities with respect to the use of, or for damages resulting from the use of any information, apparatus, method, or process disclosed in this report.

As used in the above, "person acting on behalf of the Commission" includes any employee or contractor of the Commission, or employee of such contractor, to the extent that such employee or contractor of the Commission, or employee of such contractor prepares, disseminates, or provides access to, any information pursuant to his employment or contract with the Commission, or his employment with such contractor.

ORNL-3114

Contract No. W-7405-eng-26

HEALTH PHYSICS DIVISION

OPTICAL EMISSION FROM IRRADIATED THIN METALLIC FOILS

A. L. Frank
E. T. Arakawa
R. D. Birkhoff
R. H. Ritchie
H. B. Eldridge

Submitted as a thesis to the Faculty of the Graduate School of Vanderbilt University in partial fulfillment of the requirements for the degree of Master of Science in physics.

DATE ISSUED

JUL 2 1962

OAK RIDGE NATIONAL LABORATORY
Oak Ridge, Tennessee
operated by
UNION CARBIDE CORPORATION
for the
U. S. ATOMIC ENERGY COMMISSION

MARTIN MARIETTA ENERGY SYSTEMS LIBRARIES

3 4456 0364314 5

ACKNOWLEDGMENTS

The authors take pleasure in expressing their sincere appreciation to J. A. Harter and D. Pittman for assistance with the electronics problems, and to H. H. Hubbell, Jr. and R. M. Johnson for their helpful comments.

This project was performed at the Oak Ridge National Laboratory under the provisions of the Atomic Energy Commission Radiological Fellowship held by one of us (ALF) and administered by W. W. Grigorieff of the Oak Ridge Institute of Nuclear Studies.

TABLE OF CONTENTS

CHAPTER		PAGE
I.	Introduction	1
II.	Theory	4
	A. The Ferrell Theory	4
	B. The Ritchie-Eldridge Theory	5
	C. Bremsstrahlung Calculation of Gluckstern, Hull, and Breit	7
	D. Summary	8
III.	Apparatus	21
	A. Electron Gun	21
	B. Accelerator	23
	C. Seya-Namioka Vacuum Scanning Monochromator	24
	1. Theory	24
	2. Construction	29
	3. Gratings	31
	4. Focus	31
	5. Transmission Cutoff	31
	6. Camera Attachment	33
	7. Phototube Attachment	33
	D. Irradiation Chamber	34
	1. Construction	34
	2. 0° Angle	36
	3. 30° Angle	38
	4. 72° Angle	38

CHAPTER PAGE

5. Chamber Accessories 39

6. Polarizer 39

E. Instruments for Beam Current Measurement 41

IV. Technique and Calibrations 42

A. Spectrometer Response 42

B. Data Correction 43

C. Wave Length Calibration 46

D. Preparation of Thin Foils 46

1. Vacuum Evaporation 47

2. Vacuum Evaporation in Irradiation Chamber 48

3. Evaporation in External Vacuum System 49

4. Current Source 51

E. Foil Thickness Measurements 51

1. Electrobalance Method 51

2. Optical Method 52

V. Procedure 54

VI. Results 55

VII. Conclusions 82

Bibliography 83

LIST OF FIGURES

PAGE

1. Theoretical Spectral Distributions from Ag (t = 1200 Å; $\theta = 30^{\circ}$; E = 40, 60, 80 kev) 11
2. Theoretical Spectral Distributions from Ag (t = 600, 1200, 1600 Å; $\theta = 30^{\circ}$; E = 60 kev) 12
3. Theoretical Photon Yields as a Function of Beam Energy for Ag (t = 1200, 1600, 2000, 2400 Å; $\theta = 30^{\circ}$; λ = 2386, 3265, 3650 Å) 13
4. Theoretical Spectral Distributions from Ag (t = 1200 Å; θ = 4°, 30°, 72°; E = 60 kev) 14
5. Theoretical Light Intensities as a Function of Foil Thickness (λ = 3265 Å; $\theta = 30^{\circ}$; E = 20, 40, 80, 120 kev) 15
6. Theoretical Photon Yields as a Function of Angle for Ag (t = 800 Å; E = 40 kev; λ = 2386, 3650, 5169 Å) 16
7. Theoretical Spectral Distributions from Al (t = 125 Å; $\theta = 30^{\circ}$; E = 40, 70, 100 kev) 17
8. Theoretical Spectral Distributions from Al (t = 125, 250, 500 Å; $\theta = 30^{\circ}$; E = 40 kev) 18
9. Theoretical Photon Yields as a Function of Beam Energy for Al (t = 125, 250, 375, 500 Å; $\theta = 30^{\circ}$; λ = 1200, 3408 Å) 20
10. Schematic Diagram of Accelerator, Irradiation Chamber, and Monochromator 22
11. Schematic Diagram of Light Path in Monochromator 26
12. Monochromator with Irradiation Chamber, Fore Pump, and Photomultiplier Equipment 30

PAGE

13. Grating in Holder, Camera, and Slit Assembly 32

14. Irradiation Chamber 35

15. Irradiation Chamber Accessories 37

16. Attachment for Measuring Polarization 40

17. Spectral Response of Monochromator and Photomultiplier . . . 44

18. Schematic of Optical Foil Thickness Measurement 53

19. Spectral Distributions from Ag ($t = 800$ Å; $\theta = 30^\circ$; $E = 50$, 70, 90, 110 kev) 56

20. Spectral Distributions from Ag ($t = 1200$ Å; $\theta = 30^\circ$; $E = 40$, 70, 100 kev) 57

21. Spectral Distributions from Ag ($t = 1200$ Å; $\theta = 72^\circ$; $E = 40$, 60, 80, 100, 115 kev) 58

22. Spectral Distributions from Ag ($t = 1600$ Å; $\theta = 30^\circ$; $E = 50$, 70, 90, 110 kev) 59

23. Spectral Distributions from Ag ($t = 2000$ Å; $\theta = 72^\circ$; $E = 50$, 70, 90, 110 kev) 60

24. Spectral Distributions from Ag ($t = 1200$, 1600, 2000, 2400 Å; $\theta = 30^\circ$, $E = 50$ kev) 61

25. Spectral Distributions from Ag and the Ritchie-Eldridge Theory ($t = 1200$ Å; $\theta = 30^\circ$; $E = 40$, 70 kev) 62

26. Uncorrected Spectral Distributions from Ag ($\theta = 2^\circ$, 4°, 30°, 72°) 63

27. Spectral Distributions from Ag ($t = 800$, 1200 Å; $\theta = 4^\circ$, 30°, 72°; $E = 50$ kev) 64

28. Theory and Experimental Points on the Angular Distribution from Ag ($\lambda = 3500$ Å; $t = 800$ Å) 65

PAGE

29. Light Intensities from Ag as a Function of Beam Energy and the Ritchie-Eldridge Theory (t = 800, 1200 Å; $\theta = 30^{\circ}$; λ = 3500 Å) 66

30. Light Intensities from Ag as a Function of Beam Energy and the Ritchie-Eldridge Theory (t = 650, 800 Å; $\theta = 30^{\circ}$; λ = 2400 Å) 67

31. Light Intensities as a Function of Polarizer Angle for Ag (t = 800 Å; $\theta = 30^{\circ}$; λ = 3500, 5000 Å) 68

32. Spectral Distributions from Al (t = 125 Å; $\theta = 30^{\circ}$; E = 40, 60, 80, 100 kev) 70

33. Spectral Distributions from Al (t = 250 Å; $\theta = 30^{\circ}$; E = 40, 60, 80, 100, 115 kev) 71

34. Spectral Distributions from Al (t = 375 Å; $\theta = 30^{\circ}$; E = 40, 60, 80, 100, 115 kev) 72

35. Spectral Distributions from Al (t = 250 Å; $\theta = 72^{\circ}$; E = 40, 60, 80, 100 kev) 73

36. Spectral Distributions from Al (t = 375 Å; $\theta = 72^{\circ}$; E = 40, 60, 80, 100 kev) 74

37. Spectral Distributions from Al (t = 125, 250, 375, 500 Å; E = 60 kev) 75

38. Photomultiplier Currents as a Function of Beam Energy for Al (t = 125, 250, 375, 500 Å; λ = 3500 Å) 76

39. Electrometer Currents as a Function of Foil Thickness for Al (λ = 3500 Å; E = 40, 60, 80, 100, 115 kev) 77

40. Photon Yield as a Function of Foil Thickness for Al and the Ritchie-Eldridge Theory (E = 40 kev) 79

PAGE

41. Light Intensities as a Function of Polarizer Angle for Al ($\theta = 30^{\circ}$, $\lambda = 3500, 4400, 5000$ Å) 80

42. Spectral Distributions from Ag, Al, and Au ($\theta = 30^{\circ}$; E = 60 kev) 81

OPTICAL EMISSION FROM IRRADIATED THIN METALLIC FOILS*

Thin metallic foils were irradiated with a 15 microampere beam of electrons from an accelerator operating between 50 to 115 kev. The light emission spectrum from the foils was analyzed with a Seya-Namioka Vacuum UV Monochromator with an EMI 6256B photomultiplier tube as detector. The metals irradiated were silver, aluminum, and gold with the former being unbacked and the latter two supported on thin organic substrates.

The silver and aluminum data were compared with the theories for the emission of radiation from a dielectric as derived by Ritchie and Eldridge, and by Ferrell. Substantial agreement was found between the former theory and the measurements.

---

*Thesis prepared by Allen Lee Frank under the direction of Drs. E. T. Arakawa and R. D. Birkhoff, Oak Ridge National Laboratory, and approved by Professors P. H. Latimer and E. A. Jones.

I. INTRODUCTION

When a monochromatic beam of high energy electrons passes through a thin metallic foil, the spectrum of the emerging electrons shows a number of energy loss peaks which are characteristic of the irradiated metal. For some metals, loss peaks are found to occur as multiples of one fundamental energy loss. A comparison of the areas under these multiple peaks leads to the conclusion that a single energy loss mechanism is involved which brings about sharp multiple losses with high probability.

In a series of articles, Pines and Bohm[1] developed a theory of collective electron interaction which was later expanded by Ferrell[2] and Ritchie,[3] and which predicted closely the loss peaks for certain metals. This theory describes the conduction electrons in a metal as a free electron gas which can absorb energy from impinging high energy charged particles by long range interactions. The electron continuum, or plasma, absorbs a discrete amount of energy, $\hbar\omega_p$, from the charged particle and is set into oscillation with a frequency ω_p. For a free electron gas $\omega_p = (\frac{4\pi ne^2}{m})^{1/2}$ where n is the free electron density. Interband

---

[1] D. Bohm and D. Pines, Phys. Rev. 82, 625 (1951); D. Pines, and D. Bohm, Phys. Rev. 85, 338 (1952); D. Bohm and D. Pines, Phys. Rev. 92, 609 (1953); D. Pines, Phys. Rev. 92, 626 (1954).

[2] R. A. Ferrell, Phys. Rev. 101, 555 (1956); R. A. Ferrell, Phys. Rev. 107, 450 (1957).

[3] R. H. Ritchie, Phys. Rev. 106, 874 (1957); R. H. Ritchie, Phys. Rev. 114, 644 (1959).

transitions,[4] core electron interactions,[5] and metal surface effects[6] may act to change ω_p from the free electron frequency. Such metals as aluminum, magnesium, and the alkali metals, which closely approximate a free electron gas, are found to exhibit the plasma response; the situation is less clear for the heavier metals where the above effects may play more important roles.

In a recent paper Ferrell[7] suggested that an independent check on the validity of the plasma theory would be possible from a measurement of the electromagnetic radiation emitted by the irradiated foil when the plasma decayed. Ferrell predicted about one photon at the plasma frequency for every thousand energetic electrons passing through a sodium foil of optimum thickness. Another advantage of the optical studies would be an increased accuracy in the determination of the plasma energy.

Because of difficulties in working in the far ultraviolet and in the ready oxidation of the metals showing the plasma response, the only radiation from metals detected so far is from silver. In 1931, using seven volt electrons, Mohler and Boeckner[8] observed a strong 3600 Å peak in the spectrum of emitted light. More recently two other groups have studied the silver peak using high energy electrons and thin foils. Steinman[9] and Brown, et al[10] irradiated thin silver foils with 25 and

---

[4] E. N. Adams, Phys. Rev. 98, 947 (1955).

[5] P. A. Wolff, Phys. Rev. 92, 18 (1953).

[6] C. J. Powell, J. L. Robins, and J. B. Swan, Phys. Rev. 110, 657 (1958).

[7] R. A. Ferrell, Phys. Rev. 111, 1214 (1958).

[8] F. L. Mohler, and C. Boeckner, Bur. Standards J. Research 6, 751 (1931).

[9] Wulf Steinman, Phys. Rev. Letters 5, 470 (1960).

[10] R. W. Brown, P. Wessel, and E. P. Trounson, Phys. Rev. Letters 5, 472 (1960).

22 kev electron beams, respectively. The former analyzed the light emitted from the backward or incident beam side of the foil and the latter from the forward side. Steinman measured the spectrum as a function of foil thickness and Brown as a function of angle of emission. The results of these experiments seemed to be in accord with the predictions of Ferrell.

II. THEORY

Two theories describing the emission of light from irradiated metallic films have recently appeared.

A. The Ferrell Theory[11]

The Ferrell theory[11] develops a series of equations which describe the variation of light intensity at and near the plasma frequency as a function of foil thickness, electron beam energy, and angle of photon emission. The spectrum is found to consist of a narrow distribution centered at a wave length corresponding to the plasma frequency.

The dependence of the photon yield per incident electron on foil thickness is given by:

$$Y(\tau) = \frac{e^2}{\hbar c} \frac{v}{c} \left[\frac{\sin^2 \left(\frac{\pi\tau}{\lambda_{ex}}\right)}{\pi \; \tau/\lambda_{ex}} \right] \tag{1}$$

where τ is the foil thickness, $\lambda_{ex} = \beta \, \lambda_p$ where λ_p is the plasma photon wave length, and v is the electron velocity.

The angular distribution is given by the equation:

$$I(\theta) = \cos \theta \left[1 + \frac{1}{\tau_d \, \omega_p} \; \frac{\lambda_p}{\pi\tau} \; \frac{\cos \theta}{\sin^2 \theta} \right]^{-1} \tag{2}$$

where τ_d is the mean lifetime of the plasmon with respect to damping, and θ is the angle between photon emission and foil normal.

The angular distribution at a frequency ω different from the plasma frequency ω_p is given by the equation:

---

[11] Ferrell, loc. cit.

$$I(\theta, \omega) = I(\theta) \left[1 + 4\tau_t^2 (\omega - \omega_p')^2\right]^{-1} \tag{3}$$

where τ_t is the total mean lifetime of the plasmon and ω_p' is the altered plasma frequency. ω_p' is defined by the equation:

$$\omega_p' = \omega_p(1 - \frac{k\tau}{4}) \tag{4}$$

where $k = \frac{\omega}{c} \sin\theta$, the tangential component of momentum carried off by the emitted photon. For most experimental situations $1 \gg \frac{k\tau}{4}$ and therefore $\omega_p' \approx \omega_p$.

This distribution function may be written by combining the above equations after normalization by $\frac{\pi}{2\tau_d}$ to provide the appropriate yield.

$$\mu_p(\theta, \tau, \omega, v) = \frac{e^2}{4\pi^2\hbar c} \left(\frac{v}{c}\right)^2 \frac{\omega_p \sin^2\theta \cos\theta \sin^2(\pi\tau/\lambda_{ex})}{(\omega-\omega_p)^2 + \frac{\omega_p^2}{4}\left(2nk + \frac{\pi\tau}{\lambda_{ex}} \frac{\sin^2\theta}{\cos\theta}\right)^2} \tag{5}$$

where $\mu_p(\theta, \tau, \omega, v)$ is the number of photons emitted per incident electron at angle θ per unit solid angle in the frequency interval $d\omega$ at ω. In this equation the small difference between ω_p' and ω_p has been neglected.

B. The Ritchie-Eldridge Theory

Ritchie and Eldridge[12] have discussed the emission of radiation from a foil using an approach similar to that of Ginsburg and Frank.[13] Their result contains the modification of transition radiation by the dielectric behavior of the foil may be written:

---

[12] R. H. Ritchie, "Optical Emission from Irradiated Foils I." (To be submitted for publication in Phys. Rev.).

[13] V. L. Ginsburg and I. M. Frank, J. Exptl. Theoret. Phys. (U.S.S.R.) 16, 15 (1945).

$$n(\theta, t, \omega, \beta) = \sum_{p_f} \frac{d^2n}{d\omega d\Omega} = \frac{Z^2e^2}{\pi^2\hbar c}\frac{\beta^2}{\omega}\mu(1-\mu^2)\ |D|^2 \tag{6}$$

where

$$|D|^2 = \frac{1}{|\Delta|^2}\left|\left[\frac{\beta\sigma + e}{1-\mu^2\beta^2} - \frac{1}{1-\beta\sigma}\right](\mu\epsilon + \sigma)e^{-it\sigma} + \left[\frac{\beta\sigma - \epsilon}{1-\beta^2\mu^2} + \frac{1}{1+\beta\sigma}\right](\mu\epsilon-\sigma)e^{it\sigma}\right.$$

$$\left. -2\sigma\epsilon\left[\frac{1}{1-\beta\mu} - \frac{1+\beta\epsilon\mu}{1-\beta^2\sigma^2}\right]e^{-\frac{it}{\beta}}\right|^2 \tag{7}$$

Here the dielectric constant

$$\epsilon = \epsilon_1 + i\epsilon_2 \tag{8}$$

$$\sigma = Re^{i\Phi} \tag{9}$$

$$R = \left[(\epsilon_1 - 1 + \mu^2)^2 + \epsilon_2^{\ 2}\right]^{1/4} \tag{10}$$

$$\Phi = \frac{1}{2}\tan^{-1}\left[\frac{\epsilon_2}{(\epsilon_1 - 1 + \mu^2)}\right] \tag{11}$$

$$\beta = \frac{v}{c} \tag{12}$$

$$\mu = \cos\theta \tag{13}$$

$$t = \frac{a\omega}{c} \tag{14}$$

$$\Delta = (\mu\ \epsilon - \sigma)^2\ e^{it\sigma} - (\mu\ \epsilon + \sigma)^2\ e^{-it\sigma} \tag{15}$$

and a is the foil thickness. $\frac{d^2n}{d\omega d\Omega}$ is the number of photons emitted per unit interval at frequency ω, per unit solid angle in the direction θ with respect to foil normal. This result is valid for all velocities of the incident particle, as long as only low energy photons, $\hbar\omega \ll mc^2$ are considered, and admits arbitrary variation of the dielectric constant with frequency. Calculations using this equation are best handled with the aid of a digital computer. Ritchie and Eldridge have shown that their result reduces to that of Ferrell when $\epsilon = 1 - (\frac{\omega_p}{\omega})^2 + i\epsilon_2$, corresponding to the dielectric constant of a free electron gas under the condition $t \ll 1$, $\beta \ll 1$ ($\frac{t}{\beta}$ unrestricted), $\epsilon_2 \ll 1$, and $\theta \ll 1$.

C. Bremsstrahlung Calculation of Gluckstern, Hull, and Breit

The differential cross section for bremsstrahlung production has been obtained by Gluckstern, Hull, and Breit[14] and has been integrated over the direction of the emerging electron by Gluckstern and Hull.[15] In the limiting case of photon energies small compared to the electron energy, the cross section for finding a photon of energy k in a solid angle $2\pi \sin\theta_o d\theta_o$ generated by an electron of velocity βc is

$$d\sigma_{II} = Z^2\left[\frac{e^2}{\hbar c}\right]\left[\frac{e^2}{m_o c^2}\right]^2 \frac{(1-\beta^2)}{\beta^2}\frac{dk}{k}\frac{(\cos\theta_o - \beta)^2}{(1-\beta\cos\theta_o)^4} \times \sin\theta_o d\theta_o$$

$$\times\left\{\ln\frac{(m_o c^2)^2\beta^2}{(1-\beta^2)\left(k^2\left[\frac{1-\beta\cos\theta_o}{\beta}\right]^2 + \frac{Z^{2/3}(m_o c^2)^2}{(108)^2}\right)} + O_{II}(1)\right\} \tag{16}$$

for photons polarized in the plane of the electron and photon and

$$d\sigma_{III} = Z^2\left[\frac{e^2}{\hbar c}\right]\left[\frac{e^2}{m_o c^2}\right]^2 \frac{(1-\beta^2)}{\beta^2}\frac{dk}{k}\frac{1}{(1-\beta\cos\theta_o)^2} \times \sin\theta_o\, d\theta_o$$

$$\times\left\{\ln\frac{(m_o c^2)^2\beta^2}{(1-\beta^2)\left(k^2\left[\frac{1-\beta\cos\theta_o}{\beta}\right]^2 + \frac{Z^{2/3}(m_o c^2)^2}{(108)^2}\right)} + O_{III}(1)\right\} \tag{17}$$

for photons polarized perpendicular to this plane. For the experimental situation of interest here where $k < 20$ ev, $\beta > .2$, and $Z > 4$, the first term in the denominator of the logarithm is always very small compared to the second term and the argument of the logarithm reduces to

$$\frac{(108)^2\beta^2}{Z^{2/3}(1-\beta^2)} \tag{18}$$

---

[14] R. L. Gluckstern, M. H. Hull, Jr., and G. Breit, Phys. Rev. 90, 1020 (1953).

[15] R. L. Gluckstern and M. H. Hull, Jr., Phys. Rev. 90, 1030 (1953).

The total cross sections for light emission integrated over all photon directions are:

$$\int_0^{4\pi} d\sigma_{II} = \frac{2}{3} Z^2 \left[\frac{e^2}{\hbar c}\right] \left[\frac{e^2}{m_o c^2}\right]^2 \frac{1}{\beta^2} \frac{dk}{k} \left\{ \ln \frac{(108)^2 \beta^2}{Z^{2/3}(1-\beta^2)} + O_{II}(1) \right\} \qquad (19)$$

$$\int_0^{4\pi} d\sigma_{III} = 2 Z^2 \left[\frac{e^2}{\hbar c}\right] \left[\frac{e^2}{m_o c^2}\right]^2 \frac{1}{\beta^2} \frac{dk}{k} \left\{ \ln \frac{(108)^2 \beta^2}{Z^{2/3}(1-\beta^2)} + O_{III}(1) \right\} \qquad (20)$$

D. Summary

The theories of Ferrell, Ritchie-Eldridge, and Gluckstern et al. may be compared in several ways.

Transition radiation results from the annihilation of a dipole perpendicular to the foil surface and should then be polarized in the plane containing the electron beam and the photon direction. Bremsstrahlung results from the acceleration of the passing electron in a direction parallel to the surface of the foil. The result of the integration over all electron directions shown in Section C indicates that the ratio of the bremsstrahlung component polarized like transition radiation to the component polarized at right angles to this direction should be unity at 0° and 180° and should fall to zero at $\cos^{-1}\beta$. At this angle the light from transition radiation and from bremsstrahlung should be plane polarized in directions at right angles to each other and thus readily separable with a polarizer. The ratio of the two bremsstrahlung components is simply $\left(\frac{\cos\theta - \beta}{1-\beta\cos\theta}\right)^2$.

Both the Ferrell and Ritchie-Eldridge theories predict that the photon intensity will depend on the square of the sine of the thickness. The results differ somewhat in that the Ferrell minima go to zero intensity while the Ritchie-Eldridge minima do not. The bremsstrahlung intensity is

derived for isolated atoms and thus is proportional to film thickness. No estimates of the effect of interference in finite foils are available.

Both the Ferrell and the Ritchie-Eldridge theories predict that the intensity should be proportional approximately to E. The non-relativistic bremsstrahlung intensity varies as $\frac{1}{E}$.

The Ferrell and Ritchie-Eldridge theories give approximately the same result for angular dependence of transition radiation. The intensity is zero at $\theta = 0^{\circ}$ and 90° and reaches a maximum at some intermediate angle which depends on the wave length. The bremsstrahlung radiation follows an approximate cosine θ distribution when β is small.

The spectral distributions of the three theories are very different. Ferrell gives a simple frequency resonance equation. The Ritchie-Eldridge theory gives a much more complicated dependence on frequency and the bremsstrahlung spectrum goes as the inverse of the frequency.

Some predictions of the Ritchie-Eldridge theory are plotted for various representative values of the parameters. The photon spectrum $N(\lambda)$ is the number of photons emitted by the foil per steradian per cm of wave length per incident electron at an angle θ to the foil normal, and the intensity $E(\lambda)$ is the product of $N(\lambda)$ and the photon energy in electron volts.

The optical constants required for the calculations were taken from the data of Berning, Haas, and Madden[16] and Haas and Waylonis[17] for aluminum and by Taft and Philipp[18] for silver.

---

[16] P. H. Berning, G. Haas, and R. P. Madden, J. Opt. Soc. Am. 50, 586 (1960).

[17] G. Haas and J. E. Waylonis, "Optical Constants of Aluminum," (meeting of the Optical Society of America, October 13, 1960).

[18] E. A. Taft and H. R. Philipp, Phys. Rev. 121, 1100 (1961).

The theory as applied to silver is shown in Figures 1 - 6. Figure 1 shows the intensity of light emitted by a 1200 Å thick foil at 30° from the foil normal for three beam energies. It is seen that the emission is approximately proportional to energy except at the peak wave length. Figure 2 shows the spectral distribution at 30° for a 60 kev beam for three foil thicknesses. The dependence of emission on wave length for various foil thicknesses and beam energies is better demonstrated on Figure 3. It is seen that the intensity is nearly independent of foil thickness except at the plasma peak at $\lambda = 3265$ Å. This is due to the fact that the plasma peak is a volume effect, whereas the radiation at other wave lengths due to the annihilation, or creation of a dipole by an electron and its image charge at the vacuum-metal interface is a surface effect. Figure 4 shows the spectral distribution for a 1200 Å foil for 60 kev electrons at three angles to the foil normal.

The dependence of intensity at $\lambda = 3265$ Å on foil thickness for various electron energies is given by Figure 5 which shows clearly its oscillating character. Figure 6 shows the angular dependence of the emission at three wave lengths. The variation of the angle of peak intensity with wave length is readily apparent.

A summary of the Ritchie-Eldridge theory for aluminum is provided in Figures 7 - 10. Unfortunately, the optical constants in the region where the plasma peak is expected to occur (800 - 900 Å) are not available. However it is of interest to investigate the intensity dependence at the longer wave lengths where data are available. Figure 7 shows that the intensity depends linearly on beam energy at the long wave lengths but not at the shorter wave lengths. Figure 8 shows the intensity as a function of wave length for various thicknesses. The thicker foils emit

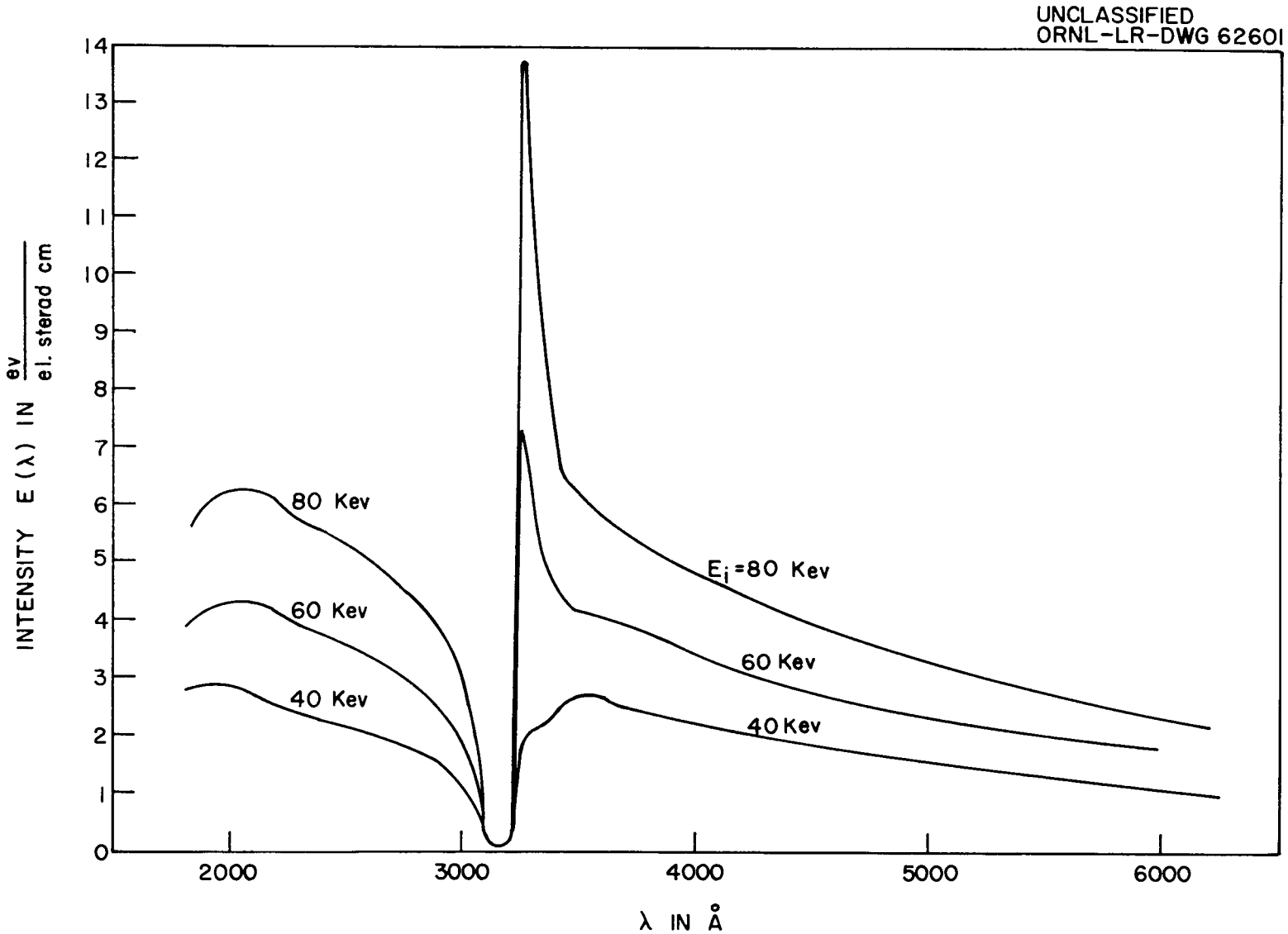

Figure 1. Theoretical Spectral Distributions from Ag (t = 1200 Å; θ = 30°; E = 40, 60, 80 kev).

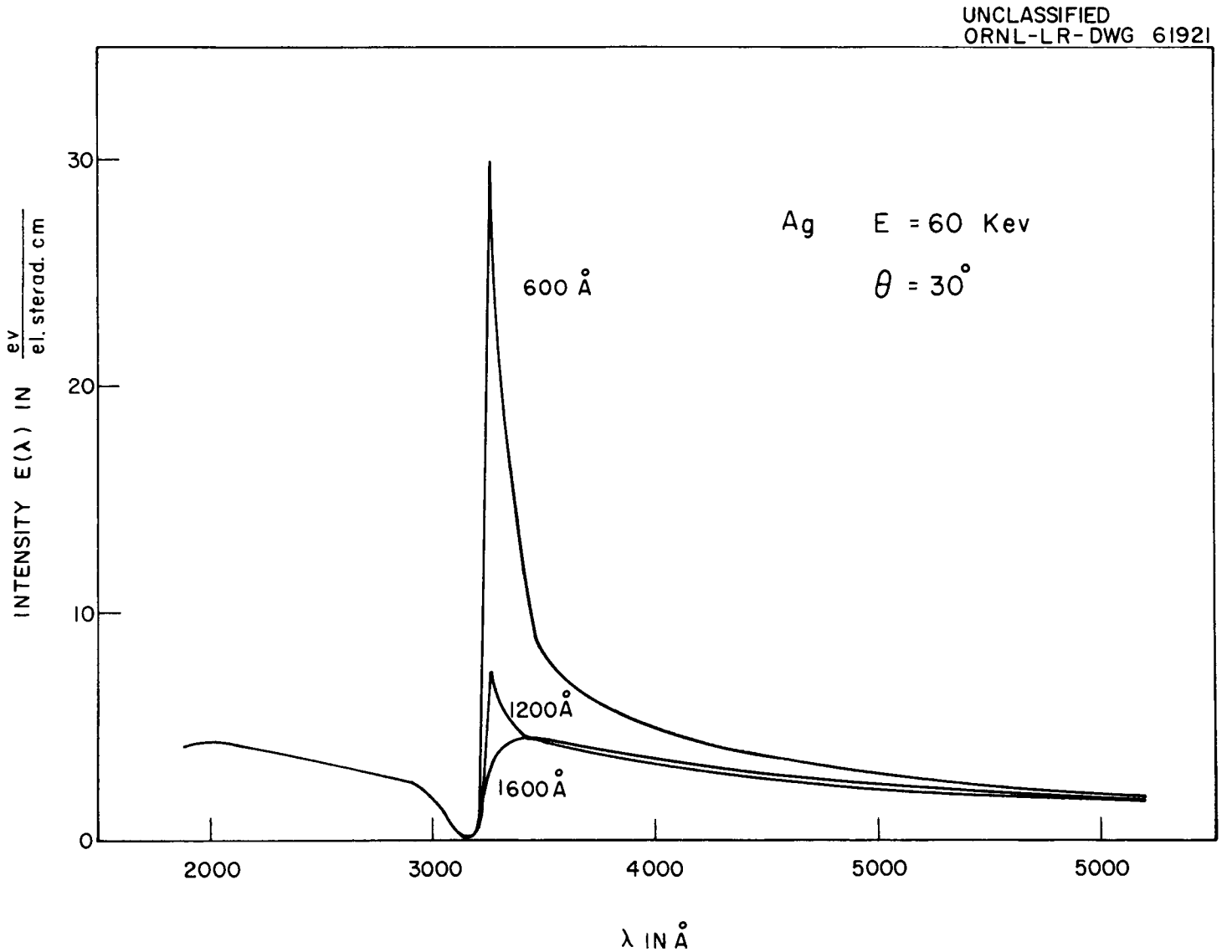

Figure 2. Theoretical Spectral Distributions from Ag (t = 600, 1200, 1600 Å; θ = 30°; E = 60 kev).

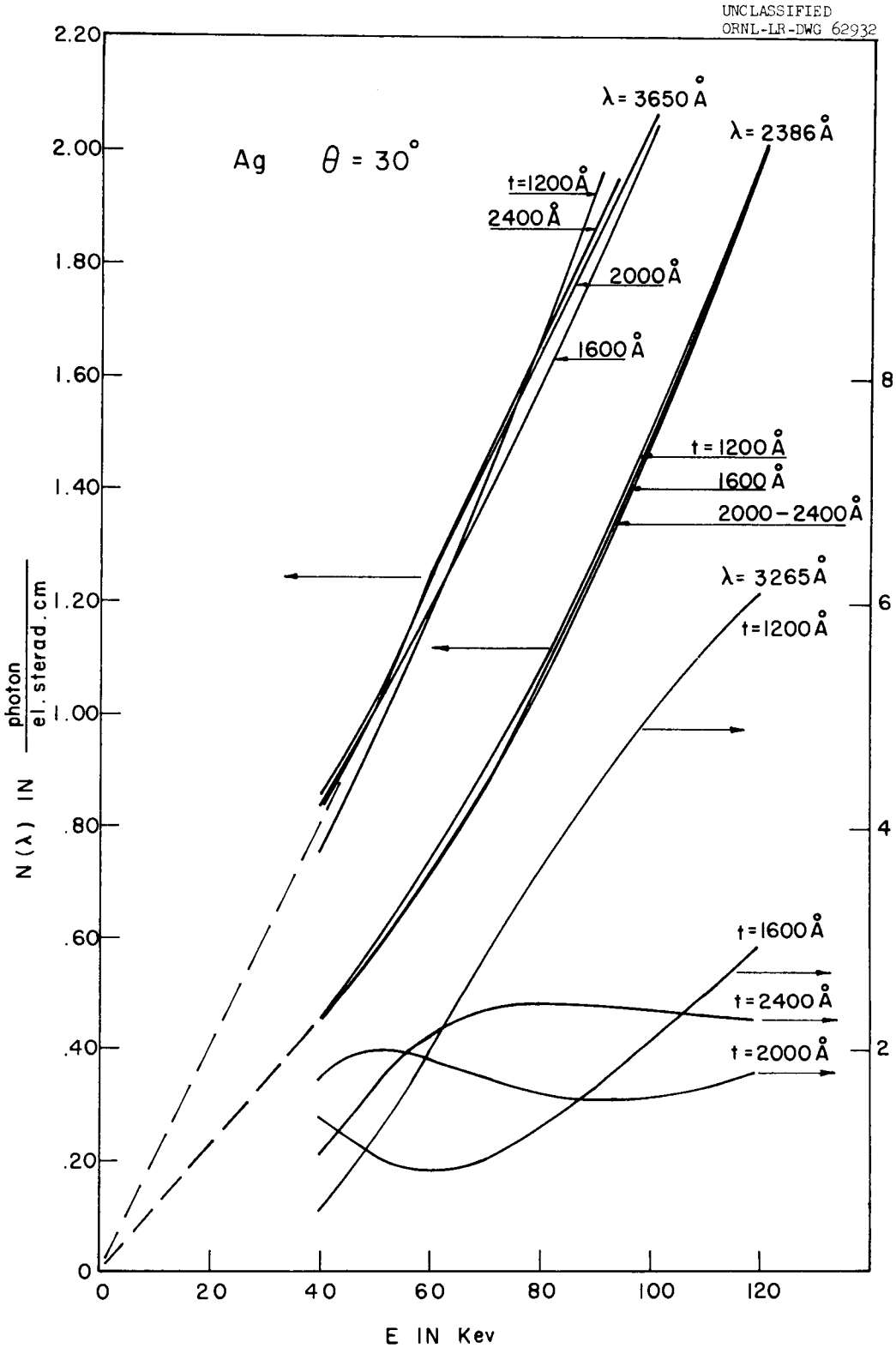

Figure 3. Theoretical Photon Yields as a Function of Beam Energy for Ag (t = 1200, 1600, 2000, 2400 Å; θ = 30°; λ = 2386, 3265, 3650 Å).

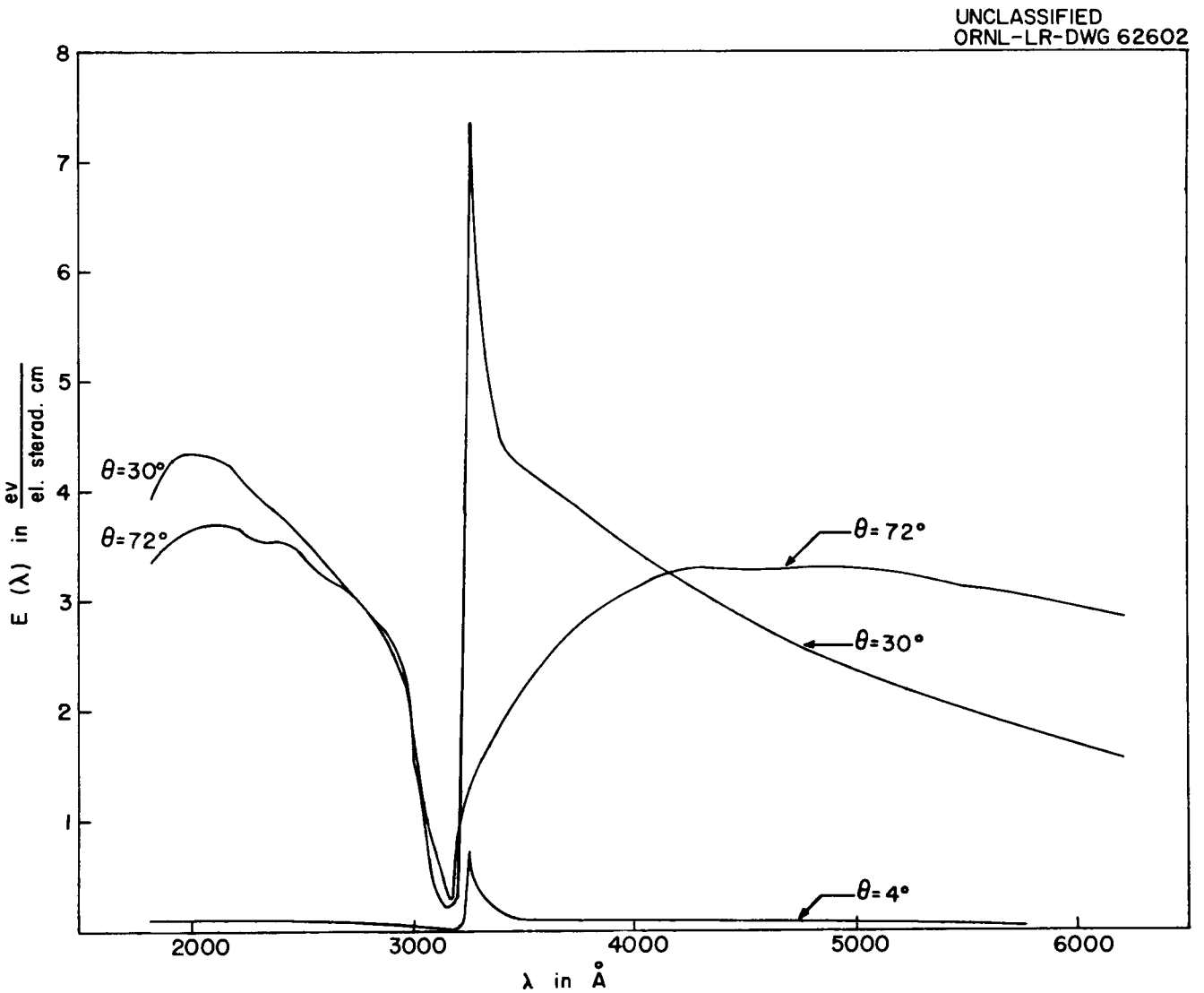

Figure 4. Theoretical Spectral Distributions from Ag (t = 1200 Å; θ = 4°, 30°, 72°; E = 60 kev).

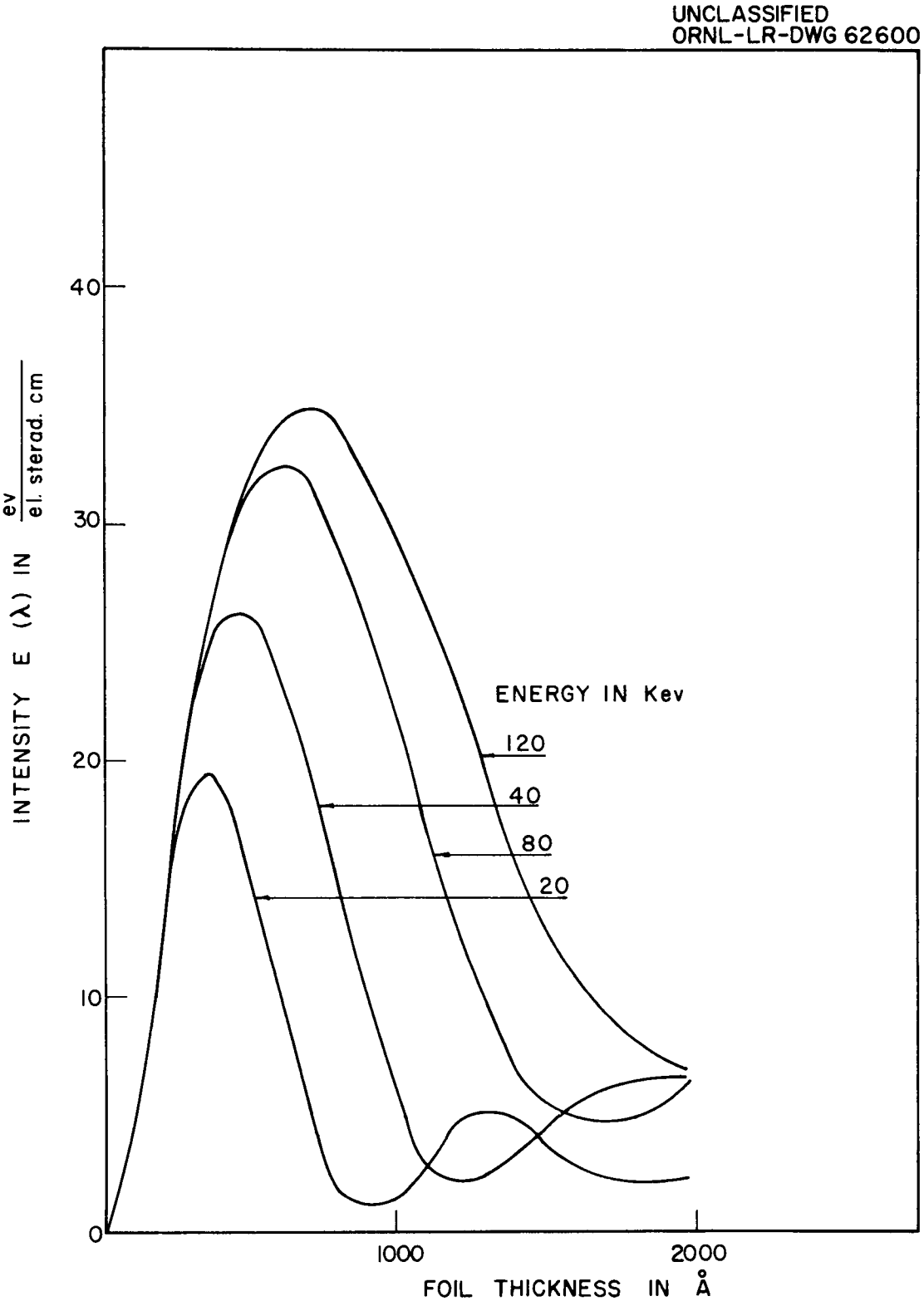

Figure 5. Theoretical Light Intensities as a Function of Foil Thickness (λ = 3265 Å; θ = 30°; E = 20, 40, 80, 120 kev).

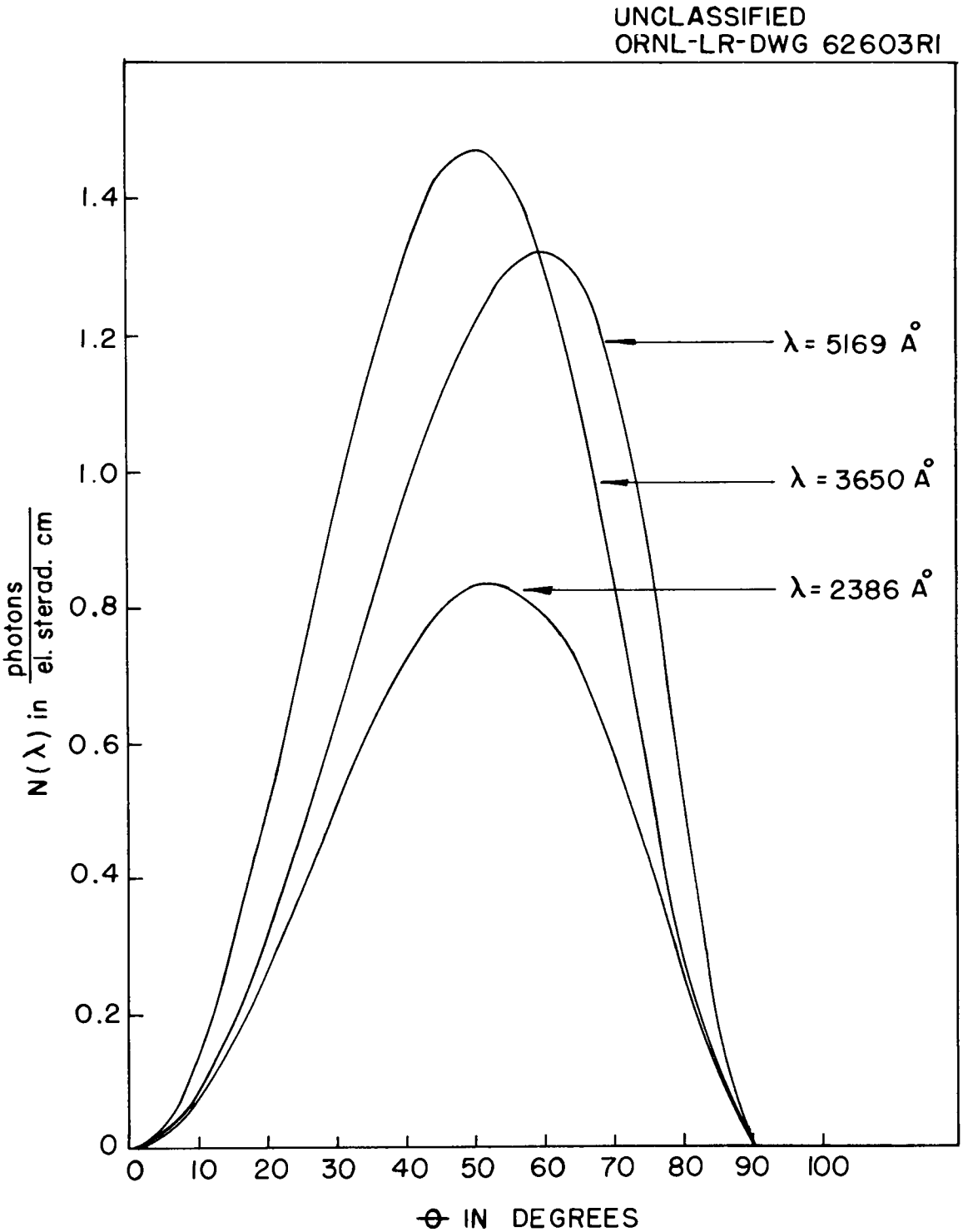

Figure 6. Theoretical Photon Yields as a Function of Angle for Ag ($t = 800$ Å; $E = 40$ kev; $\lambda = 2386, 3650, 5169$ Å).

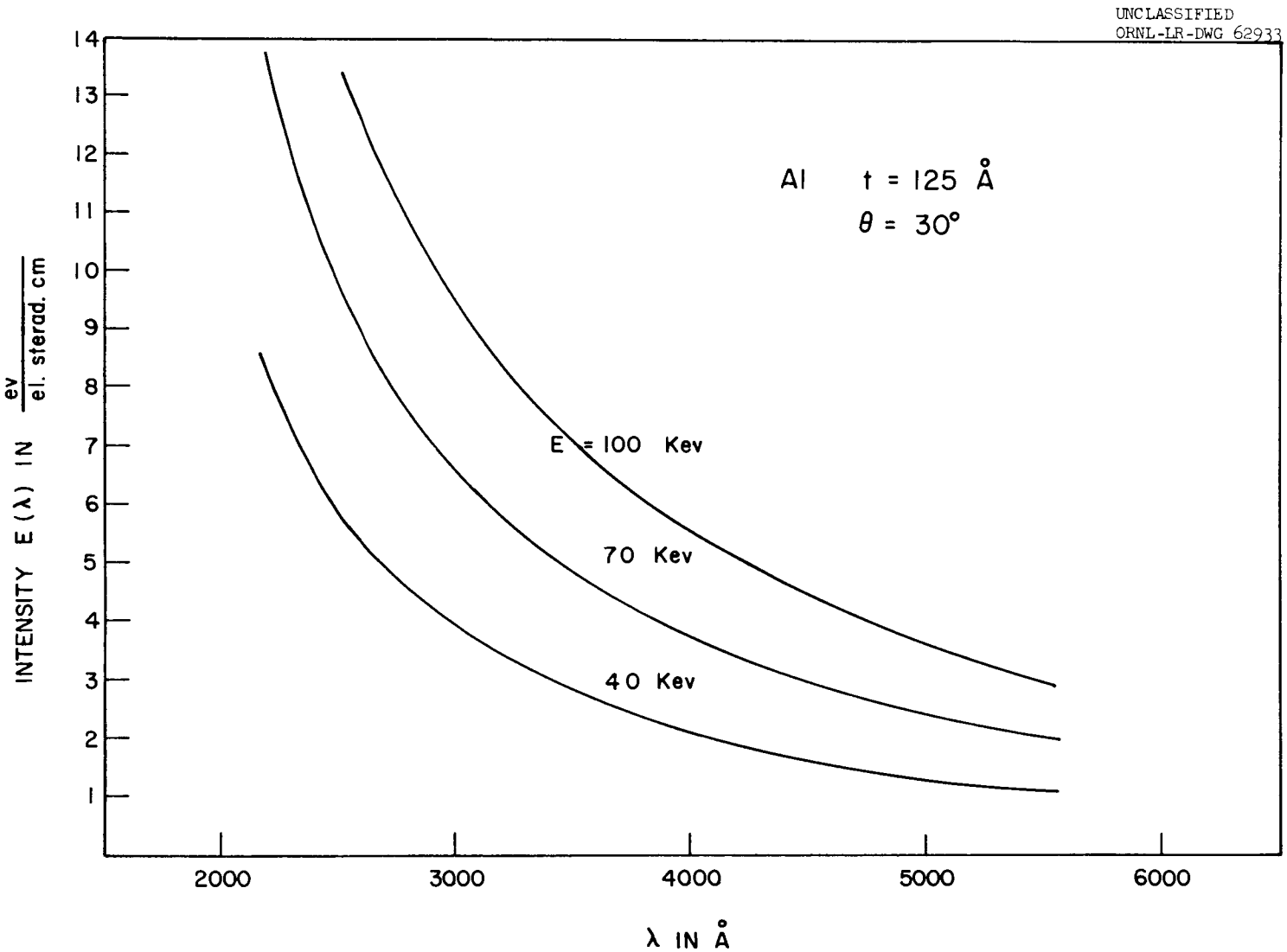

Figure 7. Theoretical Spectral Distributions from Al (t = 125 Å; θ = 30°; E = 40, 70, 100 kev).

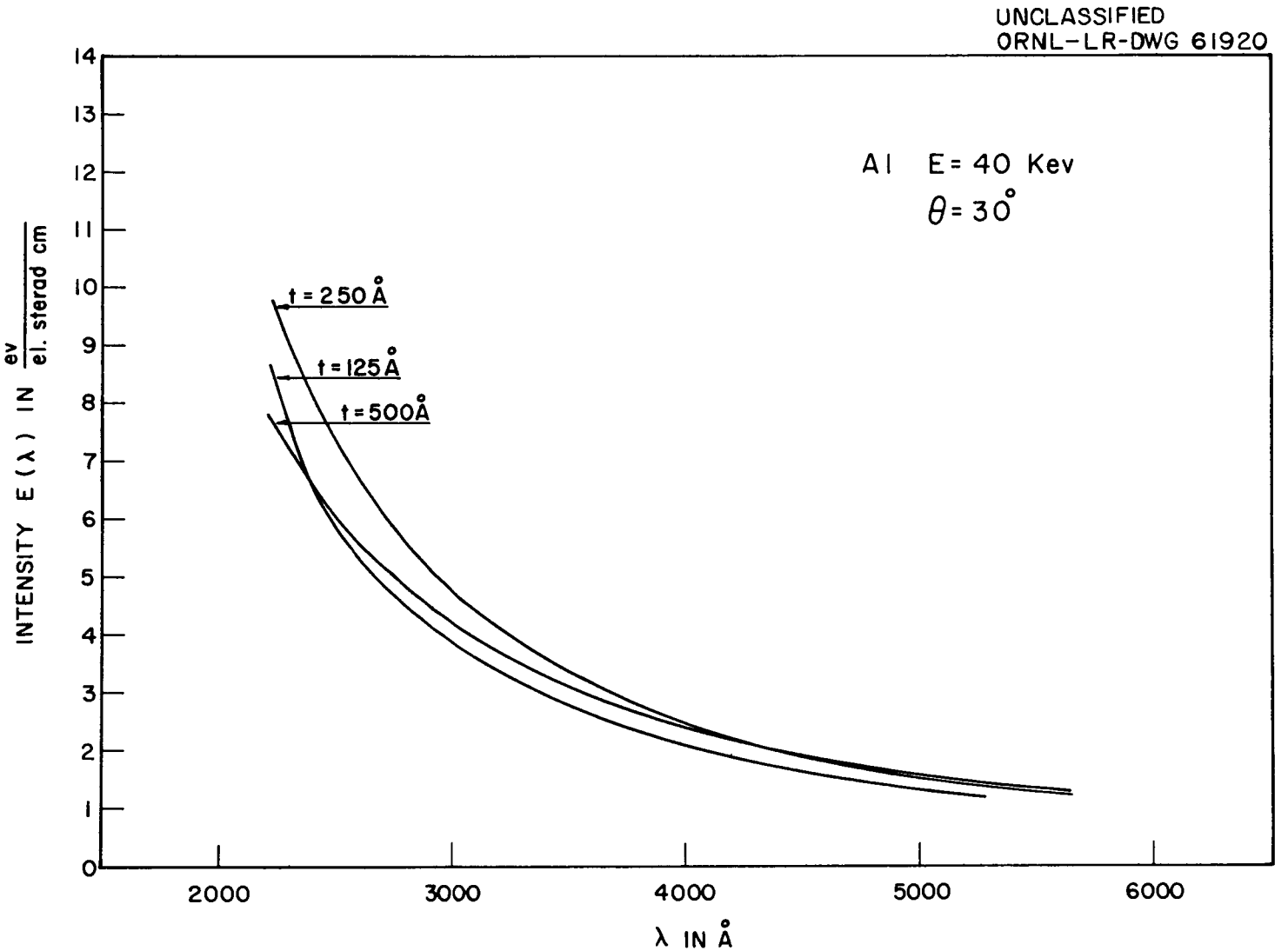

Figure 8. Theoretical Spectral Distributions from Al (t = 125, 250, 500 Å; θ = 30°; E = 40 kev).

less at short wave lengths nearer the plasma wave length and their emission falls off more slowly as wave length is increased. Figure 9 shows the photon number versus beam energy for two different wave lengths and various thicknesses. It is again seen that the intensity varies markedly with thickness close to the plasma peak, whereas it is nearly independent of foil thickness at the longer wave lengths.

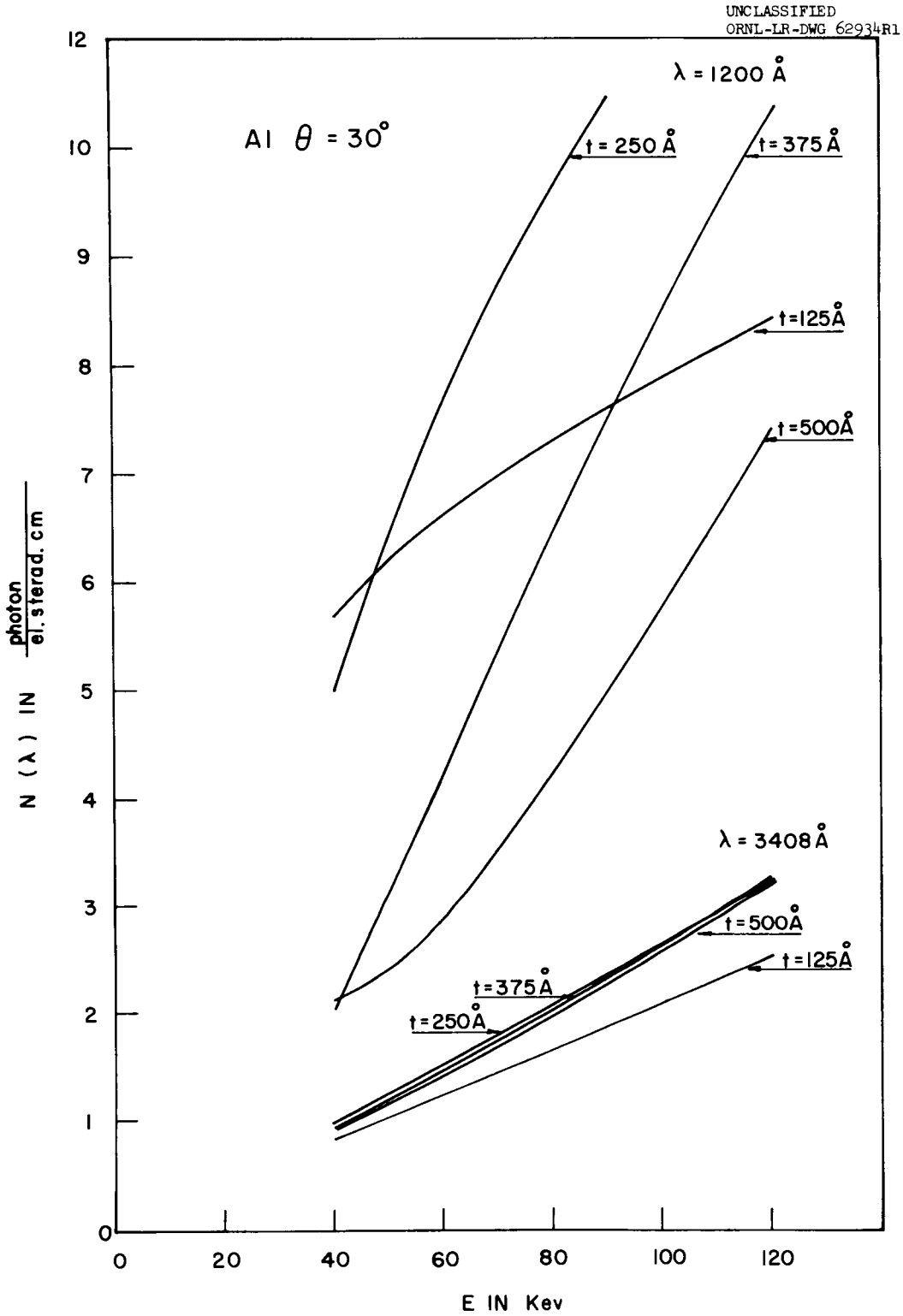

Figure 9. Theoretical Photon Yields as a Function of Beam Energy for Al (t = 125, 250, 375, 500 Å; $\theta = 30^{\circ}$; λ = 1200, 3408 Å).

III. APPARATUS

The apparatus shown in Figure 10 consisted of an electron gun, a linear accelerator, a target foil, a Faraday cup, a target foil housing, a vacuum monochromator, and a photon detector. The gun delivered a monoenergetic beam of electrons which were accelerated to a particular energy. The accelerated beam was then defined by one or more collimators before impinging on the thin target foil and emerging into the Faraday cup. The vacuum monochromator focused the light emitted from the foil within a small solid angle at some particular angle onto a photon detector. The detector was either film or a photomultiplier tube.

A. Electron Gun

Two different electron guns were used in this work. The first gun was much the same as that described by Zeimer, Johnson, and Birkhoff.[19] The electrode structure from a General Electric 3MP1 cathode-ray tube was inserted into and insulated from a brass tube. The latter could be inserted into the end of the accelerator through an O-ring seal. The gun was modified by removing the deflection plates, the base, the filament, and the cathode. A directly heated cathode was made from a Westinghouse 1709 12-volt spot light bulb which has a linear filament. This filament, coated with a special emission coating manufactured by the Kulite Tungsten Company, Ridgefield, New Jersey, proved to be superior to uncoated filaments in lifetime and electron emission.

---

[19] P. L. Zeimer, R. M. Johnson, and R. D. Birkhoff, "Measurement of Stopping Power of Copper by Calorimetric Methods," ORNL-2775, 1959, Oak Ridge National Laboratory, Oak Ridge, Tennessee.

UNCLASSIFIED
ORNL-LR-DWG 50834ARI

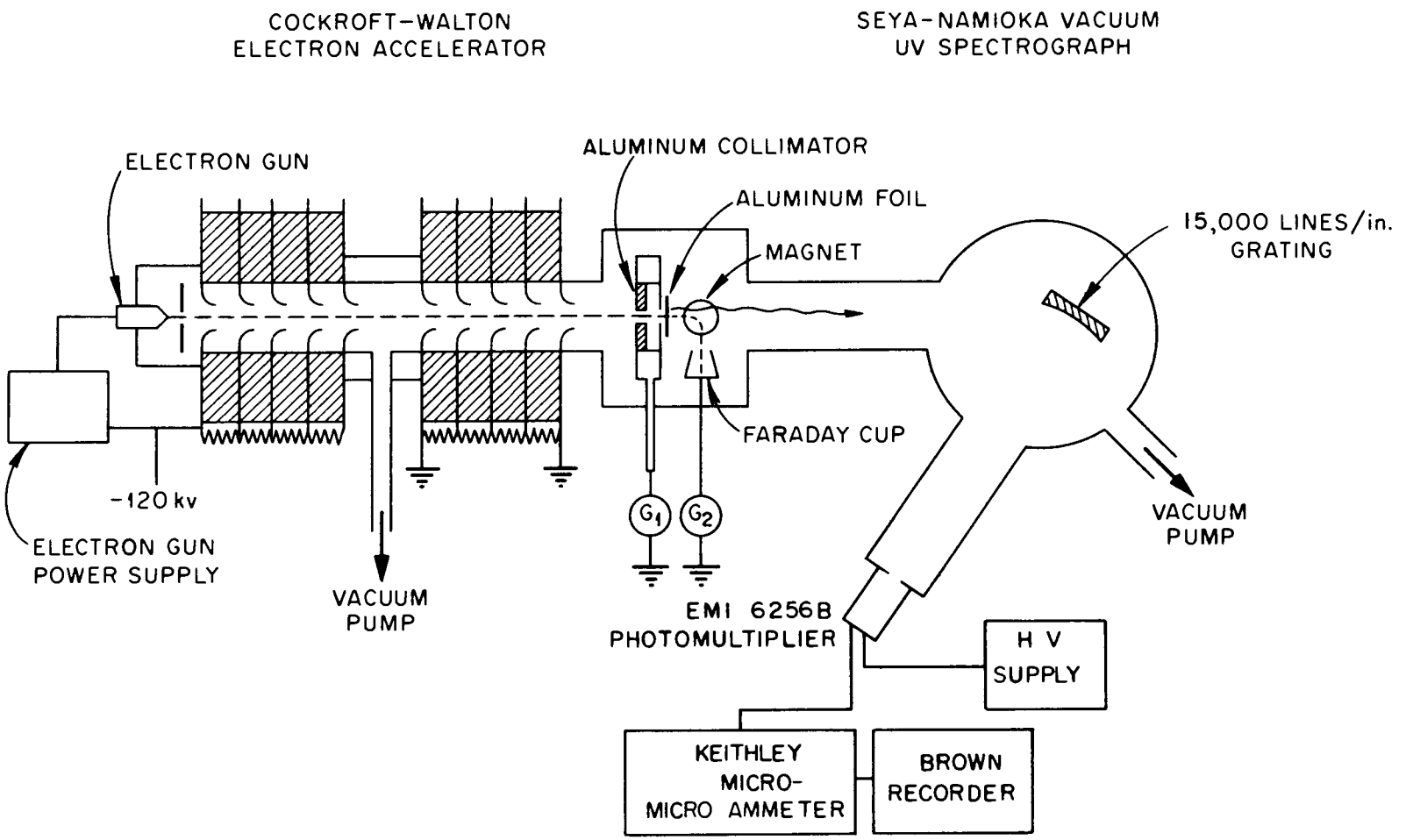

Figure 10. Schematic Diagram of Accelerator, Irradiation Chamber, and Monochromator.

The second gun was designed for easier alignment of the filament with respect to the electrodes. The glass envelope was removed from a Westinghouse 1709 tube and the filament on its base was placed in position through the side of the brass tube structure. A window in the face of the gun then allowed unhampered vision of the filament position. For several reasons the deflection plates in the gun were electrically connected to the second anode rather than being removed as in the first gun. This electrical connection was as effective as removal in nullifying the effects of the deflection plates without precluding future use of them. Also in removing the deflection plates it is easy to damage the electrodes. The kovar seals were recessed into the brass end plate to give them protection from being accidentally broken.

The power supply for the electron gun was that used by Zeimer, et al.[20] except for a 2.5 ohm resistance in series with the filament. This change permitted more precise control of the filament emission.

B. Accelerator

The Cockcroft-Walton accelerator consisted of a vacuum-tight arrangement of alternate electrodes and ceramic insulators. The electrodes were separated electrically by six fifty-megohm resistors across which the high voltage was applied from a Westinghouse center-grounded 250 KV x-ray power supply. Only one side of the power supply was used which limited the maximum electron beam energy to 125 kev.

Surrounding the accelerator were three degaussing coils to nullify the earth's magnetic field and the fringe fields of other electrical

---

[20] Ibid.

devices nearby and to help in directing the beam into the target foil. Also helping in the positioning of the beam was an insulated collimator at the end of the accelerator which was connected to ground through a sensitive galvanometer. Beam width and position could be judged by galvanometer deflection as a function of the current in the degaussing coils.

The accelerator vacuum system included a liquid-nitrogen trap, an oil diffusion pump, another liquid-nitrogen trap, and a fore pump.

C. Seya-Namioka Vacuum Scanning Monochromator

1. Theory

A Jarrell-Ash model 78-650 Seya-Namioka Vacuum Scanning Monochromator was used to analyze the spectra of light emitted by the foils. The theory for this given type of monochromator has been developed by M. Seya,[21] and the first such machine was constructed by T. Namioka.[22] Some of the advantages of this design are: 1) only one reflecting surface is needed in the ultraviolet region where all materials reflect poorly; 2) the total ruled portion of the grating is used for all wave lengths which results in an improvement in resolution and transmission; 3) the instrument is light, small, and portable so that it can be used easily in various positions with other apparatus; and 4) with fixed entrance and exit slit positions, the instrument can be used from 500 to 6000 Å with only a slight defocusing of the image by simply rotating the grating. It can be seen that a rotation of the grating with fixed entrance and exit slits will take the grating surface off the Rowland circle. The

---

[21] M. Seya, Science of Light 2, No. 1, 8 (1952),

[22] T. Namioka, Science of Light 3, No. 3, 15 (1954).

theory derived by Seya demonstrates that the grating may be rotated enough to give the monochromator an operating region of a few thousand angstroms without a large drop in resolution or transmission.

Using the equation for the focal properties of a concave grating developed by H. G. Beutler,[23] Seya studied the focusing of a grating when subjected to a rotation about a vertical central axis.

The light path function, F (see Figure 11) for a concave grating is expressed by:

$$F = AP + BP + \frac{w}{d} m \lambda \tag{21}$$

where d is the ruling separation, w is the horizontal component of P on the grating, λ is the wave length of the light considered, and m is an interger expressing the order of the image.

AP and BP can be expressed as:

$$AP = F_1 + F_2 + F_3 + \ldots \tag{22}$$

$$BP = F'_1 + F'_2 + F'_3 + \ldots \tag{23}$$

where F_1, F'_1, F_2, and F'_2, etc. are written in terms of the entrance and exit slit distances from the center of the grating surface, r and r'; the radius of curvature of the grating, R; the entrance and exit slit angles, α and β; and the width and length of the grating face, w and l.

The constancy of the terms $(F_1 + F'_1 + \frac{w}{d} m \lambda)$ and $(F_2 + F'_2)$ determine the image formation while $(F_3 + F'_3)$, $(F_4 + F'_4)$, etc. describe astigmatism, spherical and chromatic aberrations, and higher order aberrations. Beutler's derivations show that

$$F_1 = r - w \sin \alpha \tag{24}$$

---

[23] H. G. Beutler, J. Opt. Soc. Am. 35, 311 (1945).

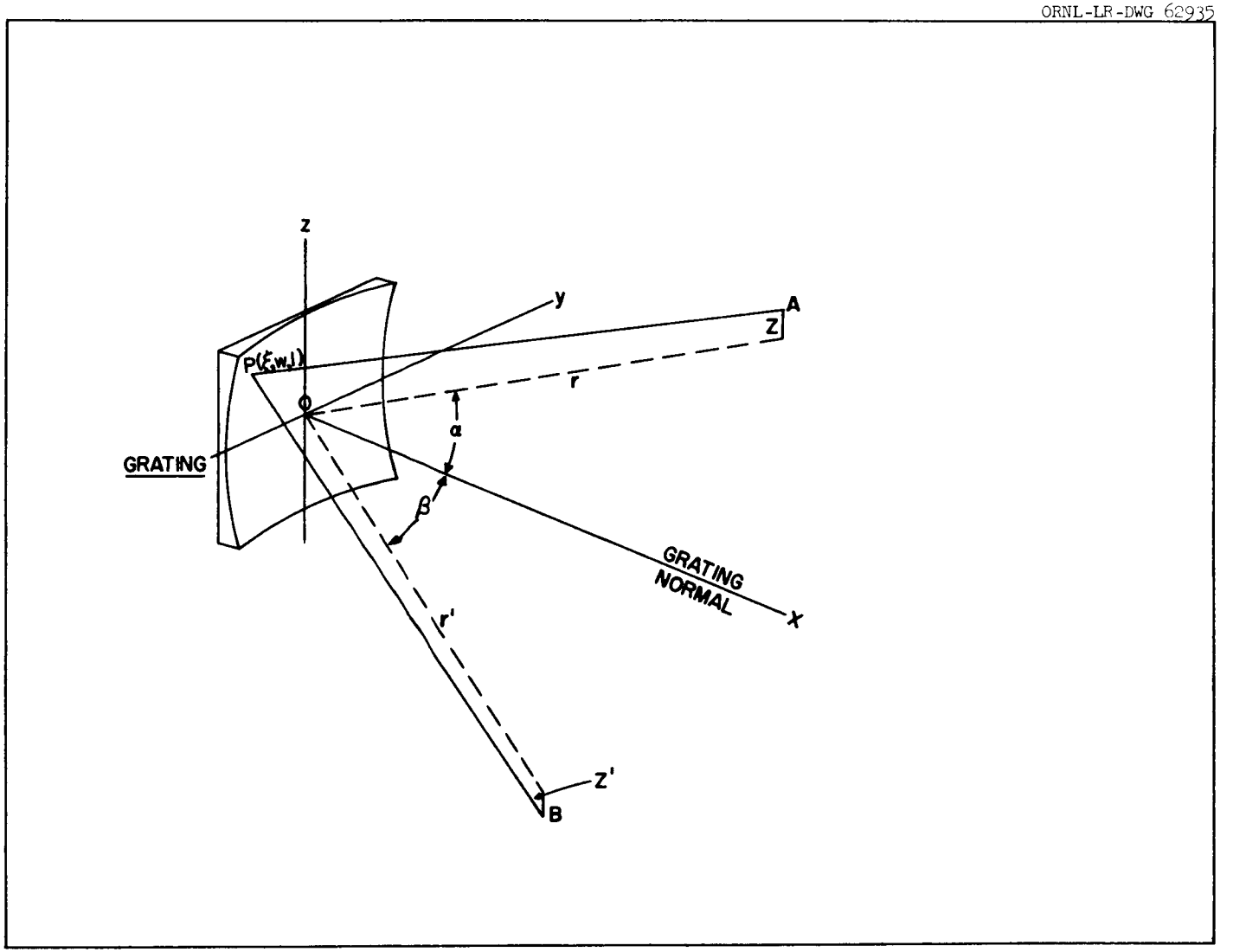

Figure 11. Schematic Diagram of Light Path in Monochromator.

$$F_2 = 1/2\ w^2 \left(\frac{\cos^2 \alpha}{r} - \frac{\cos \alpha}{R}\right) + 1/2\ w^2 \frac{\sin \alpha}{r} \left(\frac{\cos^2 \alpha}{r} - \frac{\cos \alpha}{R}\right)$$

$$+ 1/2\ w^4 \frac{\sin^2 \alpha}{r^2} \left(\frac{\cos^2 \alpha}{r} - \frac{\cos \alpha}{R}\right) + \ldots \tag{25}$$

$$F'_1 = r' - w \sin \beta \tag{26}$$

$$F'_2 = 1/2\ w^2 \left(\frac{\cos^2 \beta}{r'} - \frac{\cos \beta}{R}\right) + 1/2\ w^2 \frac{\sin \beta}{r'} \left(\frac{\cos^2 \beta}{r'} - \frac{\cos \beta}{R}\right)$$

$$+ 1/2\ w^4 \frac{\sin^2 \beta}{r'^2} \left(\frac{\cos^2 \beta}{r'} - \frac{\cos \beta}{R}\right) + \ldots \tag{27}$$

Using Fermat's principle, the constancies of the image terms are expressed as:

$$\partial \frac{(F_1 + F'_1 + \frac{w}{d} m \lambda)}{\partial w} = 0 \tag{28}$$

and

$$\partial \frac{(F_2 + F'_2)}{\partial w} = 0 \tag{29}$$

These differentials yield the equations

$$d\ (\sin \alpha + \sin \beta) = m \lambda \tag{30}$$

and

$$w \left[\frac{\cos^2 \alpha}{r} - \frac{\cos \alpha}{R} + \frac{\cos^2 \beta}{r'} - \frac{\cos \beta}{R} \right]$$

$$+ 3/2\ w^2 \left[\frac{\sin \alpha}{r} \left(\frac{\cos^2 \alpha}{r} - \frac{\cos \alpha}{R}\right) + \frac{\sin \beta}{r'} \left(\frac{\cos^2 \beta}{r'} - \frac{\cos \beta}{R}\right) \right] = 0 \tag{31}$$

Equation (30) is the familiar equation for wave reinforcement while Equation (31) describes the focal conditions in terms of the slit angles and distances.

To employ the Seya mounting, it is necessary to find a condition for image formation at some point which is independent of grating rotation. Analysis of Equation (31) shows that there are only two straightforward conditions wherein the left side reduces identically to zero. If the entrance and exit slits and the grating lie on a Rowland circle, then

$$\frac{\cos^2 \alpha}{r} - \frac{\cos \alpha}{R} = \frac{\cos \alpha}{R} - \frac{\cos \alpha}{R} = 0 \tag{32}$$

and

$$\frac{\cos^2 \beta}{r'} - \frac{\cos \beta}{R} = \frac{\cos \beta}{R} - \frac{\cos \beta}{R} = 0 \tag{33}$$

and therefore the equation is satisfied. For the Wadsworth mounting where $r = \infty$, and $\beta = 0$, the equation is also identically satisfied. These are the only two mountings which give perfect focus. However another condition can be derived which produces a close approximation to a focus.

If Equation (31) is considered to be an expansion of $\frac{w}{R}$, the second and higher order terms can be neglected or considered as aberrations for an approximate solution. Equation (31) then reduces to:

$$\frac{\cos^2 \alpha}{r} - \frac{\cos \alpha}{R} + \frac{\cos^2 \beta}{r'} - \frac{\cos \beta}{R} = 0 \tag{34}$$

The (α, r) and (β, r') which satisfy this equation give the positions of the entrance slit and its image or the exit slit.

Let f be defined as

$$f \equiv \frac{\cos^2 \alpha}{r} + \frac{\cos^2 \beta}{r'} - \left(\frac{\cos \alpha + \cos \beta}{R}\right) \tag{35}$$

A condition for image formation independent of grating rotation means that there must be found an $f = 0$ where r, r', and $(\alpha - \beta)$ are independent of α.

Letting $C = \alpha - \beta$ and $\alpha = \alpha_o + \Delta \alpha$ and substituting in Equation (35), one finds that the condition for $f = 0$, regardless of the value of $\Delta \alpha$, is given by the determinantal equation:

$$\begin{vmatrix} \cos^2\alpha_o & \cos^2(\alpha_o - C) & -[\cos \alpha_o + \cos(\alpha_o - C)] \\ -\sin 2\alpha_o & -\sin 2(\alpha_o - C) & \sin \alpha_o + \sin(\alpha_o - C) \\ -2 \cos 2\alpha_o & -2 \cos 2(\alpha_o - C) & \cos \alpha_o + \cos(\alpha_o - C) \end{vmatrix} = 0$$

This equation was investigated in a detailed graphical analysis by Seya. The behaviors of r and r' as functions of α_o in the range between 20°

and 34° were explored for values of C around 70°. This study resulted in the choice of the best values of C of 70° 15' and $\frac{R}{r}$ of 1.22247. With these choices $\frac{R}{r'}$ changed with α_o by less than 0.00023 over a wave length region from 0 to 6000 Å.

2. Construction

The monochromator was constructed in the following manner (Figure 12). The vacuum chamber consisted of a cylindrical tank 9 inches in diameter and 20 inches deep with removable top. The tank opened into two adjustable arms 3-7/8 inches in inside diameter and also into an oil diffusion pump and fore pump. Attached at the ends of the two arms were precision slits, adjustable from 0 - 400 μ. All removable parts were fitted with O-ring seals. The vacuum system consisted of a pipe leading past a cold trap into a diffusion pump backed by a fore pump. For convenience, a change was made in the system as received from the manufacturer. The diffusion pump was disconnected and a valve was placed between it and the monochromator. Thus the diffusion pump did not need to be cooled when the vacuum system was opened to the atmosphere, thus saving much time.

The grating holder was located on a rotating base at the center of the cylindrical tank. The grating rotation was controlled from outside the tank through a rotating rod. A geared transmission operated by either a hand crank or an electric motor provided twelve speeds to the rod. A counter connected to the gearing system translated grating rotation into a measure of the wave length of the light being transmitted.

A veeco type DG-2 ion gauge measured the pressure in the spectrometer from 10^{-2} to 10^{-6} mm of mercury in two ranges. A control panel

Figure 12. Monochromator with Irradiation Chamber, Fore Pump, and Photomultiplier Equipment.

contained the ion gauge switch and meter, the switches for the diffusion pump and an extra electrical outlet, the main power switch, and the control to an extra air valve located at the bottom of the tank. The monochromator was mounted on a three wheel cart which held the monochromator arms at the same level as the central axis of the accelerator.

3. Gratings

Two 0.5 meter gratings were used in the monochromator (Figure 13). The first was an aluminum replica grating ruled with 30,000 lines per inch and blazed for 1100 Å. The second was similar to the first except that it was ruled with 15,000 lines per inch and blazed for 6000 Å. The 1100 Å grating was used primarily for measurements in the 400 - 2000 Å region while the 6000 Å grating was used primarily in the 2000 - 6000 Å region. The ruled surfaces of the gratings were 44 x 44 millimeters.

4. Focus

The monochromator was focused by adjustment of the grating and the slits. With the grating clamped carefully in a prescribed position, the slits were adjusted by means of the movable arms until maximum intensity of the image was found. The Seya mounted grating is such that the monochromator could be focused exactly for only one wave length, with the efficiency falling off slightly as the grating was rotated away from that position. The monochromator was focused at the central image position for all measurements reported here.

5. Transmission Cutoff

In instances where the spectrum under 2000 Å was not be be measured, a 1/16 inch fused-quartz plate of known transmission was placed in the exit arm. This had the effect of cutting out short wave length

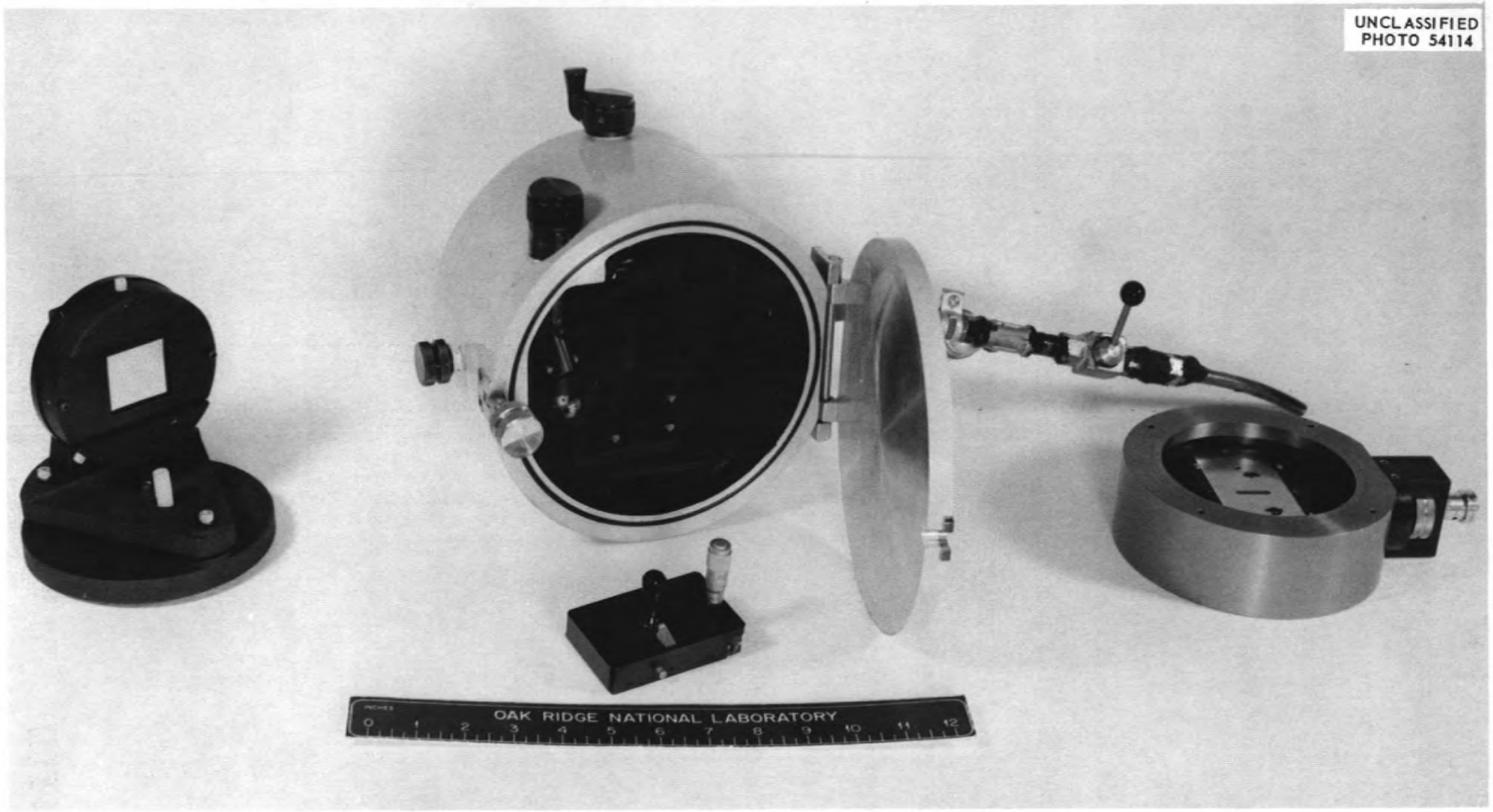

Figure 13. Grating in Holder, Camera, and Slit Assembly.

bremsstrahlung at the detector. Short wave length radiation was not diffracted well by the grating, but rather was scattered off the grating into the exit slit.

6. Camera Attachment

The monochromator camera attachment was a Jarrell-Ash Model 78-656 (Figure 13). The camera replaced the exit slit and the diffracted image was focused onto a curved film holder which held a 2-1/2 inch length of 35 millimeter film. The monochromator and camera together were used as a spectrograph. A calibrated control knob on top of the camera allowed the film holder to be raised in steps from behind an opaque slide and enabled the taking of multiple exposures on a single piece of film.

The camera compartment could be isolated from the monochromator by a flap valve controlled by a hand crank at the top of the camera. This enabled the camera to be opened to atmospheric pressure for reloading of the film while the monochromator was kept at high vacuum. A separate port in the side of the camera was used to pump down the camera with a fore pump to a pressure of about 200 μ of Hg where it could be opened again to high vacuum.

Two types of film were used in the camera. For measurements of the region from under 2000 Å into the visible, special 35 mm Kodak SWR film was used. For measurements taken in the higher wave length regions, regular Kodak film of ASA speed 800 was usually used.

7. Phototube Attachment

The phototube attachment employed an EMI 6256 B photomultiplier and was mounted onto the exit slit of the monochromator in a vacuum-tight seal. The phototube was used at room temperature. Light leaks

into the container were reduced by black paint on the container and three external black bags. The quartz window of the phototube imposed an effective lower limit of approximately 2000 Å for normal usage. In order to detect shorter wave lengths the window was sometimes covered with a thin film of sodium salicylate. This transformed the phototube into a detector with constant sensitivity from 500 Å to 3000 Å, at the cost of efficiency for the longer wave lengths.

The phototube voltage was supplied by an Atomic Super-Stable High Voltage Power Supply model 312. The phototube output was measured with a Keithley model 410 D.C. micro-microammeter which fed a 10 millivolt Brown recorder. In order to utilize the full sensitivity of the electrometer, a calibrated variable negative potential was used to nullify part or all of the phototube dark current and background. Another alteration in the electrometer was the substitution of 300 μμf and 55 μμf capacitors on the 10^{-10} and 3×10^{-11} scales of the instrument. These larger input capacitances tended to damp out random fluctuations in the current. A potential divider across the electrometer output reduced the 5 volt maximum signal to the 10 millivolt maximum required by the Brown recorder.

D. Irradiation Chamber

1. Construction

The irradiation chamber was made from a brass block 5 in. x 5 in. x 3-7/8 in. with a cylindrical cavity 4-7/32 in. in diameter centered along the 3-7/8 in. axis (Figure 14). One end attached directly to the entrance arm of the monochromator while the other end held a flange which connected the chamber and accelerator.

Circular openings 2-7/8 in. in diameter were made in three sides of the chamber. These openings were provided with lucite windows and aluminum

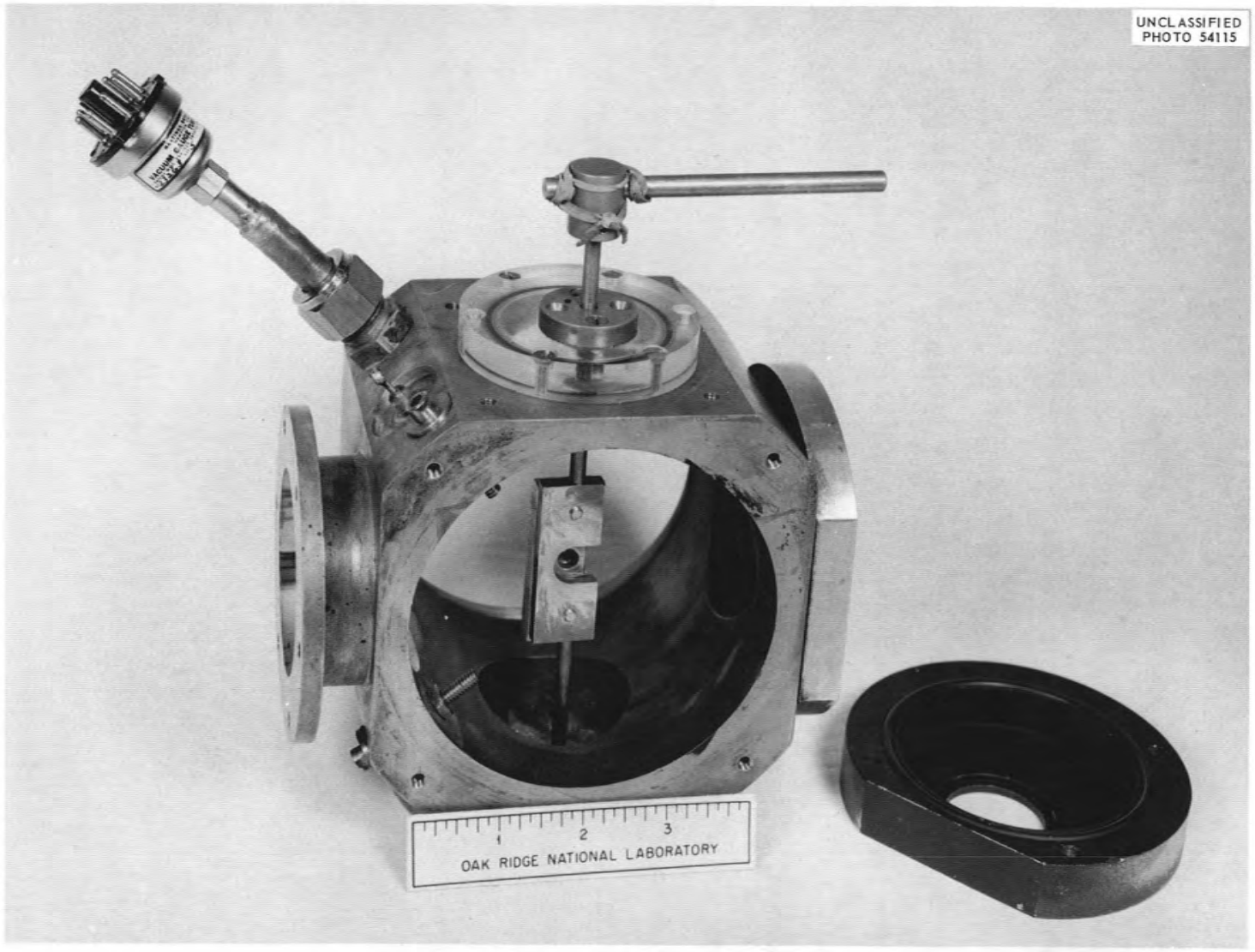

Figure 14. Irradiation Chamber.

covering caps. The lucite windows, which were made vacuum tight with O-ring seals, allowed visual inspection of the target foils. The aluminum caps, which were made light tight with O-ring seals, were used to exclude room light during a run. Two of the windows were modified to accommodate the foil holder. A brass rod with a block containing a 1.3 cm ring groove near its center fitted into a blind hole in one lucite window and out through the opposite window and aluminum cap. This arrangment was such that 1) the ring groove was centered on the central axis of the chamber; 2) when the chamber was attached to the monochromator arm, the ring groove, which contained the target foil, was at exactly the monochromator entrance slit position; 3) the rod could be rotated at will from outside the chamber; and 4) the rod was electrically insulated by the lucite windows. The third lucite window was left for miscellaneous purposes.

An opening 2-5/16 in. in diameter was cut in the fourth side of the chamber and a brass flange was welded around it. This flange was sealed with a plate which contained electrical terminals to support the filaments used for vacuum evaporation of metals (Figure 15).

Other parts of the system concerned with controlling the electron beam were the beam entrance flange and the Faraday cup. These elements were varied in position with changes in the system for viewing the foil at different angles.

2. 0° Angle

For the monochromator to view the foil at 0° (directly in the beam direction), the beam had to be diverted so that the Faraday cup would not prevent the light emitted by the foil from entering the monochromator.

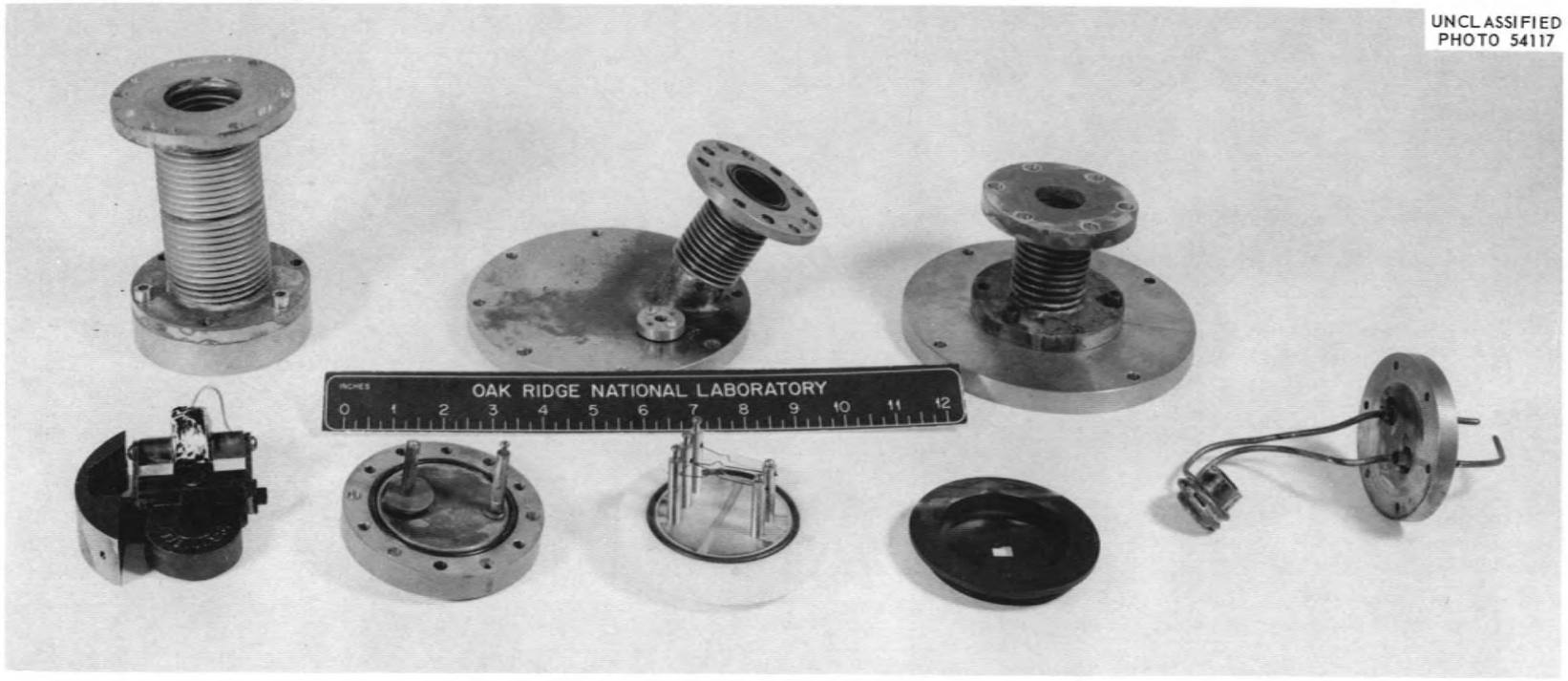

Figure 15. Irradiation Chamber Accessories.

A small permanent magnet was used to turn the electron beam through an angle of approximately 45° and into the cup after passing through the foil. The entrance to the insulated cup was small so that the 40 - 110 kev electron beams used had to impinge on the center of the target foil in order to be collected by the cup.

The beam entrance flange brought the beam straight through the center of the irradiation chamber from the accelerator. The beam was reduced to about 2 mm diameter by an aluminum collimator on the front side of the foil holder.

3. 30° Angle

The magnet was removed from the chamber when the foil was viewed at 30° to the normal. The current was collected using a cup which was supported in place by wrapping copper tubing around it and running the leads out through kovar seals in a brass plate replacing the third lucite window. Water or other coolants could be flowed through the tubing to cool the cup, but this was found to be necessary only at the highest power level ($\sim$ 5 watts). By shaping the tubing correctly, the distances were such that the cup could collect the beam without blocking the light from the foil.

The entrance flange was arranged so that the electron beam entered at a 30° angle to the axis of the chamber and on the same horizontal plane. The foil holder rod, in a vertical position, was rotated until the beam hit normal to the foil. The monochromator then viewed the foil at a 30° angle to the foil normal.

4. 72° Angle

The arrangement for viewing the foil at 72° required that the electron beam enter the third window in the side of the chamber. An entrance flange

containing a flexible sylphon bellow was arranged so that the electron beam cleared the edge of the window, was defined by the aluminum collimator on the foil holder, penetrated the target foil, and was collected by a Faraday cup. This cup was held in place by the screws provided for the magnet holder and was electrically isolated by its nylon supports. The end of the box not used in this experiment was sealed by a plain brass plate.

5. Chamber Accessories

The chamber contained two more connections to the outside. One was a kovar sealed electrical lead which was used in measuring the current collected by the Faraday cup in the 0° and 72° positions. The other was a screw fitting welded to an open port which held a thermocouple vacuum gauge. Another addition was a light baffle fitting into the monochromator arm to decrease the scattered light at the detector.

6. Polarizer

An aluminum plate with a geared rotating brass tube section at its center containing a polarizer fitted into the end of the monochromator arm in place of the light baffle (Figure 16). Another gear operating at a 9:20 ratio with the first was also contained in the plate. To rotate the tube from outside the chamber, a stainless steel rod entering through an O-ring sealed hole in the beam entrance flange was turned which rotated the tube through two universal joints. The polarizer used was a Glan prism obtained from Karl Lambrecht with a useful transmission down to 2100 Å. In this manner, light from the foil was analyzed for polarization before striking the grating. It was discovered that unpolarized light from a black body appeared to be partially polarized because the prism deviated

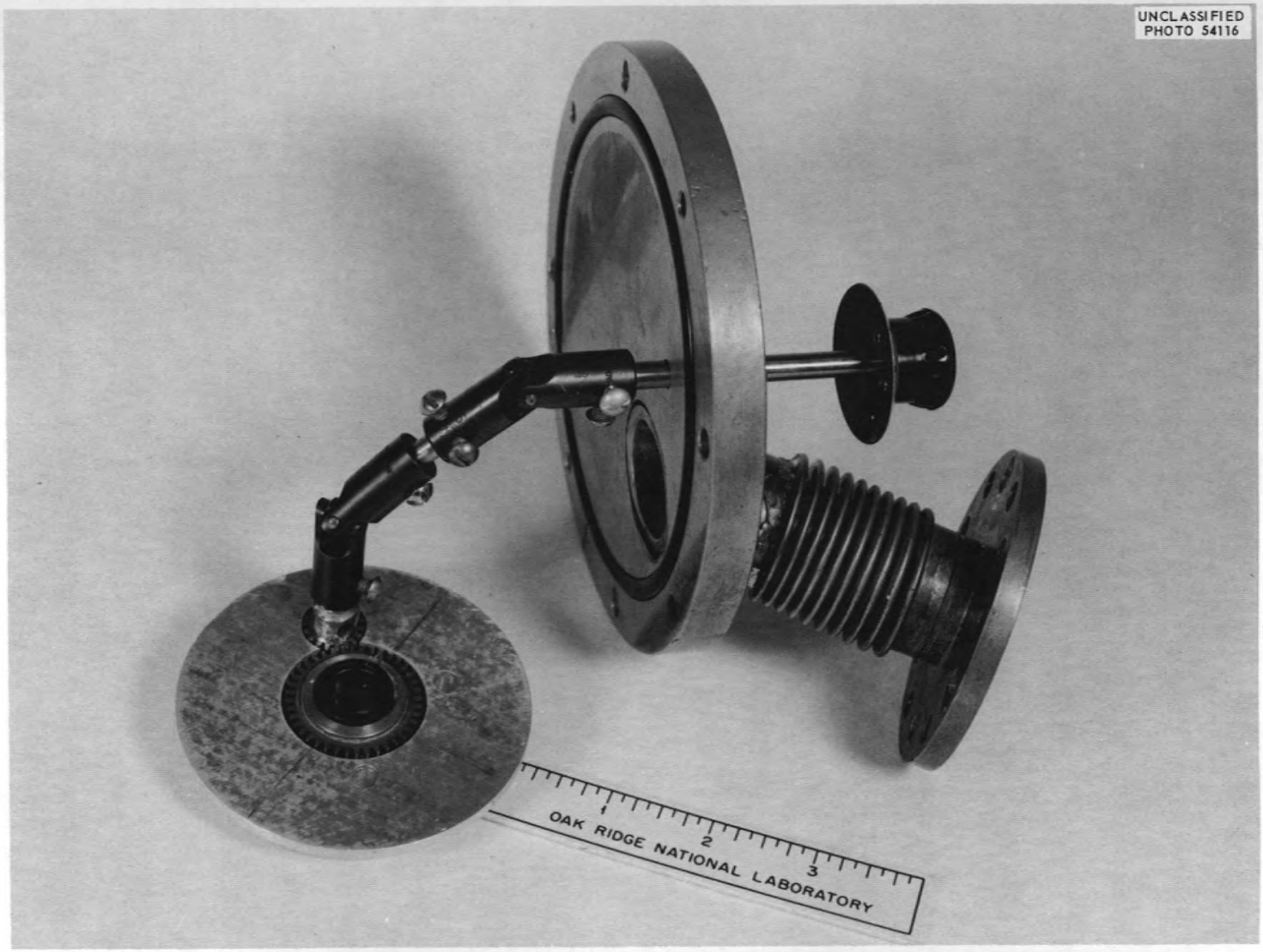

Figure 16. Attachment for Measuring Polarization.

the light so that it partially missed the grating, and because the grating reflectively depended to some extent on the direction of polarization of the incident light. A correction curve was obtained as a function of wave length and was applied to all polarization data on light from foils.

E. Instruments for Beam Current Measurement

Three instruments were used in beam current measurements. The first was a Keithley model 410 micro-microammeter which measured the current collected by the Faraday cup. The second was a Rubicon galvanometer of .00406 μ amp/mm sensitivity with an Ayrton shunt giving 1 to 10,000 times the galvanometer scale reading. This instrument was used to measure the current stopped by the foil, foil holder, and defining collimator. The third was a Leeds and Northrup 2420 galvanometer of .031 μ amp/mm sensitivity which measured the current stopped by the beam control collimator at the end of the accelerator.

IV. TECHNIQUE AND CALIBRATIONS

A. Spectrometer Response

The black body radiation emitted by a heated tungsten filament was used as a source of known spectral distribution for determining the relative response of the spectrometer.

A filament assembly containing two insulated electrodes and a glass window was connected to the entrance slit of the monochrometer. A tungsten filament of .015 in. diameter was so arranged between the inside terminal ends that it was parallel to the entrance slit and was centered on the axis of the arm of the monochrometer. The entrance slit was masked down to the point where all the transmitted light fell onto the grating.

Before heating the filament, the system was pumped down to approximately 50 microns of mercury pressure and then refilled with dry nitrogen gas to about one atmospheric pressure. The nitrogen had the double purpose of retarding filament evaporation and shortening the mean free path of molecules which were evaporated so they would not coat the grating of the monochromator. A current of up to 25 amperes was put through the filament. A Leeds and Northrup 8622-C optical pyrometer was used to read the temperature of the filament through the glass window. When the temperature of the filament reached equilibrium, the wave length region from 2000 to 6000 Å was scanned and recorded. The temperature was monitored throughout the scan.

The recorded spectrum as detected by the phototube was compared with a table of values calculated by Eldridge[24] based on a modified Planck

---

[24] H. B. Eldridge, "Weins Law Black Body Tables," Oak Ridge National Laboratory, Oak Ridge, Tennessee (1961, unpublished).

radiation spectrum. The temperature indicated by the pyrometer was corrected from color temperature to true temperature with data given by DeVos.[25] The black body spectrum for this corrected temperature was then modified for the emissivity of tungsten also given by DeVos.[26]

The values of relative intensity versus wave length thus obtained constituted the actual light spectrum incident on the grating. The resulting response of the spectrometer was then calculated by dividing the recorded spectrum by the modified black body spectrum and is shown in Figure 17.

Although the spectral response was calculated down to 2300 Å, the light intensity below about 2800 Å is so low that the accuracy of calibration is correspondingly reduced.

B. Data Correction

Each spectral distribution curve as recorded by the Brown chart recorder of the spectrometer system required two corrections before the photon spectrum emitted by a foil could be ascertained. The first correction was a subtraction of the second order spectrum and the second was a correction for the relative response of the whole spectrometer system.

Since a quartz window photomultiplier with a short wave length cut off at 1600 Å was used as a detector, a second order contribution was expected at wave lengths greater than 3200 Å with a third order contribution beginning at 4800 Å. However, since no radiation was detected

---

[25] J. C. DeVos, Physica 20, 690 (1954).

[26] G. A. W. Rutgers and J. C. DeVos, Physica 20, 715 (1954).

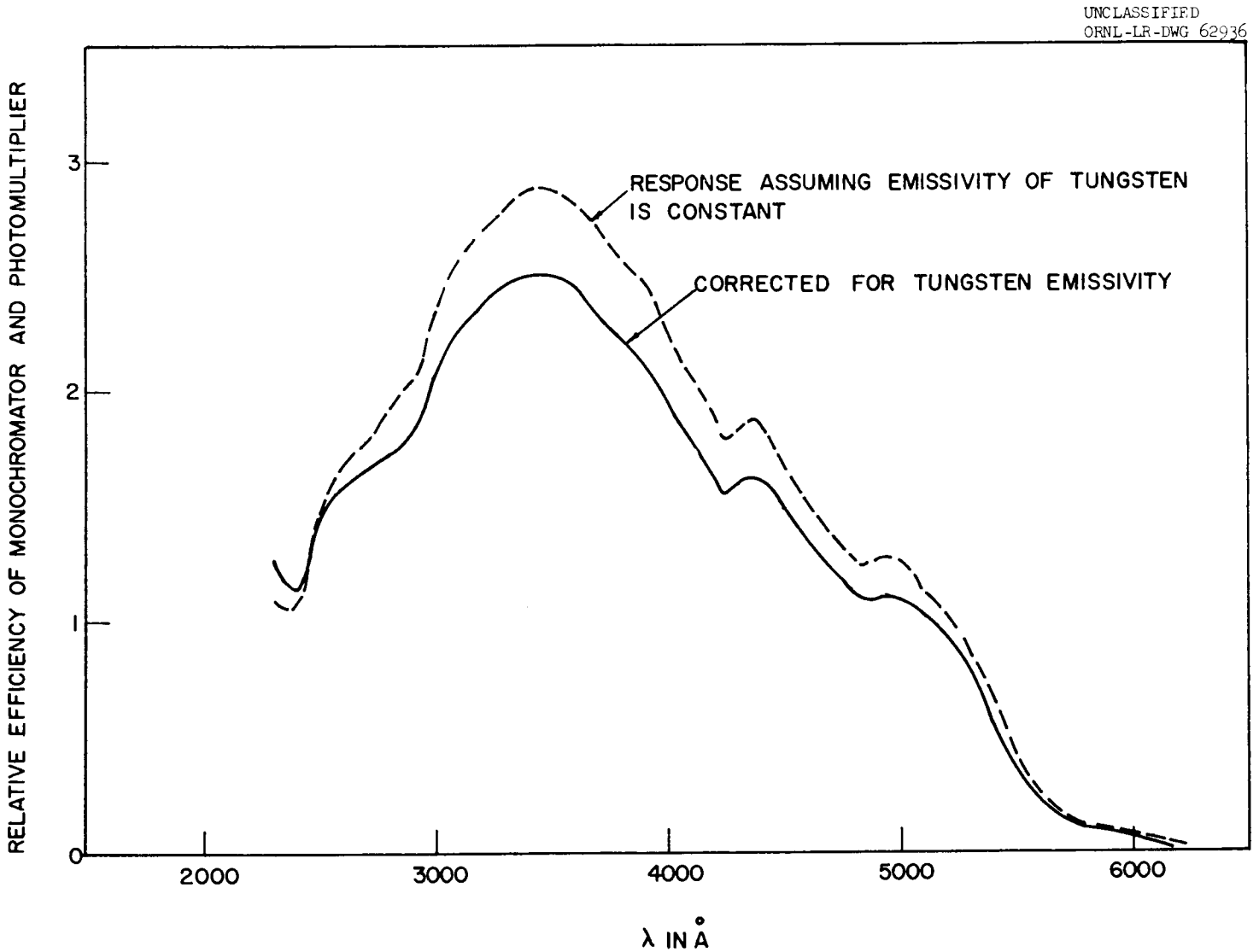

Figure 17. Spectral Response of Monochromator and Photomultiplier.

from the foils below 1900 Å, the second order contribution did not occur until 3800 Å with no third order contribution below 5700 Å.

In order to assess the second and third order contributions, two glass plates each 1/16 inch thick were inserted in the light beam. These plates, made from Corning No. 774 glass, do not transmit radiation below 3000 Å. It was observed that no radiation was detected at 5600 Å, although the recorded spectrum without the glass plates showed radiation at this wave length. All of the radiation detected at 5600 Å was therefore ascribed to the second order contribution of the radiation emitted by the foils at 2800 Å.

Theoretically, the ratio of the current recorded at 5600 Å to the current recorded at 2800 Å should be a constant for all of the runs using the same grating. It should therefore be possible to use this ratio determined in one run to correct the data in all other runs. In practice, however, slight variations in experimental conditions caused this ratio to vary. It was felt that a more precise way to correct for the second order contribution was to determine this ratio for each run, assuming that all of the radiation at 5600 Å was second order. The spectral distributions were therefore corrected using the relationship

$$I(\lambda) = I'(\lambda) - \frac{I'(5600\ \text{Å})}{I'(2800\ \text{Å})} I'(\lambda/2)$$

where $I(\lambda)$ was the spectral distribution with the second order contribution subtracted and $I'(\lambda)$ was the spectral distribution detected by the photomultiplier during an experimental run without the glass plates in the beam.

This spectral distribution was finally corrected for the response of the spectrometer system in order to obtain the spectral distribution

emitted by the foils as shown in all figures except where noted to the contrary.

C. Wave Length Calibration

The monochromator was calibrated for the 15,000 line-per-inch grating with a mercury vapor light source and a photomultiplier detector. The central image was found by scanning and the dial reading for peak maximum was carefully recorded The spectrum was then scanned to locate strong mercury lines of known wave length.

Since the monochromator dial was calibrated to read the wave length for a 30,000 line-per-inch grating, the equation to convert dial reading to true image wave length was:

$$\lambda = 2(\lambda' - \lambda_{cI})$$

where λ is the true wave length, λ' the spectroscope dial reading, and λ_{cI} the central image dial reading.

Careful scans at a few angstroms per minute showed that the wave lengths of spectral lines were reproducible to within 1 Å over the region from 500 to 6000 Å. However, since the actual scans of the foil emission spectra were done at 1000 to 2000 Å per minute, any wave length in the recorded spectrum was limited in accuracy to approximately $\pm$ 10 Å because of the relatively slow response of the electrometer and recorder. An additional source of uncertainty was the wide (2 mm) circular aperture used for a slit. At a dispersion of about 25 Å/mm, this introduced an uncertainty of about 50 Å.

D. Preparation of Thin Foils

Thin metallic target foils were produced by evaporation shortly before use, the time lapse allowed depending on the rate of deterioration

of the metal foil. The foils were evaporated in thicknesses varying from approximately 100 - 3000 Å.

1. Vacuum Evaporation

A filament of high melting point, either tungsten or tantalum, was used as a heater from which a segment of wire of the desired target metal was evaporated onto a prepared surface. The evaporation apparatus was contained in a system evacuated to a pressure of 10^{-6} millimeters of mercury. Evaporation techniques are detailed in a recent book by Holland.[27]

Tungsten wire of .015" diameter was used as the heater for aluminum and gold. These metals "wet" tungsten well enough to form a droplet and cling to the wire when they melt. Small segments of aluminum or gold wire were hung at the bottom of V-shaped dips in the tungsten wire during the evaporation, thus keeping the molten droplets from spreading away from a small region.

A tantalum trench-shaped filament or "boat" was used to evaporate silver which does not wet tungsten well. A small piece of silver was placed at some point at the bottom of the boat and surface tension in molten silver kept the evaporating area localized.

The geometry and mass to be evaporated were adjusted to produce foils of certain desired thicknesses. In the case of the wire filaments, emission was assumed to be isotropic from the droplet. By applying the inverse square law the thickness was calculated from

$$t = \frac{m}{4\pi r^2 \rho}$$

---

[27] L. Holland, VACUUM DEPOSITION OF THIN FILMS, (John Wiley and Sons, Inc., New York, 1960).

where m is the mass of metal evaporated, ρ is the density of the bulk metal, and r is the distance from source to target. It can be seen that for r sufficiently large with respect to the width of the target, the variation in foil thickness over the surface of a flat target is small. Since the radius of the foils used was 1.3 cm while r was several centimeters, the error in this approximation was negligible.

Calculations for the tantalum boat evaporations were less exact. It was assumed that the evaporated molecules left the boat isotropically over 2 π steradians. Subsequent weighing of the foils showed that the foils were thicker than calculated, the amount of disagreement depending on the shape of the boat. The shallower the boat, the closer the thickness agreed with the calculations.

2. Vacuum Evaporation in Irradiation Chamber

Vacuum evaporation in the experimental system allowed the foil bombardment to take place immediately after evaporation without exposing the foil to air with resulting contamination and oxidation. Only tungsten filament heaters were used since it was necessary to evaporate in a horizontal direction in the chamber. Metals had to be evaporated onto a substrate which would produce negligible attenuation of the electron beam and have a negligible effect on the light emission of the foil.

Four tungsten heaters were held by five brass terminals passing through a teflon plate so that when the plate was attached to the flange on the chamber all heaters were nearly horizontal. The dip points on the heaters were approximately 6.1 cm from the substrate.

The substrate used for foil support was formvar and each backing was made individually. A 1 molar solution of commercial formvar (obtained

from Shawinigan Products Corp.) in dichloroethane was prepared. One drop of this solution was then dropped from an eye dropper onto the surface of an open container filled with water. Part of the drop remained on the surface and spread over a large area. After a few seconds during which most of the dichloroethane evaporated, an aluminum plate with a 1" diameter hole in its center was raised vertically through the surface of the water. The formvar coated both sides of the aluminum plate and formed a double thickness over the 1" hole. The formvar layer was then transferred to an aluminum ring of thickness .003", O.D. = 5/8", I.D. = 7/16" by dropping the ring onto the formvar and cutting it free from the plate.

The aluminum ring covered with the formvar substrate was inserted into the ring groove in the foil holder and the latter placed in the chamber. Before evaporation, the system was evacuated to approximately 10^{-6} mm of Hg. Next the wire carrying the mass to be evaporated was outgassed. The foil holder was turned perpendicular to this filament so that the substrate would not be contaminated by the outgassing. Then an electric current was passed through the filament until the metal wire segment melted into a droplet. The current was then reduced and the foil holder was turned parallel to the filament. Finally the current was increased until the metal was seen to be evaporating rapidly.

After the completion of the evaporation from this filament, the foil was rotated until it was perpendicular to the electron beam direction. As many as three additional evaporations could be made onto the same foil.

3. Evaporation in External Vacuum System

The external evaporation system consisted of a bell jar vacuum sealed to a base which contained a port for pumping and three insulated

electric terminals. An oil diffusion pump and a fore pump reduced the pressure of the system to approximately 10^{-5} mm Hg.

The three electric terminals held two tantalum boats. One contained a measured amount of silver while the other contained a small particle of Victawet 35B, a wetting agent made by the Victor Chemical Works. Spaced at 10, 11.5, 14.1, and 20 cm above the boats were clean glass plates. (Gold Seal Micro Slides made by Clay Adams, Inc.) One evaporation onto these spaced plates gave four Ag films equally spaced in thickness.

After the system was pumped down, the Victawet boat was heated and a film of the wetting agent was evaporated onto the glass slides. Sufficient evaporation of the wetting agent was checked by noting a drastic increase in pressure. After allowing the vacuum to return to about 10^{-5} mm Hg, a shield was rotated between the Ag boat and the glass slides, and the boat was outgassed at a temperature near the melting point of Ag. Then the shield was moved aside, and the current through the boat was increased until the Ag evaporated at a rapid rate.

The Ag film was removed from the glass plates by floating it off onto a water surface. The success of floating off the Ag depended on a good film of the wetting agent between the Ag and the glass slide. The next step was to transfer part of the Ag film onto an aluminum ring. This was done by first gluing the ring onto a slightly smaller hole in an aluminum or teflon plate, and then submerging the plate in the water until the ring was covered. The Ag film adhered to the plate where the two touched and by pulling the plate vertically out of the water, the Ag film completely covered the ring. After cutting through the aluminum around the ring, the ring plus Ag film was removed from the plate and was ready to be put in the foil holder.

4. Current Source

The large current needed to raise the heaters to the necessary temperature was provided by a Type W20MT3 Variac Autotransformer made by General Radio Company operating through a G. E. 76G164 transformer to the filament or boat terminals. Heavy 50 amp cables were used for the connections.

E. Foil Thickness Measurements

1. Electrobalance Method

A detailed description of the methods and apparatus used to weigh foils on the electrobalance has been given by Ziemer, et al.[28]

A modified Cahn Model M-10 Electrobalance was calibrated for linearity with a series of standard weights. Next, a series of formvar backings were weighed which had been made in the same manner as those onto which the foils had been evaporated.

The used target foil was kept in a dessicator jar after being taken from the irradiation chamber until it was weighed. To weigh the foil, it was cut away from the support ring and placed in a small, thin metal holder which had been previously weighed. The holder was then placed on the electrobalance arm, the current to the electrobalance motor was adjusted to balance the torque due to the foil weight, and the potential across a precision resistance was read on a Leeds and Northrup K-3 potentiometer. The potential due to the foil weight was then found by subtracting the holder potential and this was multiplied by the gram per volt constant to give foil weight. In the case of backed foils, an average value for the

---

[28] Ziemer, et. al., op. cit.

formvar backing weight was subtracted. Foil thickness was then found by dividing weight by the product of the foil area and foil density. The foil density was assumed to be the bulk value.

2. Optical Method

Optical measurements of foil thickness were made by the multiple beam interferometry method. A good description of this method is given by Tolansky.[29]

The measurements were set up as in Figure 18. A thick layer of silver was vacuum evaporated onto a slide on which a layer of foil still adhered to the surface. The resulting slide was then used with a Bausch and Lomb Stereo-Microscope, a half-silvered mirror and a half-silvered optical flat. A mercury vapor light source was used in conjunction with an interference filter to produce a beam of the mercury green line of 5460 Å which was partially reflected down onto the parallel plate arrangement. Multiple interference at the silvered surfaces produced fringes visible in the microscope. The steps to be measured in the silver surface appeared as a fringe displacement as shown in the insert of Figure 18. The relationship between the fringe displacement and the height of the step t is given by $t = f(\lambda/2)$ where f is the fractional fringe shift and λ is the wave length of the light.

---

[29] S. Tolansky, AN INTRODUCTION TO INTERFEROMETRY, (Longmans, Green, and Company, London, 1955).

UNCLASSIFIED
ORNL-LR-DWG 62937

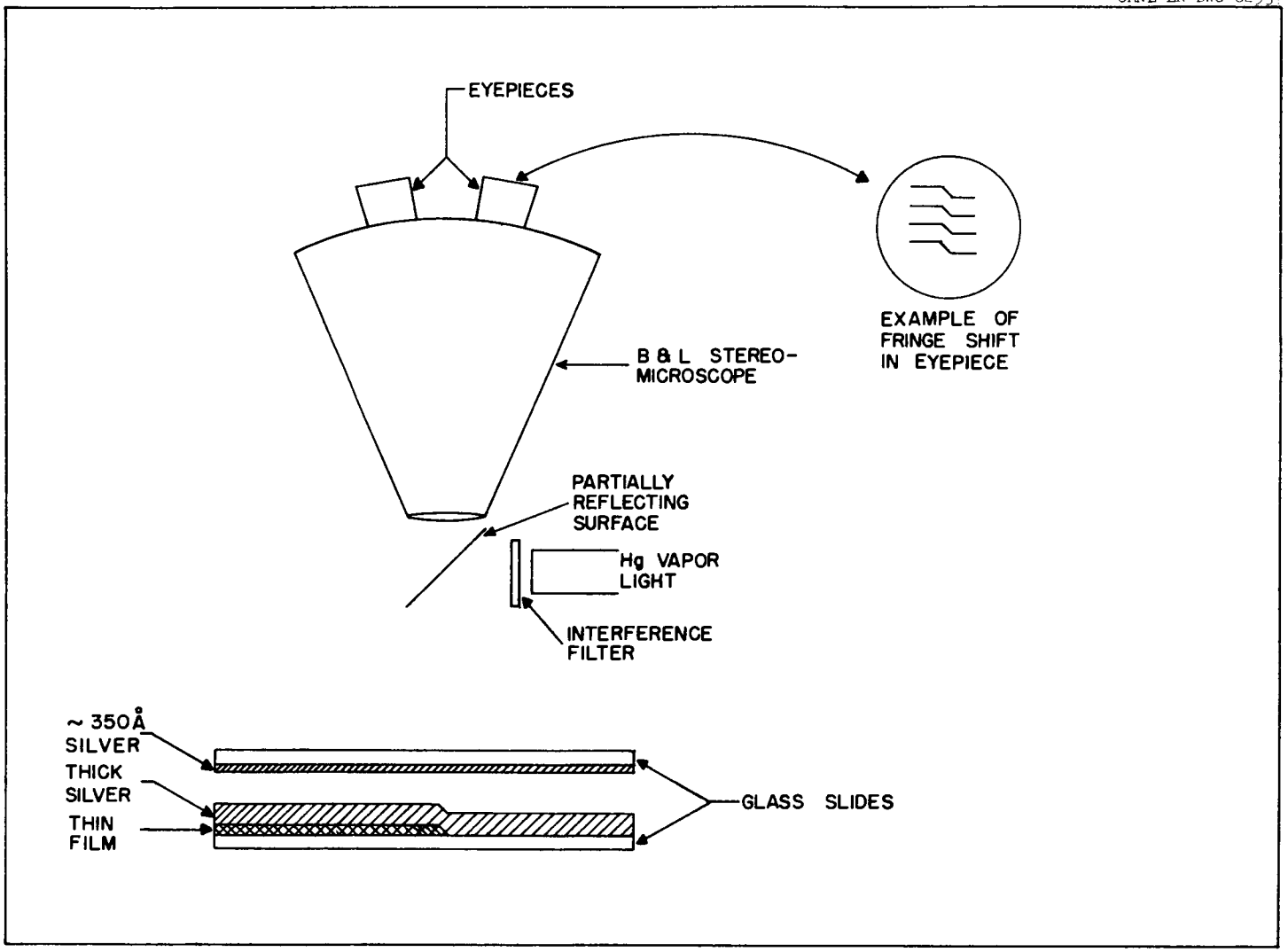

Figure 18. Schematic of Optical Foil Thickness Measurement.

V. PROCEDURE

A fore pump was used to reduce the pressure of the system to about 200 microns of mercury. Then the fore pump was closed off and the two diffusion pump fore-pump ports were opened. At this point the monochromator cold trap was filled with liquid nitrogen. At operating conditions, the vacuum varied between .5 and 5×10^{-6} mm of mercury.

The accelerator high voltage was turned on and the beam current set by adjusting the first and second anode potentials and filament current in the gun and the current in the degaussing coils around the accelerator. In some cases the grid bias was also varied. The beam current collected by the Faraday cup was found to be most stable when the current collected by the foil holder collimator system and by the beam control collimator at the end of the accelerator were minimized.

With an electron beam of about 15 microamp striking the foil, the electrometer, recorder, and phototube high voltage were turned on. The monochromator grating was then rotated to a position where the wave length transmitted was below the photomultiplier threshold and the dark current decreased to its lowest values.

The central image was scanned first to determine the consistency of the monochromator calibration. The spectrum was then scanned at 1000 or 2000 Å per minute. At this rate, the entire spectrum was recorded in not longer than five minutes. Spectra were obtained for several different electron energies, angle of observation and foil thicknesses for the same Faraday cup current.

VI. RESULTS

The results of the light emission measurements on silver foils were in approximate agreement with theoretical expectation. Thinner silver foils tended to have an emission peak in the region from 3400 to 3500 Å for certain electron beam energies. This can be seen in Figures 19 and 20 for $\theta = 30^{\circ}$ and in Figure 21 for $\theta = 72^{\circ}$. For thicker foils the sharp peak has disappeared into the broad continuum as seen in Figures 22 and 23. The effect of foil thickness on peak intensity is shown again in Figure 24. In Figure 25, the data are compared with the Ritchie-Eldridge theory and agreement may be considered to be satisfactory if allowance is made for the experimental uncertainties involved.

The change in spectral distribution for different angles of emission shows approximate agreement with the theory for the angular distribution. Figure 26 shows the uncorrected data for Ag for four angles. Figure 27 shows corrected data for three angles of emission, and Figure 28 compares four experimental points with Ferrell's theoretical angular distribution.

The variation of light intensity with beam energy for the various foil thicknesses agreed approximately with theory. Figures 29 and 30 contrast experimental points from thin foil spectra at two wave lengths with the theory of Ritchie-Eldridge. Theory and experiment are normalized to agree at 80 kev. The theoretical curves are seen to have a greater slope than the experimental points. This could be an indication of the $1/E$ bremsstrahlung increase at the lower energies.

The determination of polarization of the silver light revealed that it was partially polarized in the plane of incidence, as seen from Figure 31.

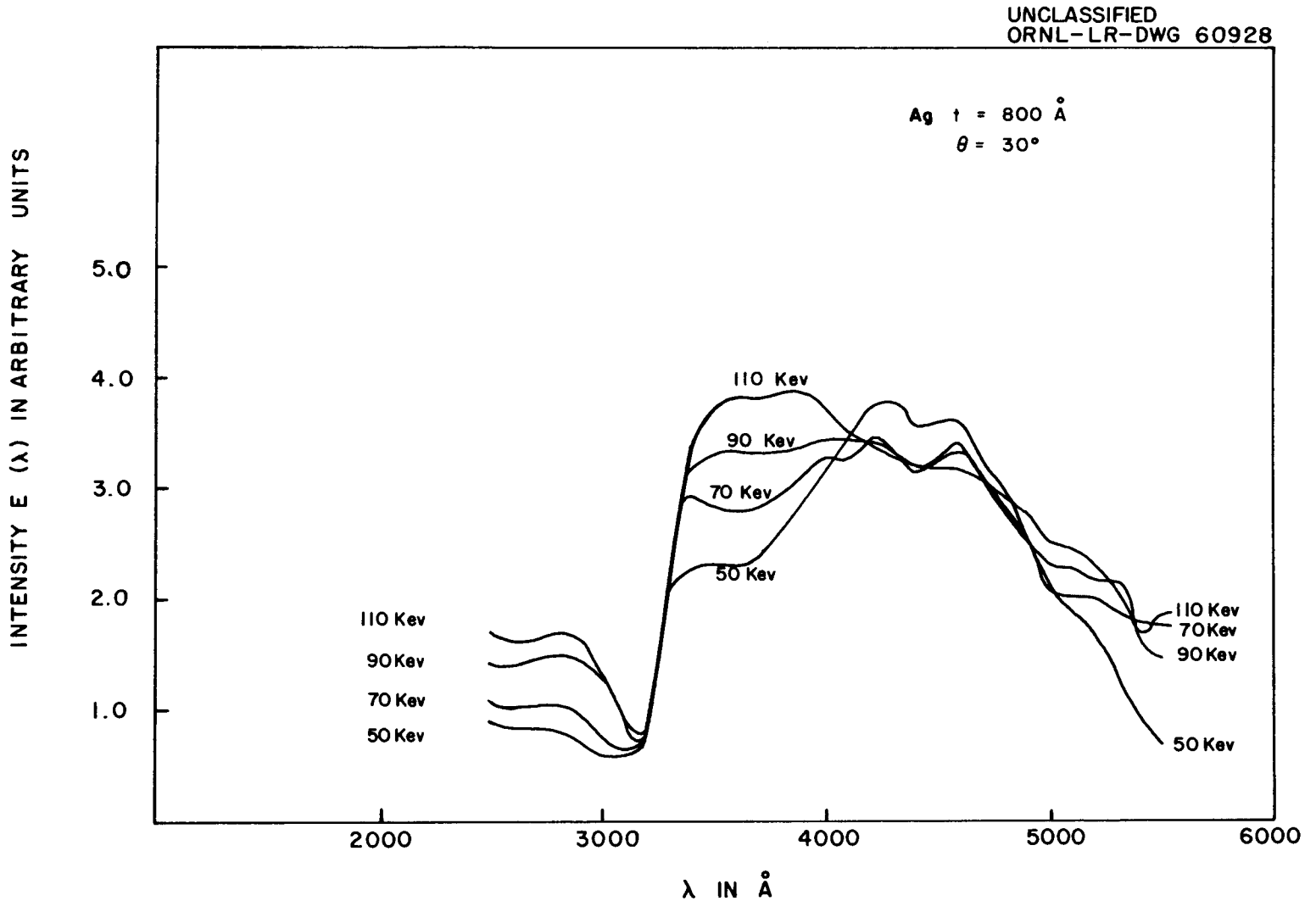

Figure 19. Spectral Distributions from Ag (t = 800 Å; θ = 30°; E = 50, 70, 90, 110 kev).

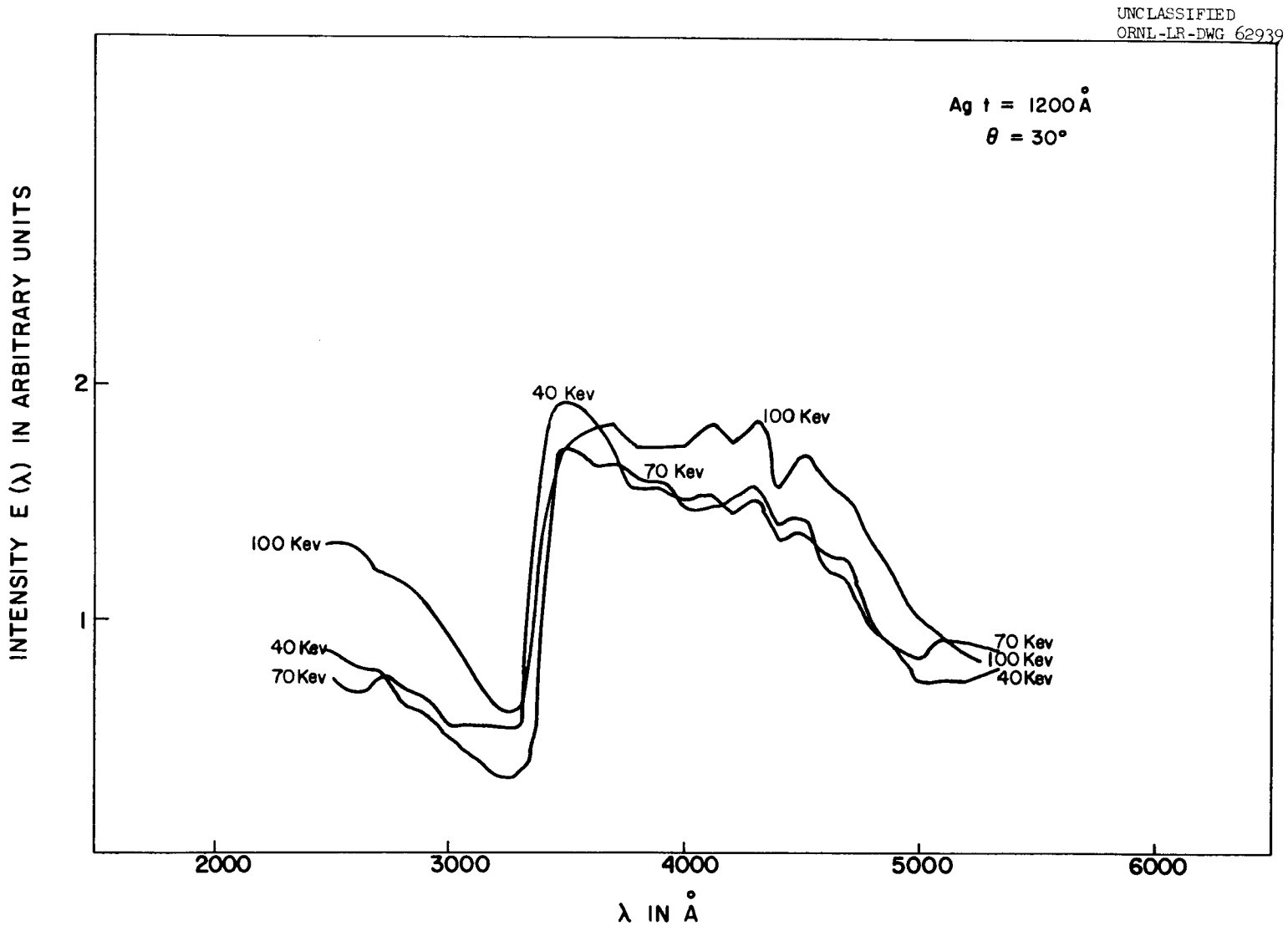

Figure 20. Spectral Distributions from Ag (t = 1200 Å; θ = 30°; E = 40, 70, 100 kev).

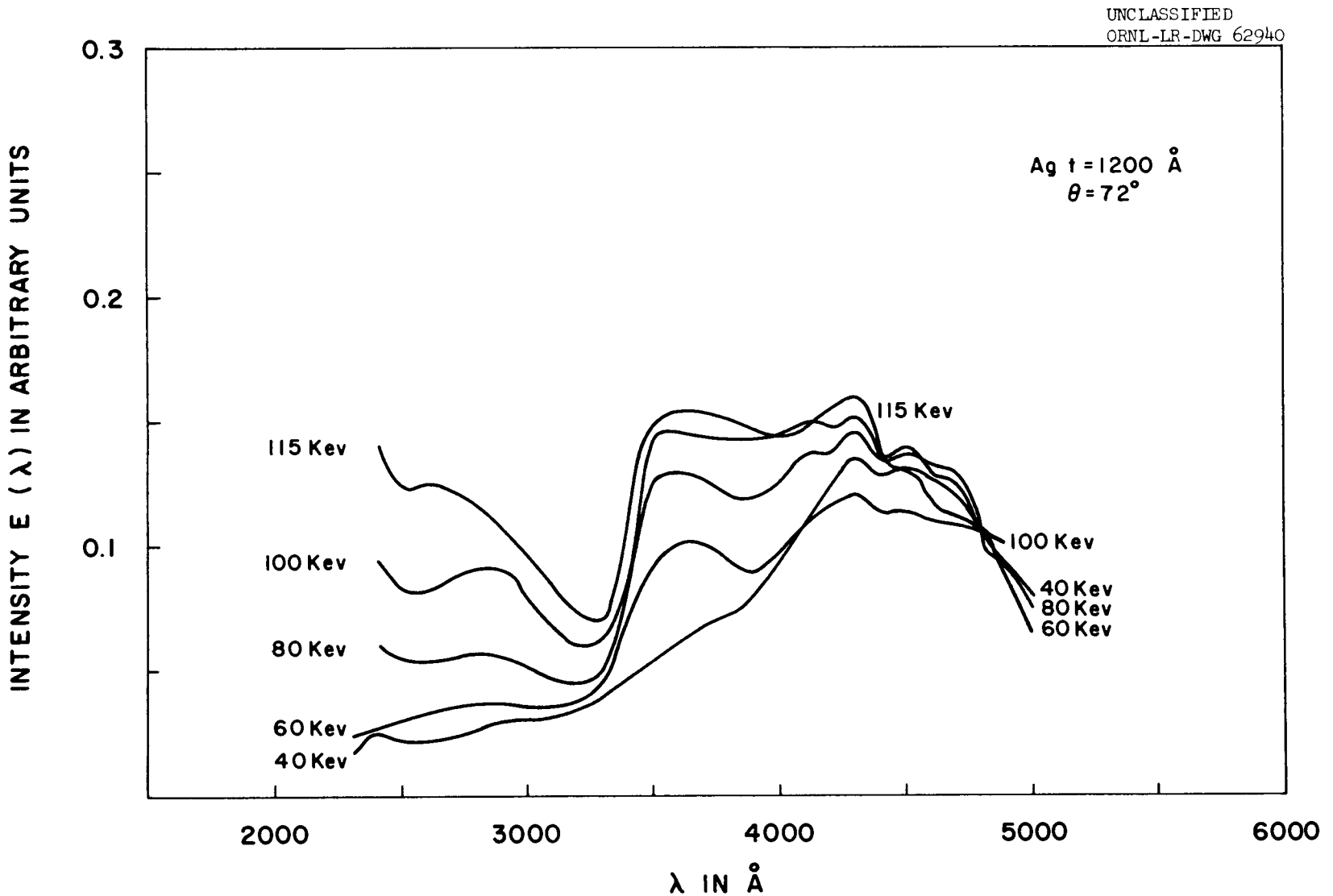

Figure 21. Spectral Distributions from Ag (t = 1200 Å; θ = 72°; E = 40, 60, 80, 100, 115 kev).

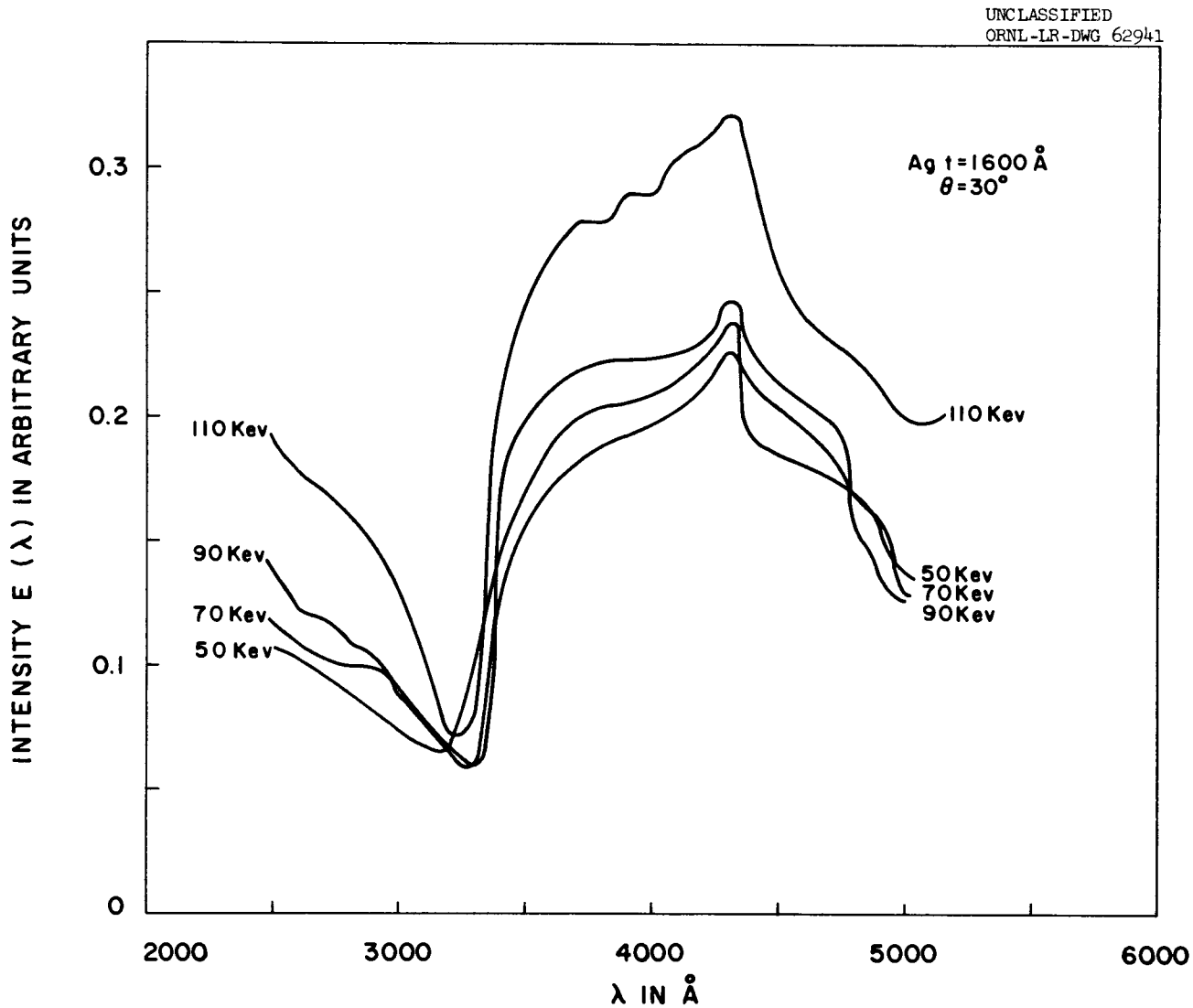

Figure 22. Spectral Distributions from Ag (t = 1600 Å; θ = 30°; E = 50, 70, 90, 110 kev).

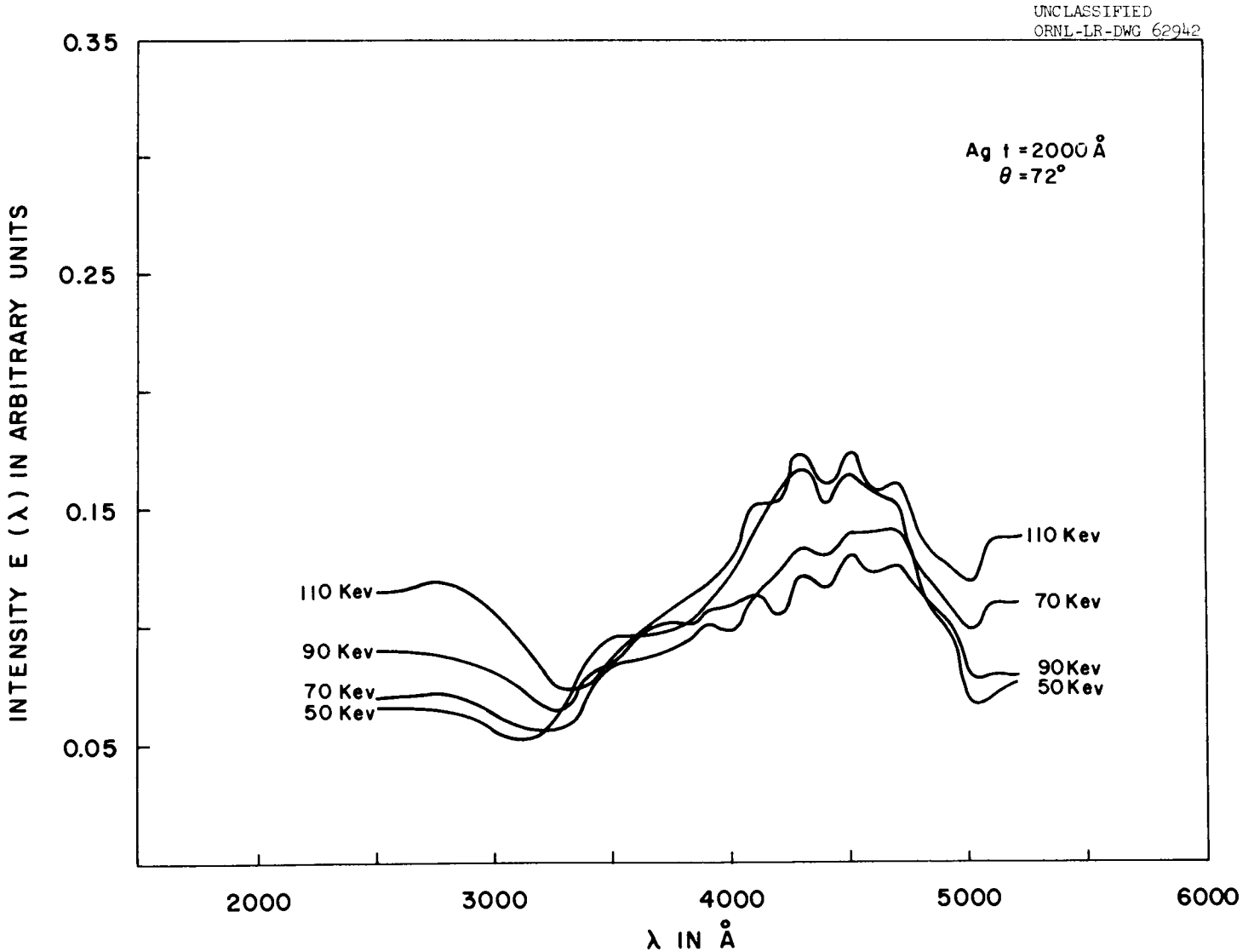

Figure 23. Spectral Distributions from Ag (t = 2000 Å; θ = 72°; E = 50, 70, 90, 110 kev).

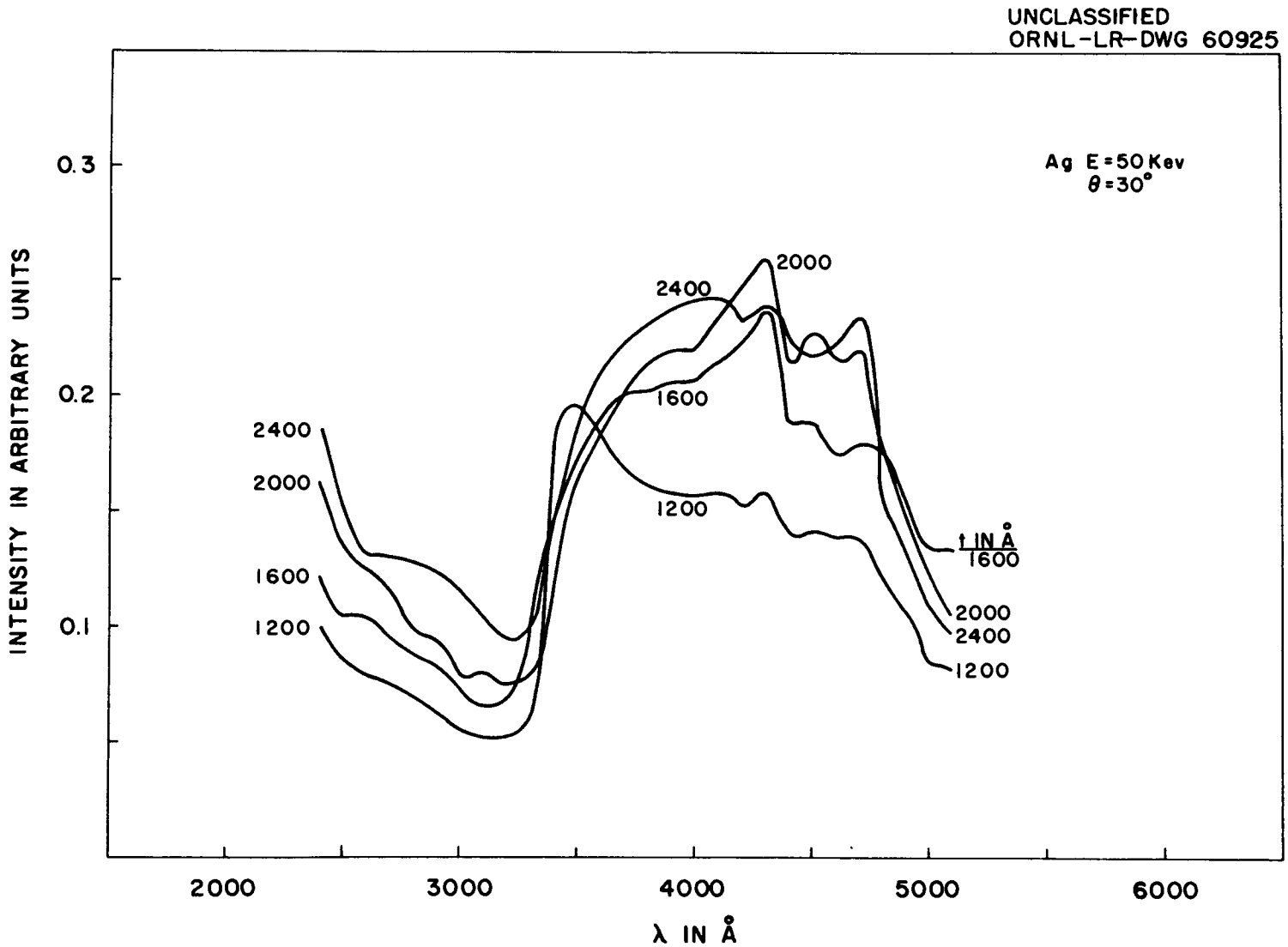

Figure 24. Spectral Distributions from Ag (t = 1200, 1600, 2000, 2400 Å; θ = 30°, E = 50 kev).

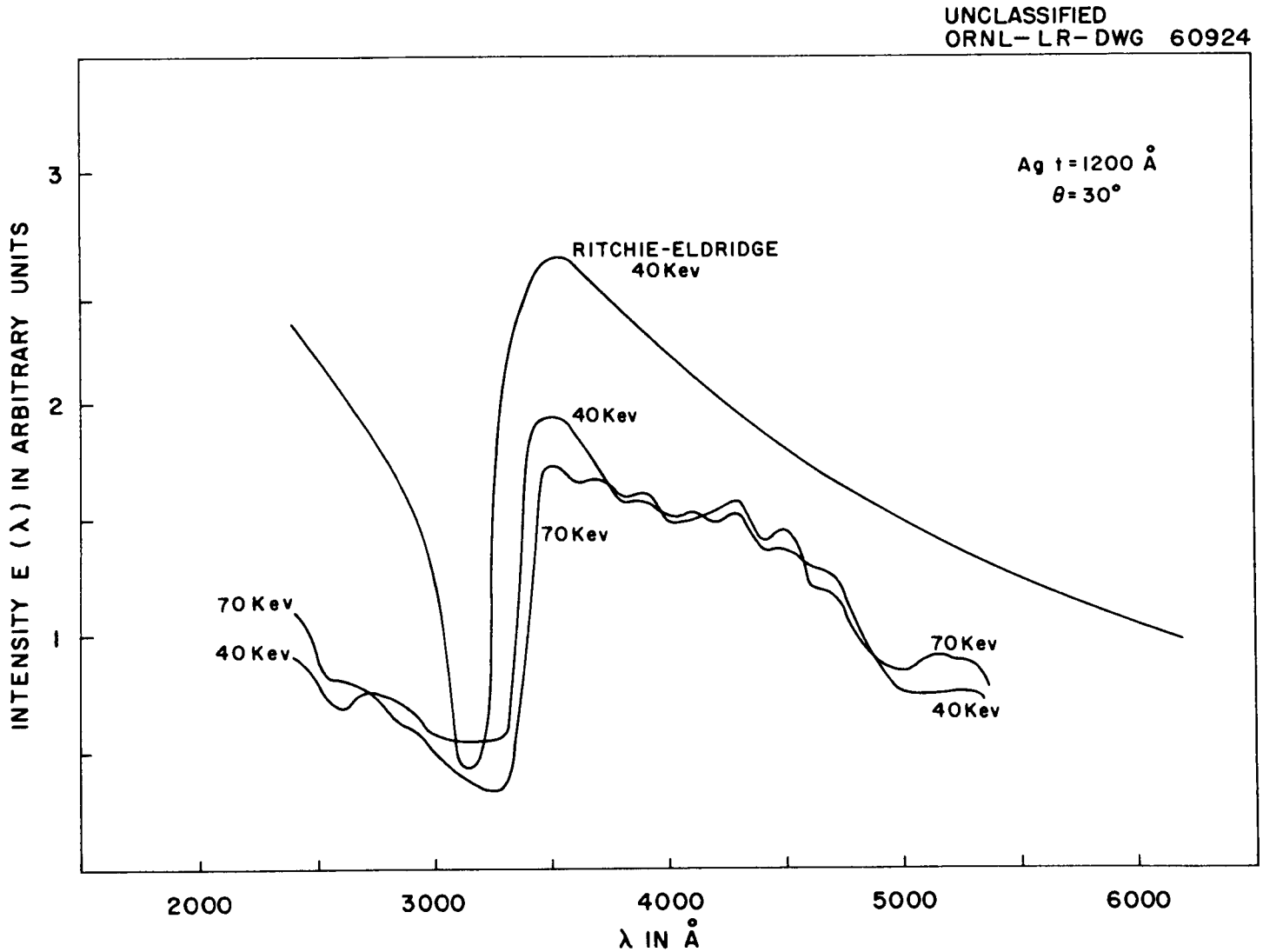

Figure 25. Spectral Distributions from Ag and the Ritchie-Eldridge Theory ($t = 1200$ Å; $\theta = 30^{\circ}$; $E = 40, 70$ kev).

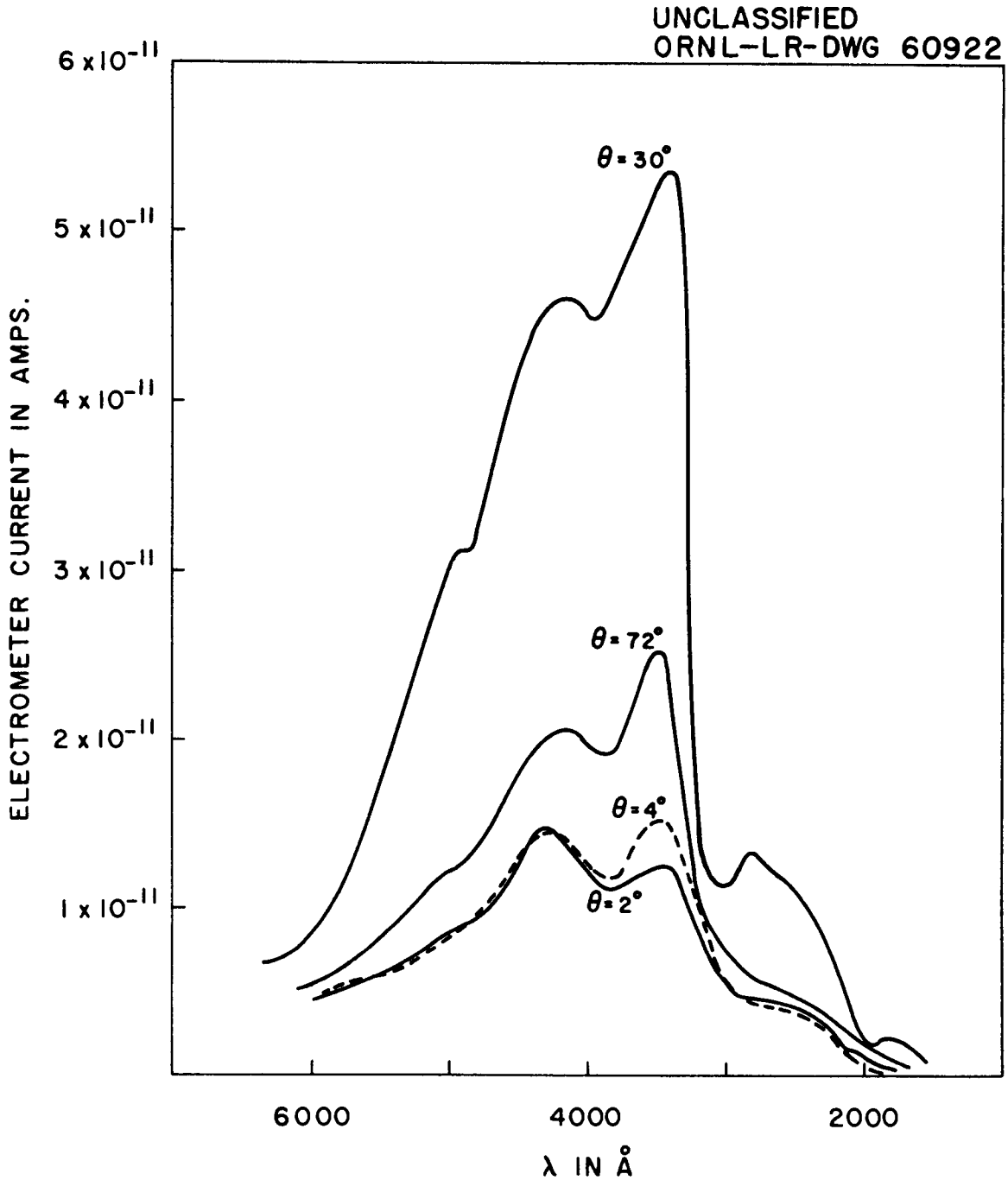

Figure 26. Uncorrected Spectral Distributions from Ag (θ = 2°, 4°, 30°, 72°).

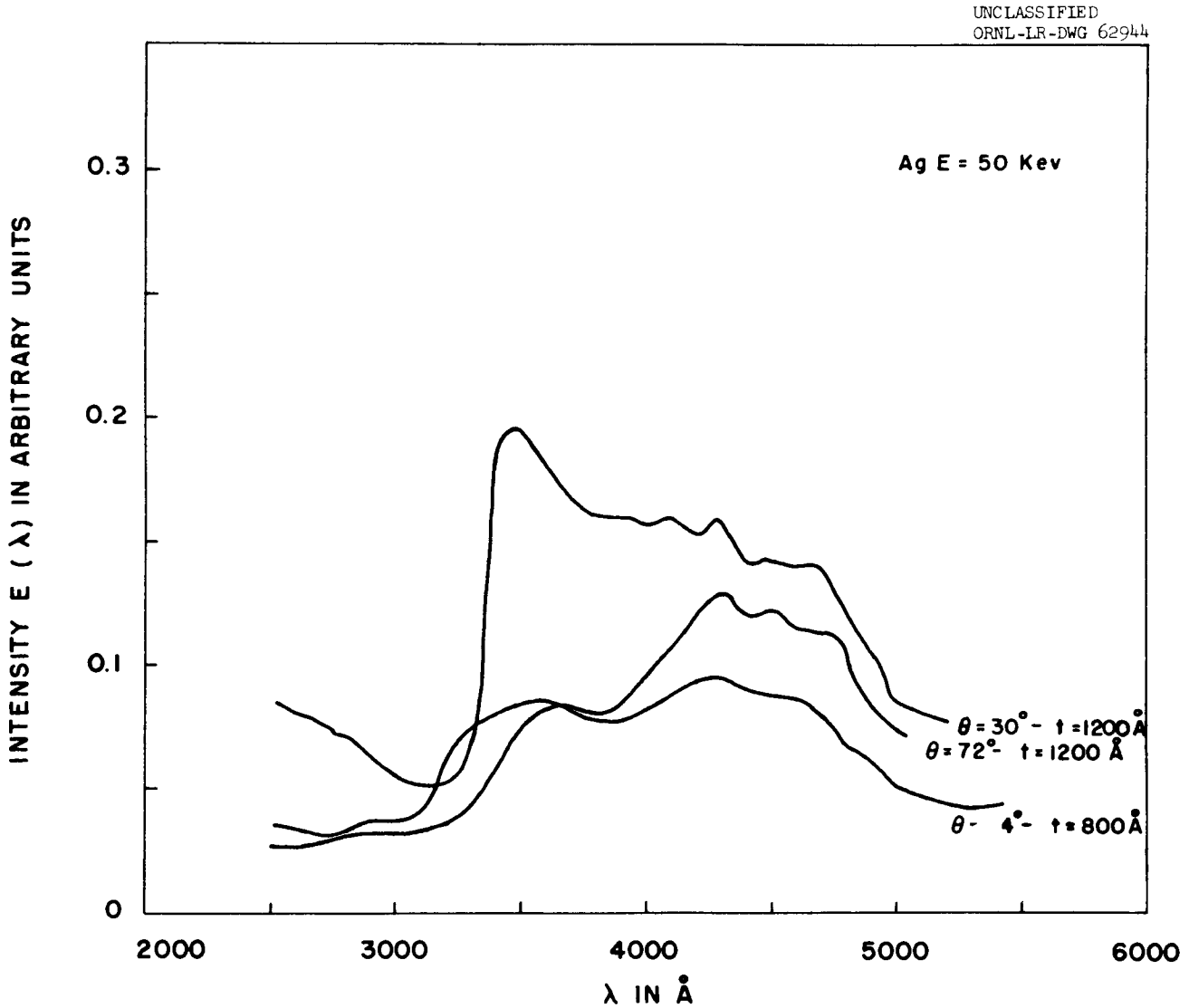

Figure 27. Spectral Distributions from Ag (t = 800, 1200 Å; θ = 4°, 30°, 72°; E = 50 kev).

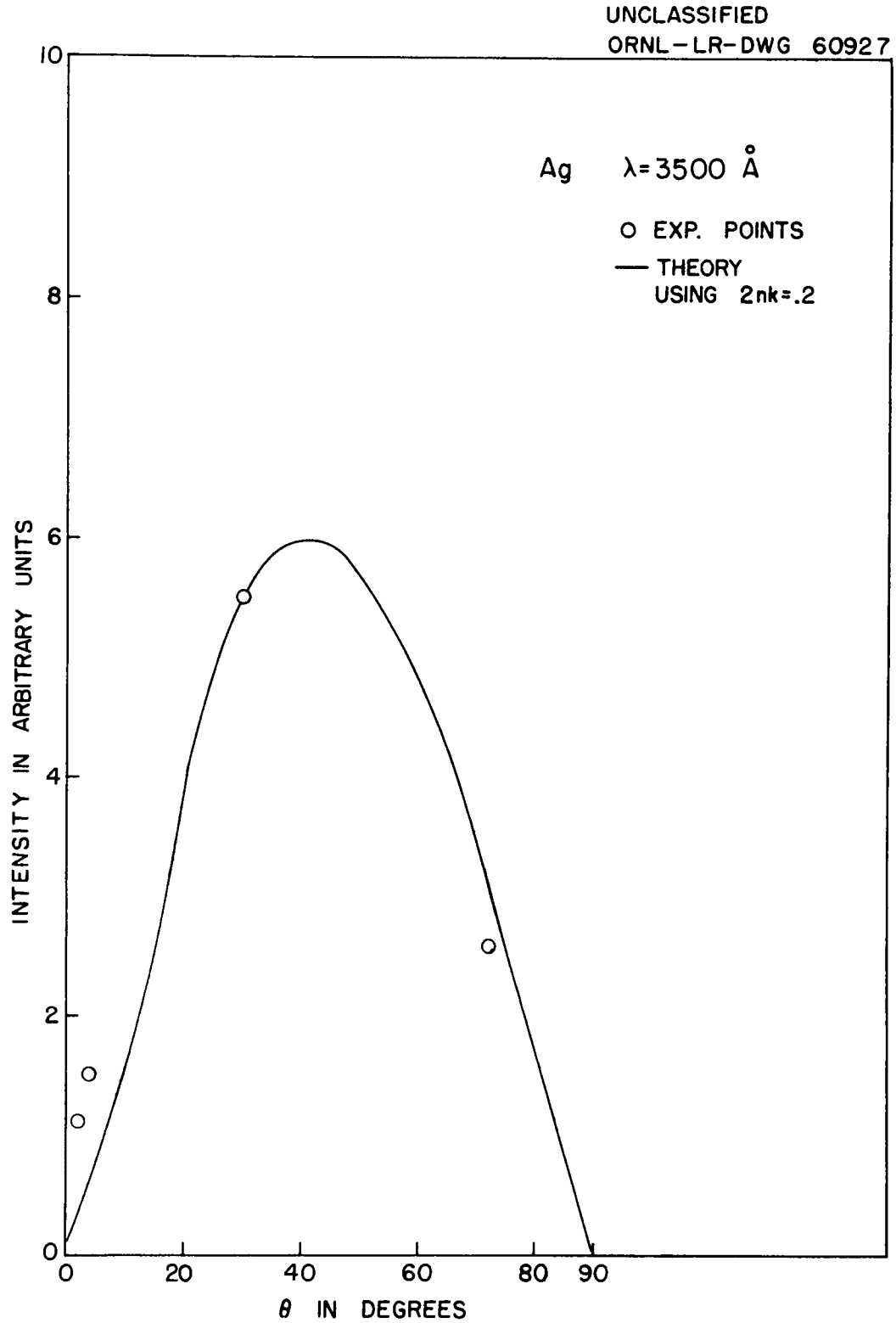

Figure 28. Theory and Experimental Points on the Angular Distribution from Ag (λ = 3500 Å; t = 800 Å).

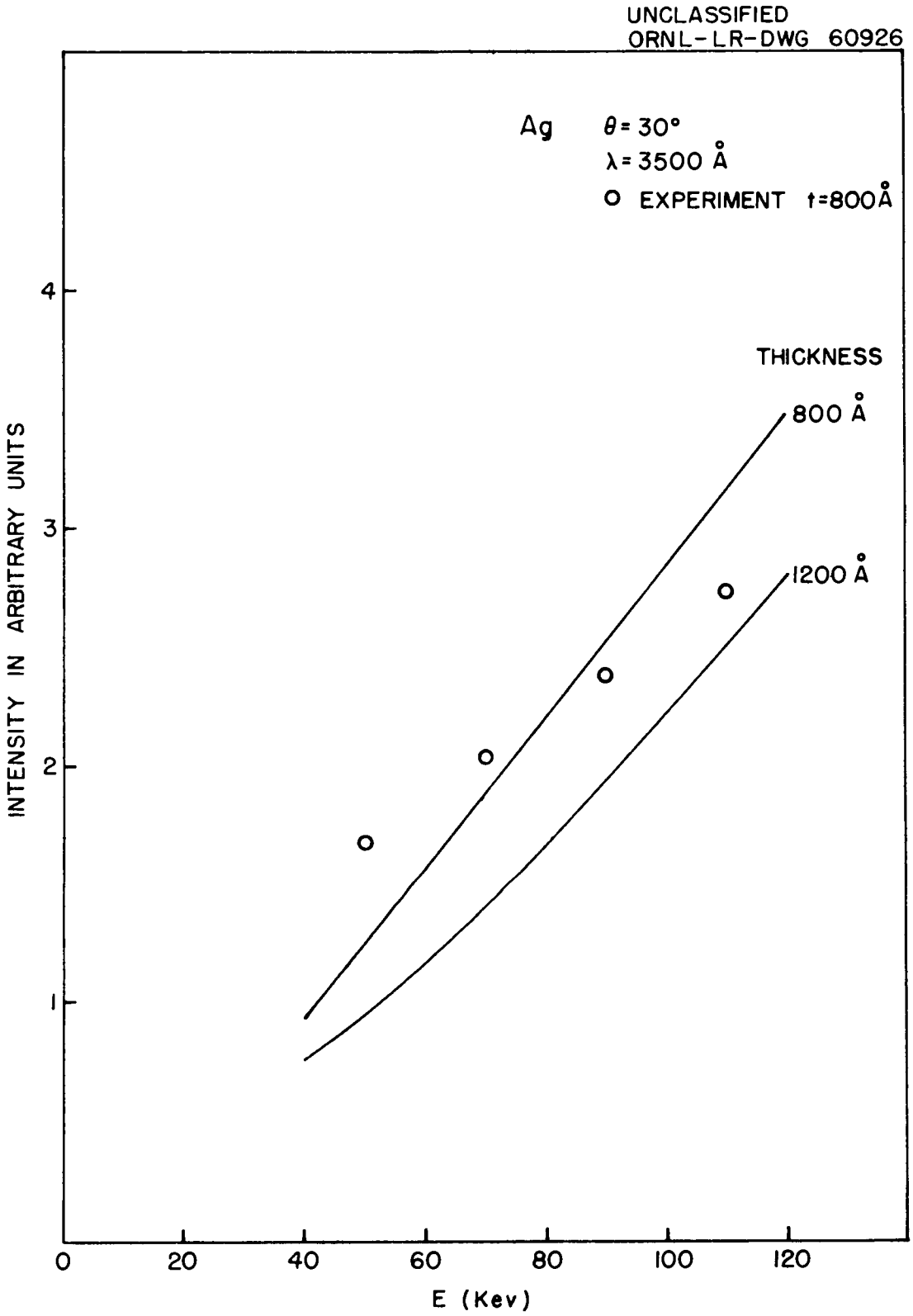

Figure 29. Light Intensities from Ag as a Function of Beam Energy and the Ritchie-Eldridge Theory (t = 800, 1200 Å; θ = 30°; λ = 3500 Å).

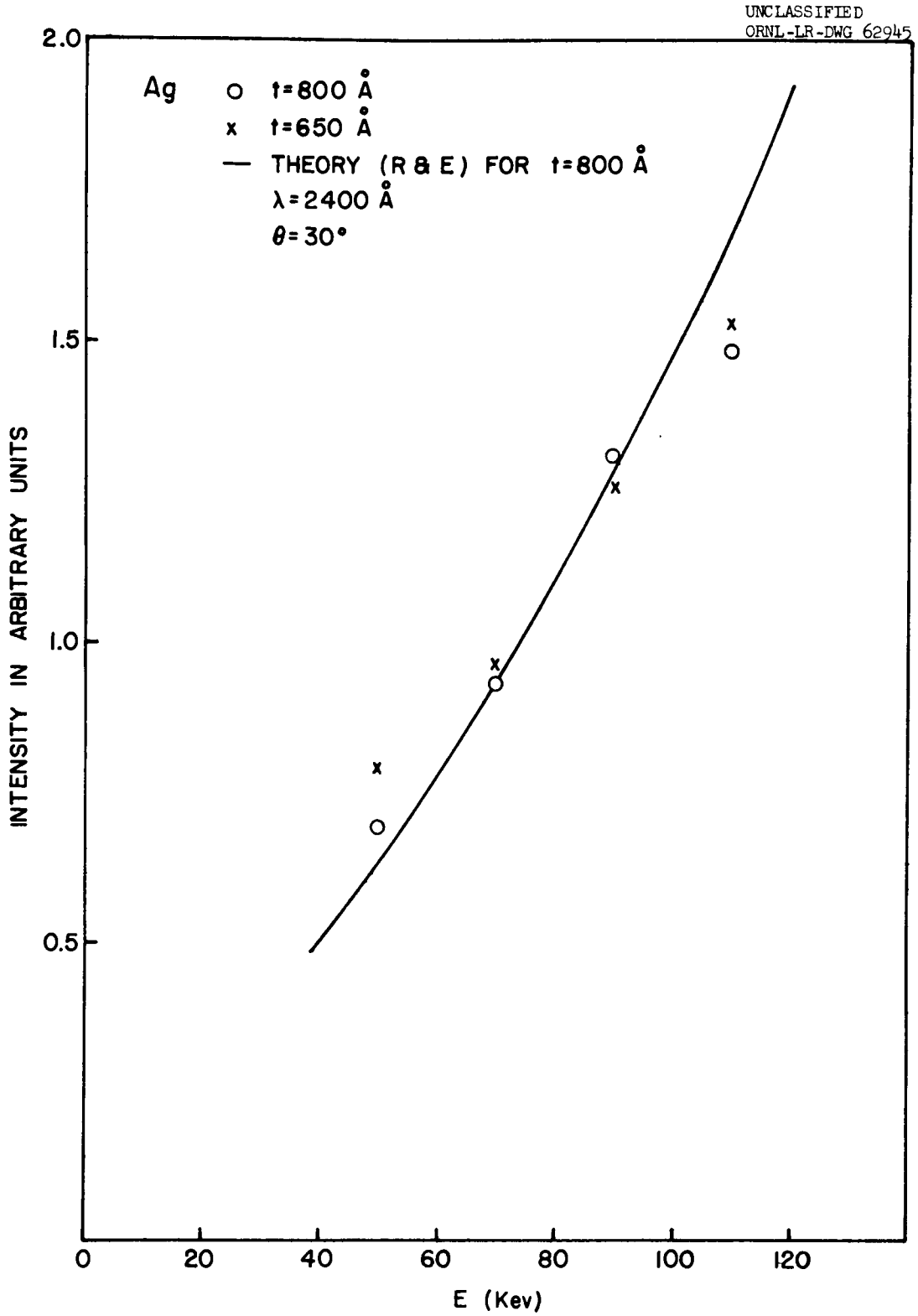

Figure 30. Light Intensities from Ag as a Function of Beam Energy and The Ritchie-Eldridge Theory (t = 650, 800 Å; $\theta = 30^{\circ}$; λ = 2400 Å).

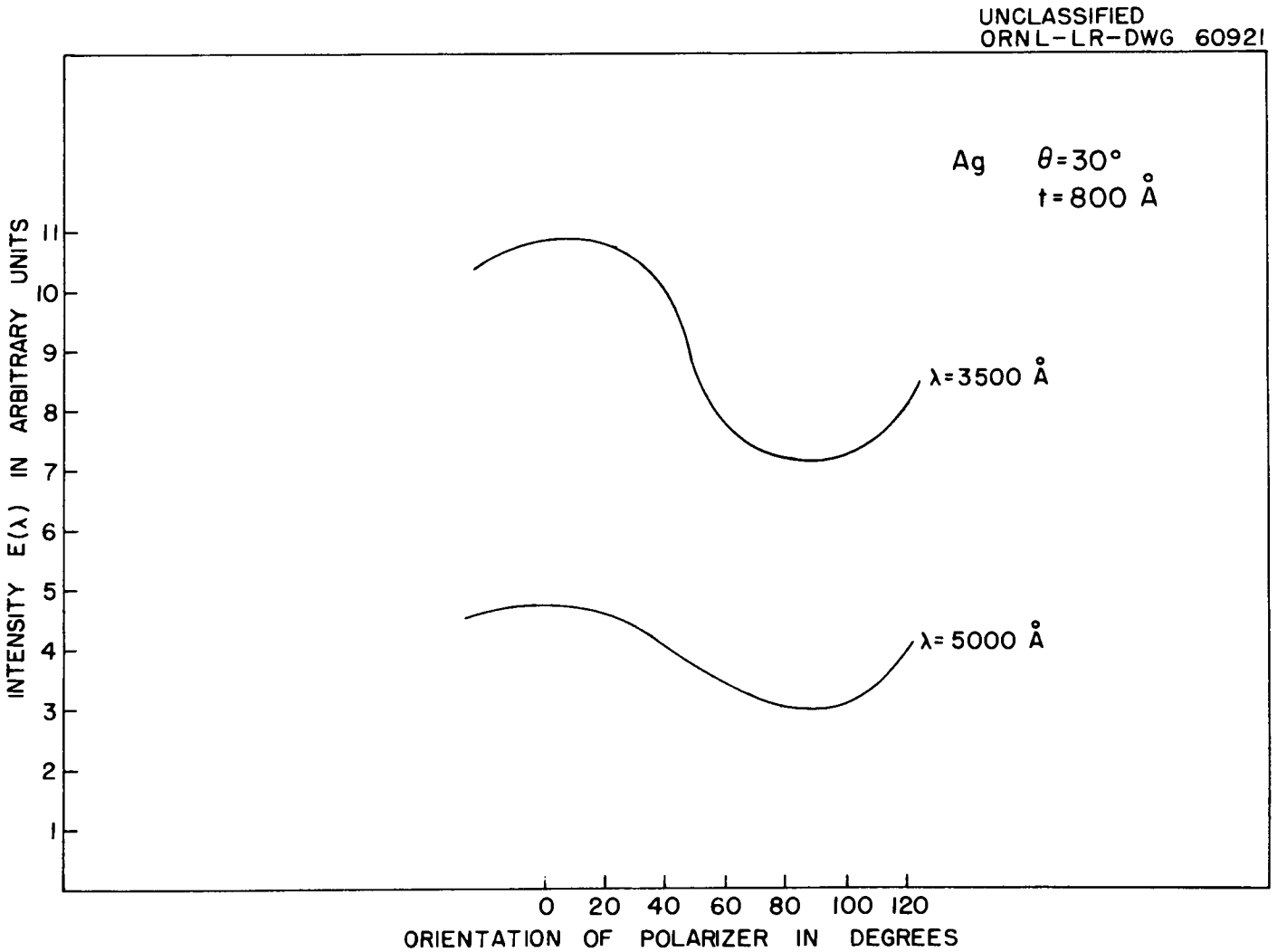

Figure 31. Light Intensities as a Function of Polarizer Angle for Al ($t = 800$ Å; $\theta = 30^{\circ}$; $\lambda = 3500, 5000$ Å).

This seems to show that transition radiation is at least a sizeable part of the light detected since bremsstrahlung is polarized principally perpendicularly to the plane of incidence.

The spectral distribution for aluminum agrees with the theoretical predictions in a general way in that there seems to be a general decrease in intensity with increasing wave length. It should also be emphasized that the experimental apparatus used did not permit investigation of the 800 - 1000 Å region where the plasma peak was expected to occur. One minor difference was that a broad band is seen with its maximum at approximately 4400 Å in Figures 32 through 36. This maximum has the greatest intensity for the thicker foils. Although the data has been corrected for instrumental response, the sharp peaks seen in the spectral distribution curves are probably not real because they seem to occur for metals other than Al; i.e., they are probably spurious reflections (ghosts) from the grating. A smoothed out spectral distribution for four foil thicknesses under identical conditions is shown by Figure 37. It should be noted also that a broad band exists in the silver foil measurements which is similar to that in aluminum. This band in silver may be partially obscured by the presence of the peak at ~ 3500 Å.

The dependence of intensity on foil thickness and electron energy is shown in Figures 38 and 39. The observation that the only curve in Figure 38 which extrapolates to zero is the one based on measurements with the polarizer tends to give support to the idea that bremsstrahlung added significantly to the light at the lower beam energies. A polarizer would cut out the larger part of the bremsstrahlung while transmitting most of the polarized transition radiation. The absolute photon yield of the aluminum foils determined experimentally agrees very well with theoretical

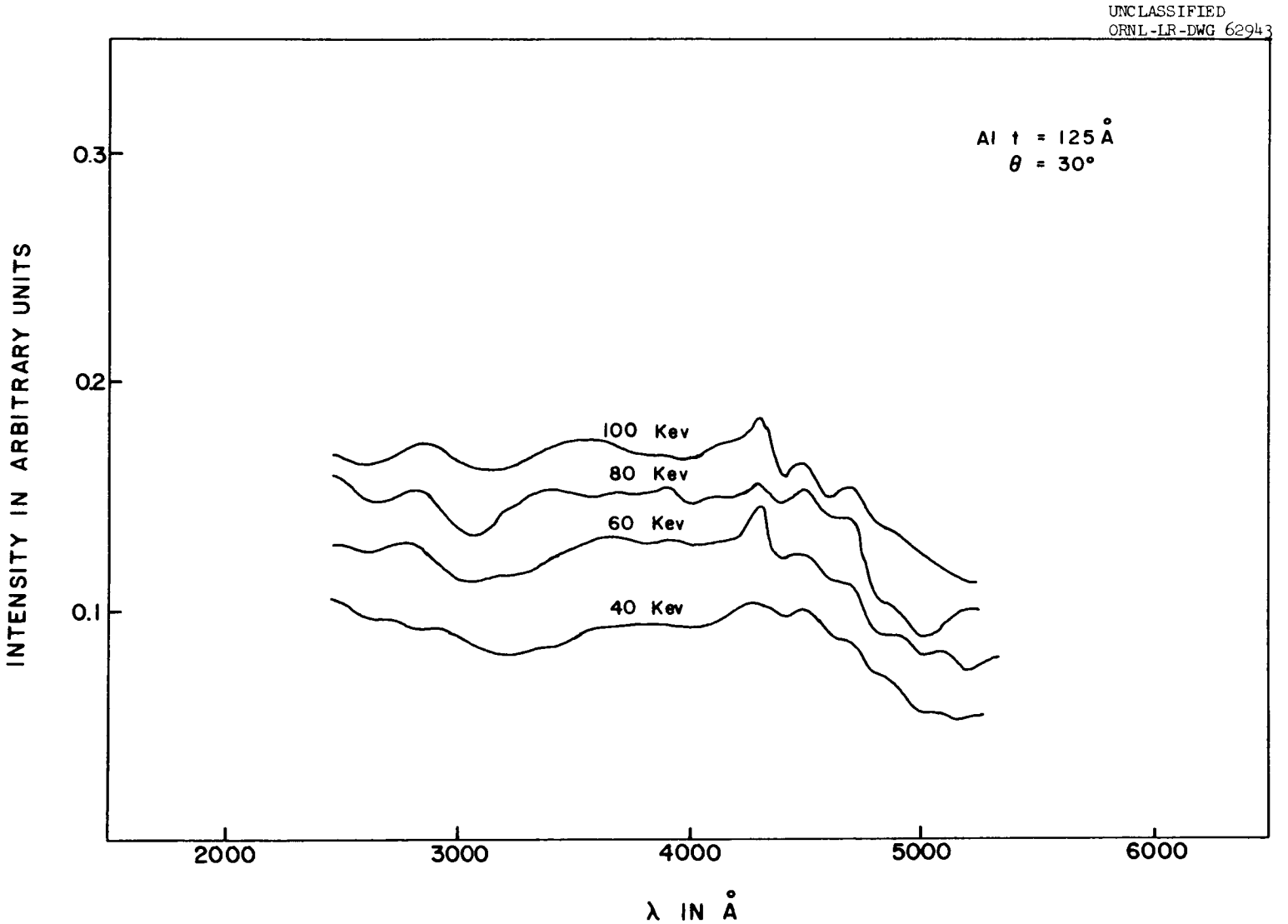

Figure 32. Spectral Distributions from Al ($t = 125$ Å; $\theta = 30^{\circ}$; E = 40, 60, 80, 100 kev).

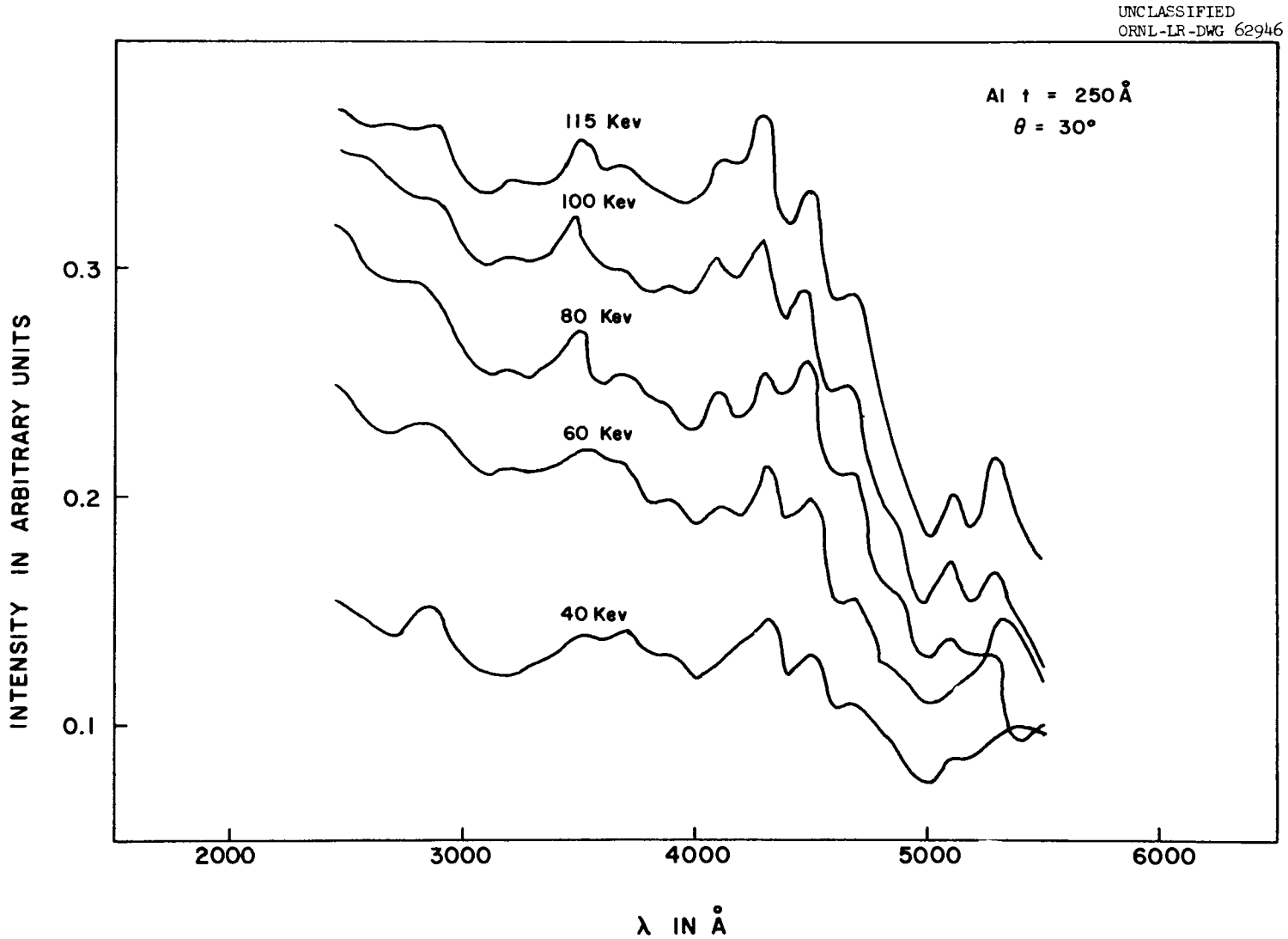

Figure 33. Spectral Distributions from Al (t = 250 Å; θ = 30°; E = 40, 60, 80, 100, 115 kev).

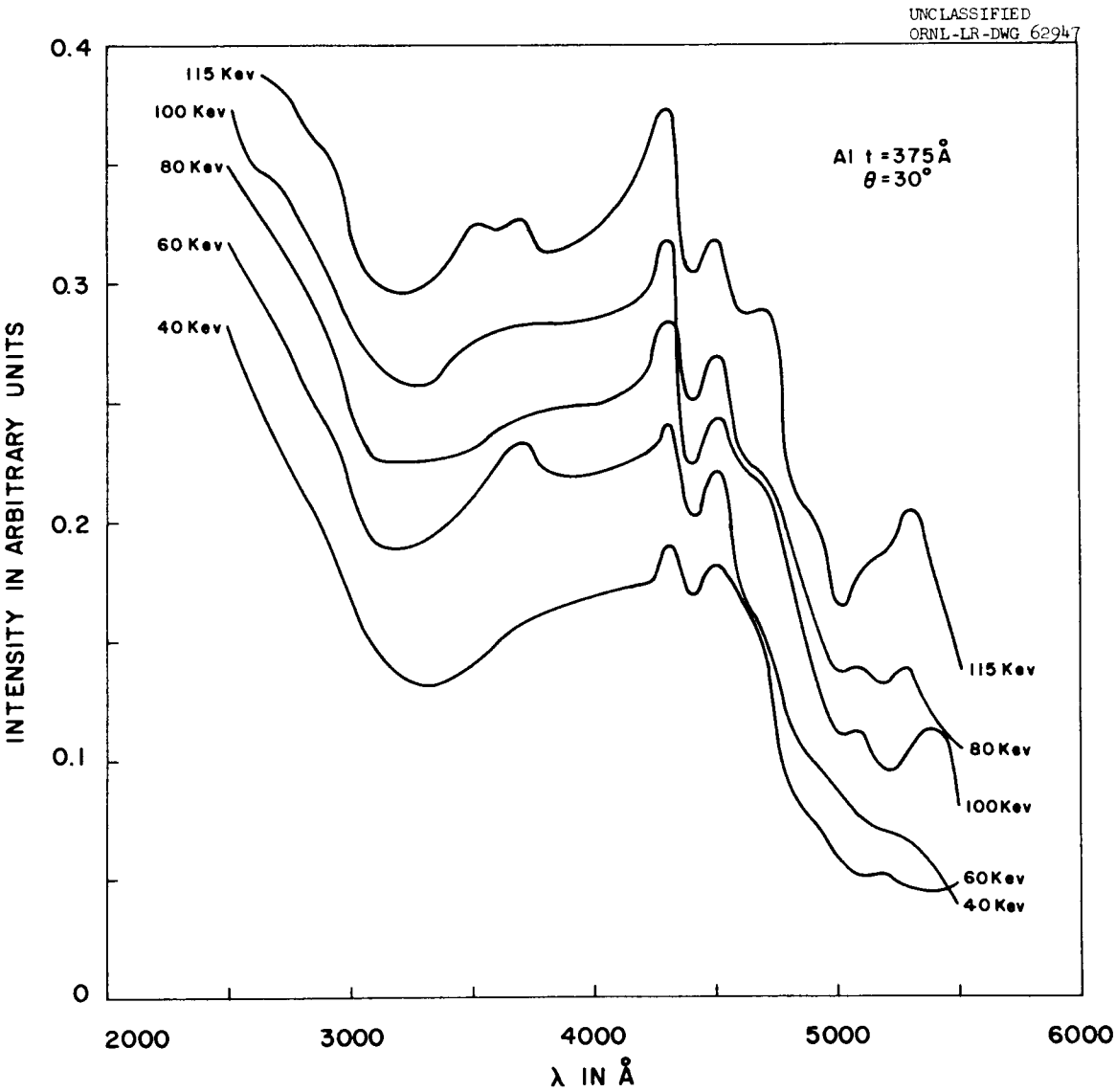

Figure 34. Spectral Distributions from Al (t = 375 Å; θ = 30°; E = 40, 60, 80, 100, 115 kev).

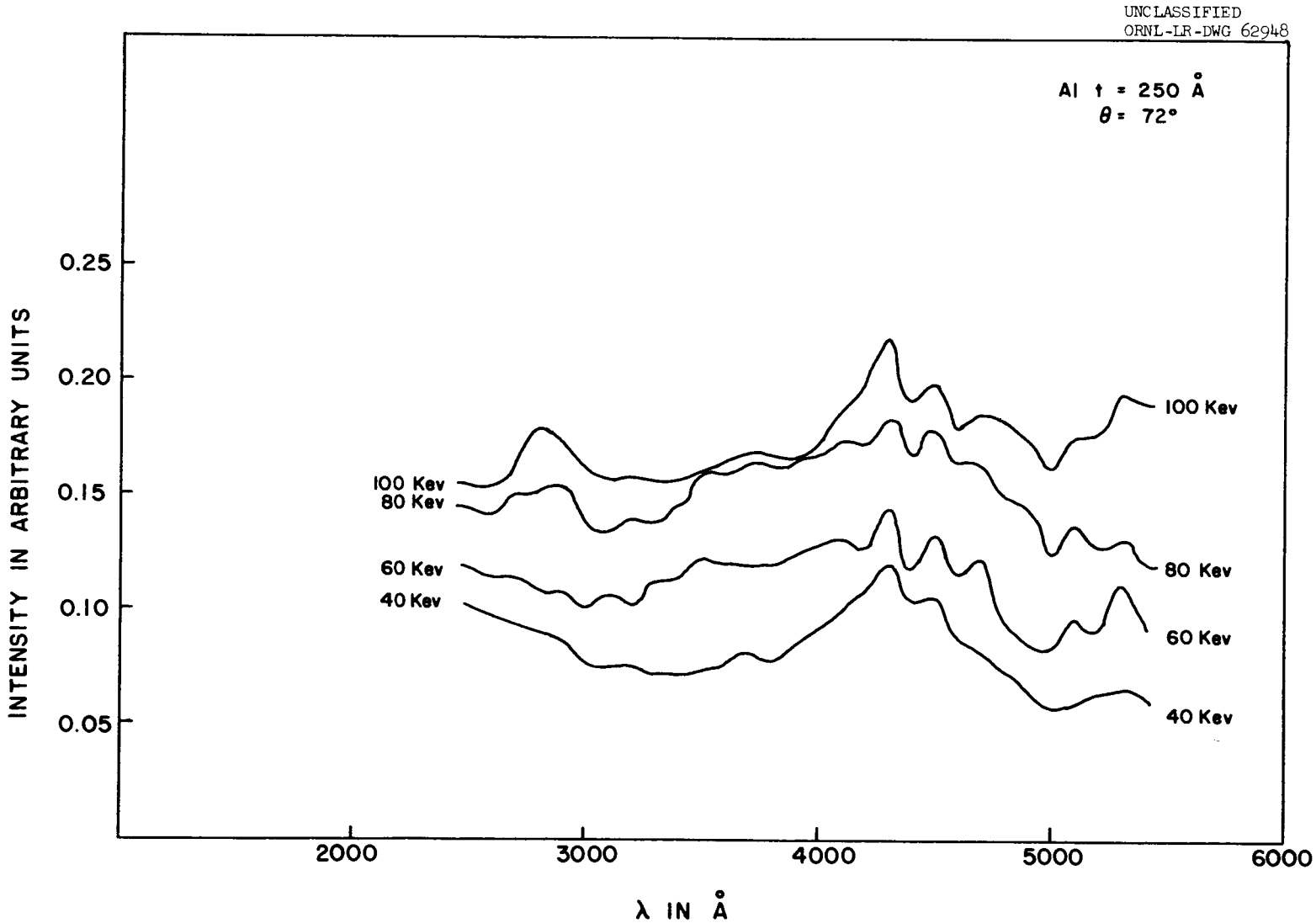

Figure 35. Spectral Distributions from Al (t = 250 Å; θ = 72°; E = 40, 60, 80, 100 kev).

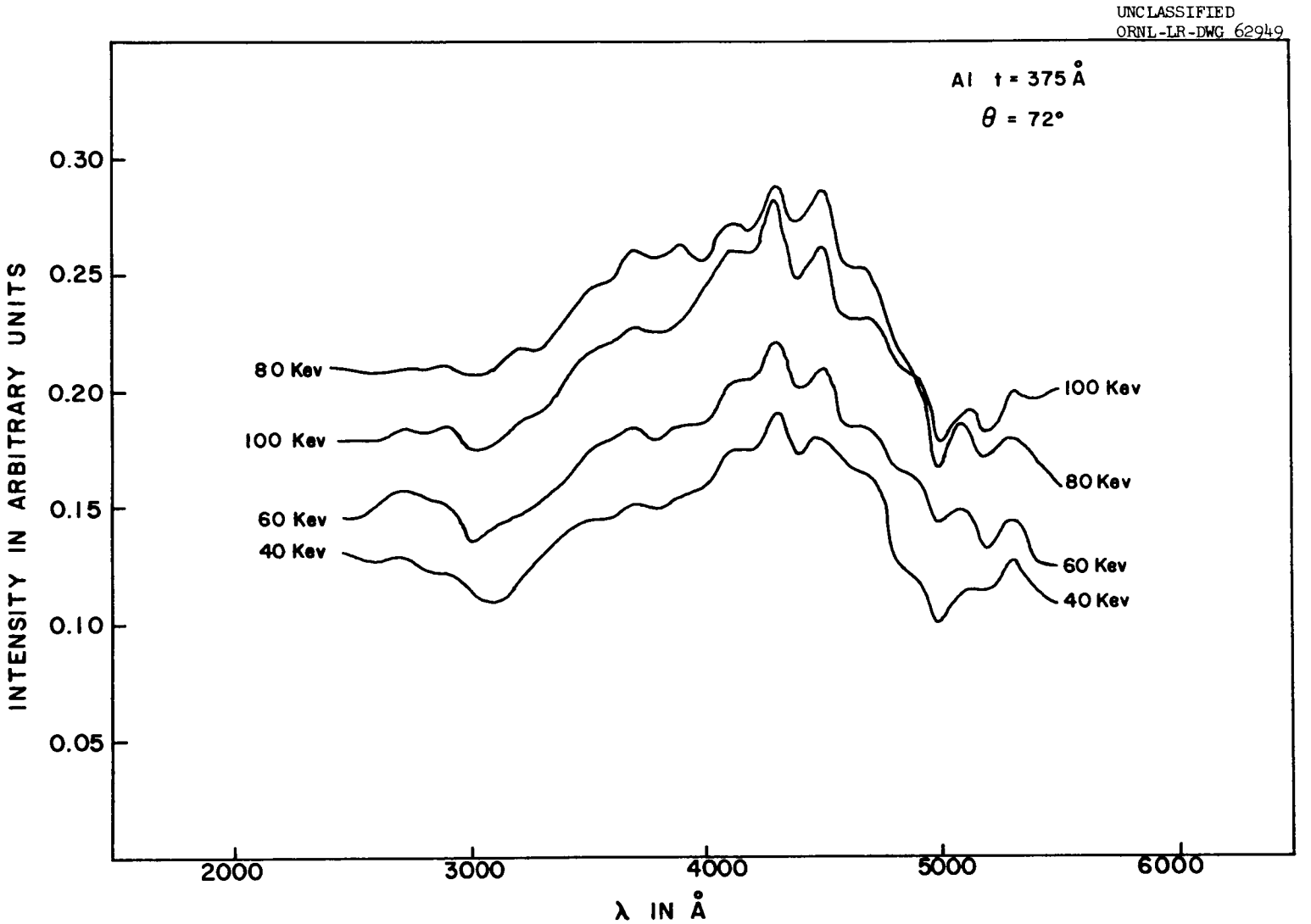

Figure 36. Spectral Distributions from Al (t = 375 Å; θ = 72°; E = 40, 60, 80, 100 kev).

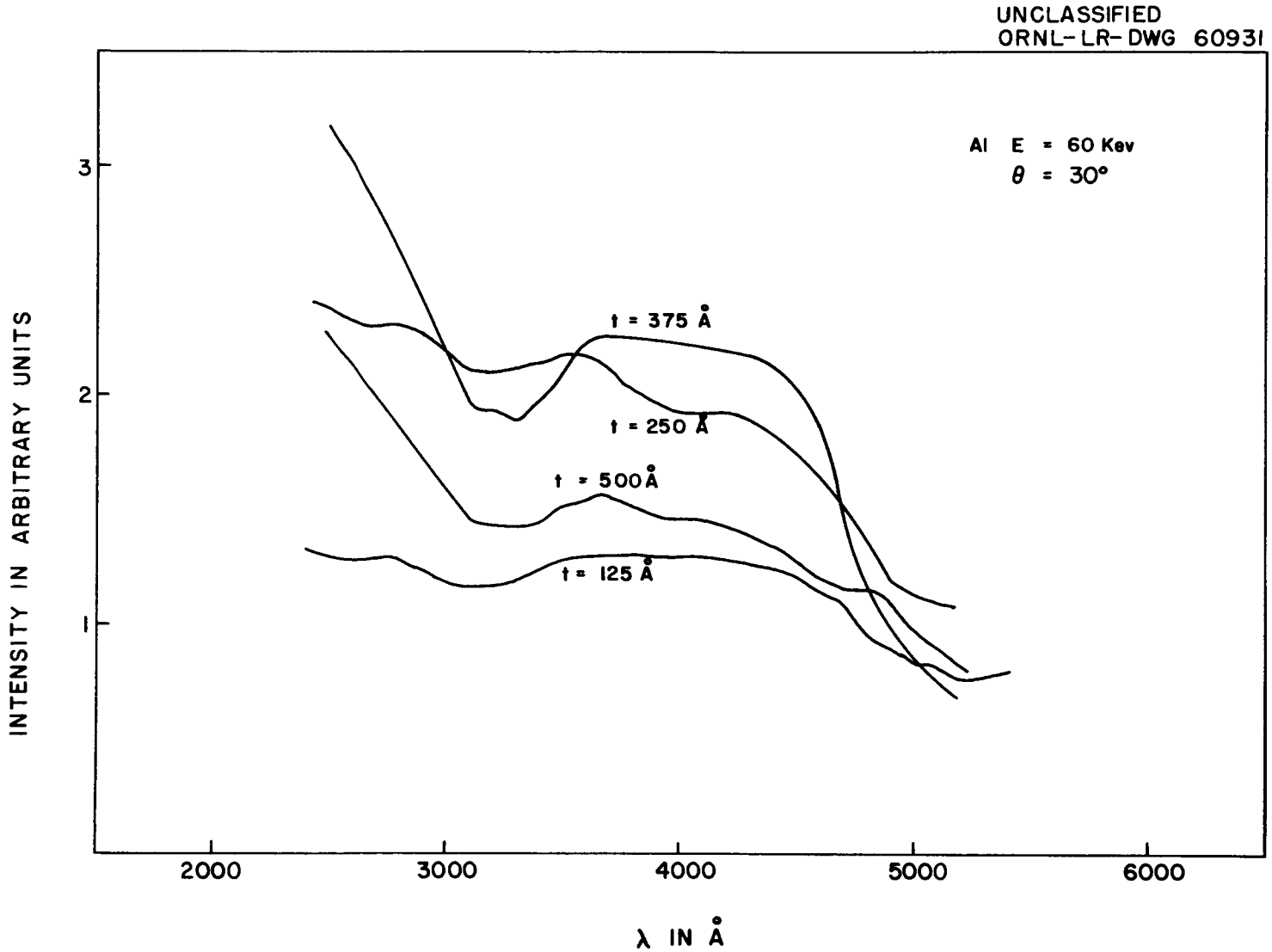

Figure 37. Spectral Distributions from Al (t = 125, 250, 375, 500 Å; E = 60 kev).

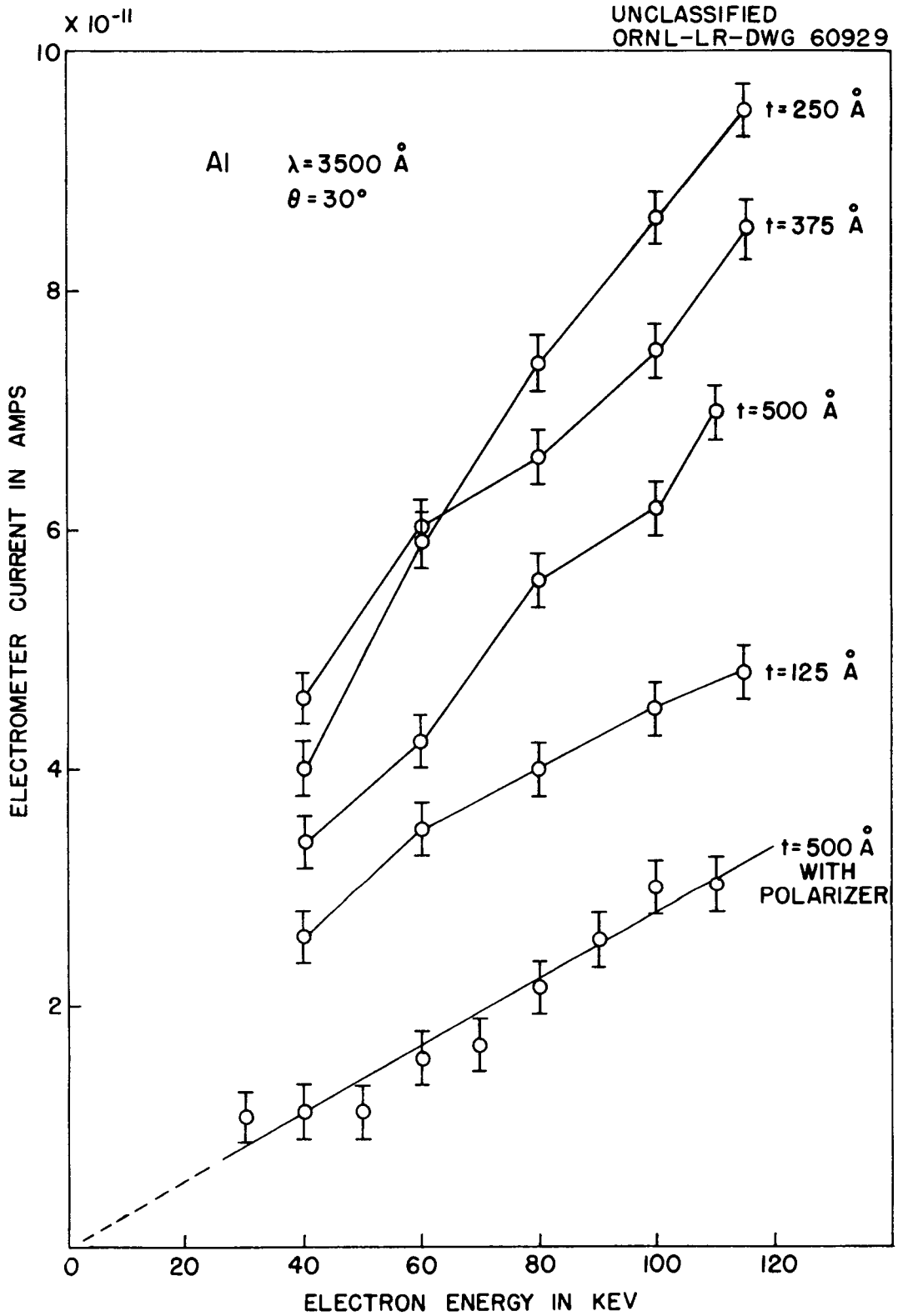

Figure 38. Photomultiplier Currents as a Function of Beam Energy for Al (t = 125, 250, 375, 500 Å; λ = 3500 Å).

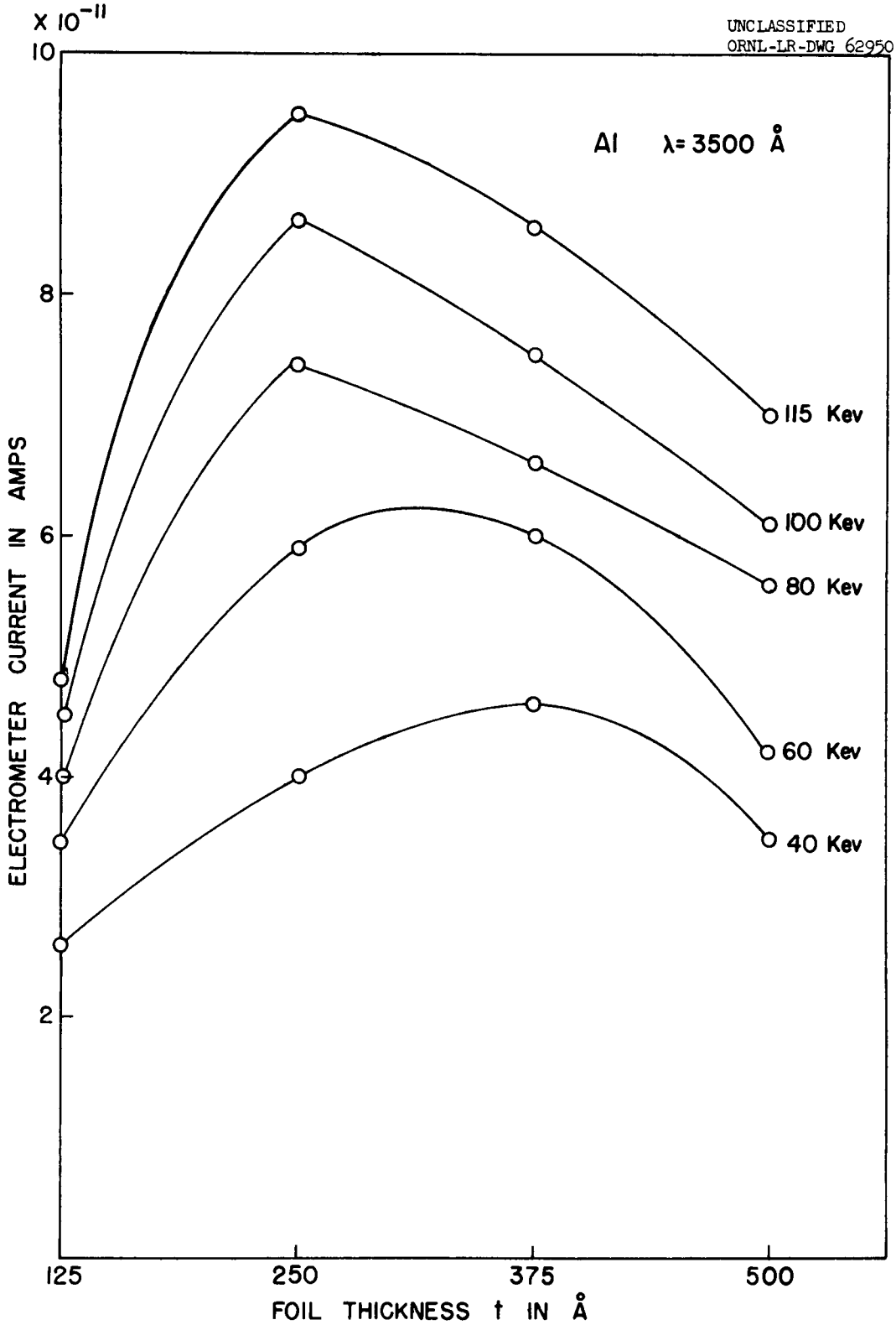

Figure 39. Electrometer Currents as a Function of Foil Thickness for Al (λ = 3500 Å; E = 40, 60, 80, 100, 115 kev).

predictions as seen in Figure 40. The experimental values were based on photocathode efficiency and photomultiplier gain as furnished by the manufacturer, a calculated solid angle for the grating, and a 30% grating efficiency.

The spectrum from aluminum proved to be more highly polarized in the plane of incidence than that from silver as shown by Figure 41. This would be expected if the component polarized out of the plane of incidence were bremsstrahlung whose intensity varies as Z^2.

In addition to foils of silver and aluminum, a thin gold foil was irradiated also. A comparison of the spectral distributions of thin silver, aluminum, and gold foils is given by Figure 42 for E = 60 kev and $\theta = 30^{\circ}$.

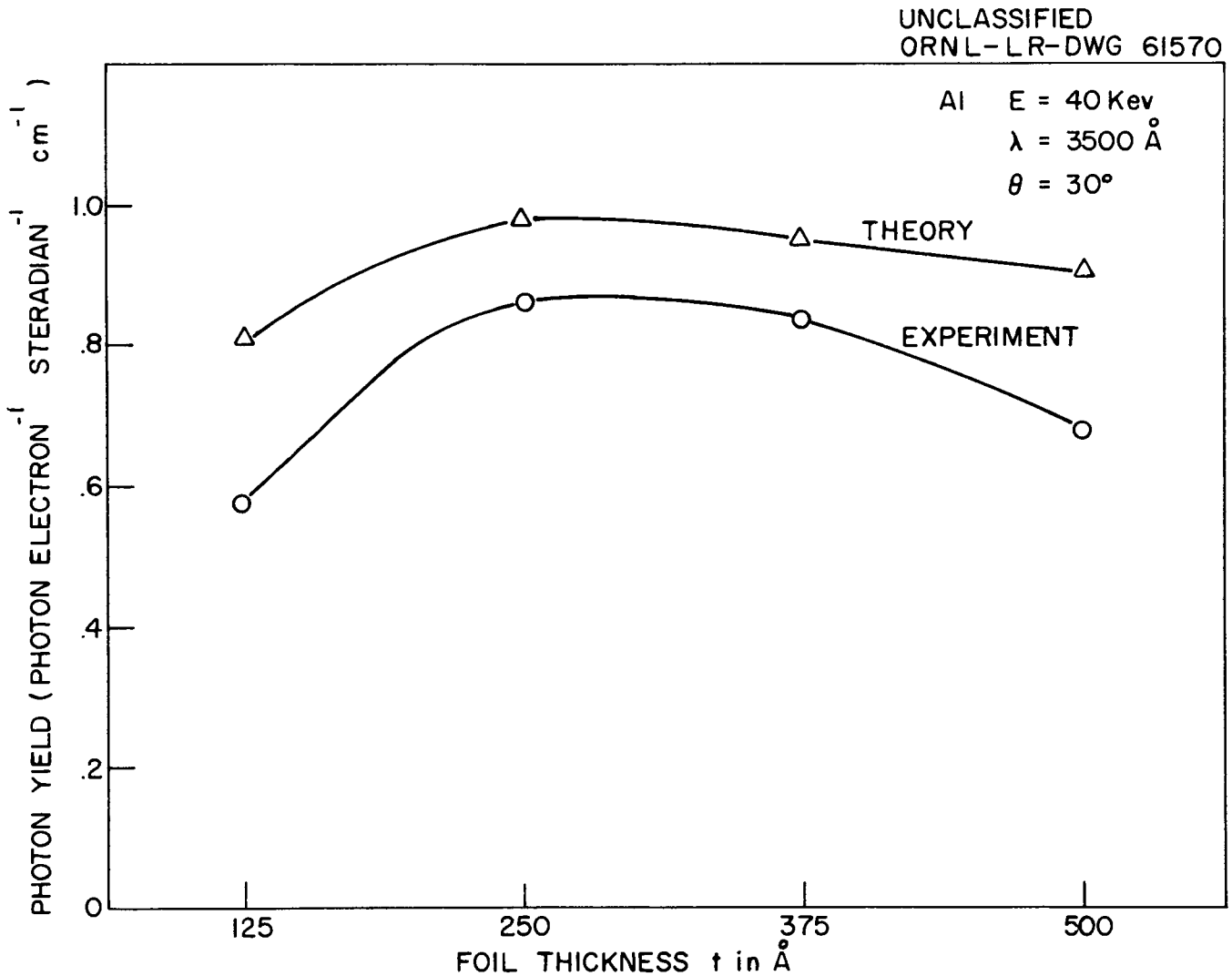

Figure 40. Photon Yield as a Function of Foil Thickness for Al and the Ritchie-Eldridge Theory (E = 40 kev).

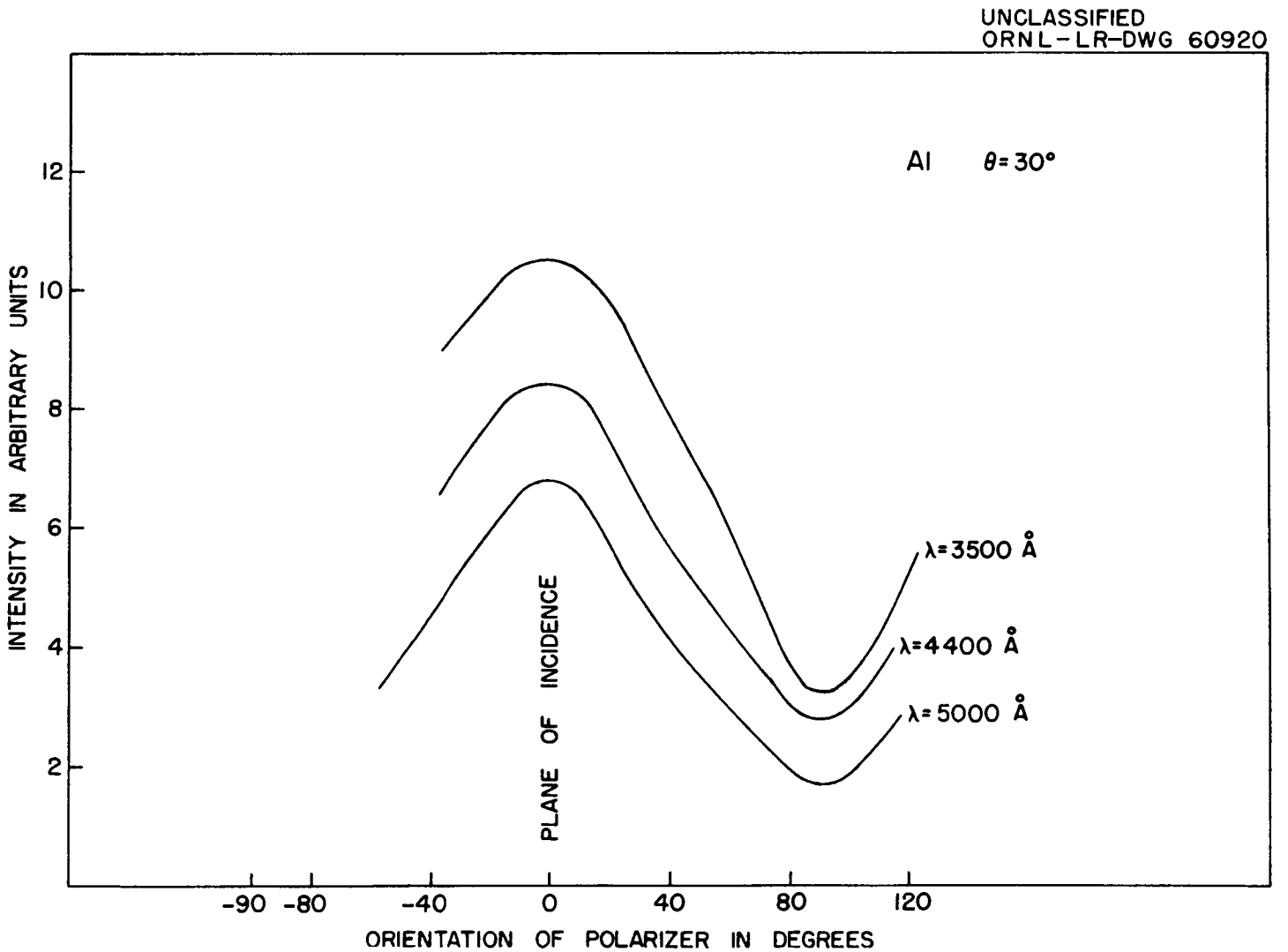

Figure 41. Light Intensities as a Function of Polarizer Angle for Al ($\theta = 30^{\circ}$, λ = 3500, 4400, 5000 Å).

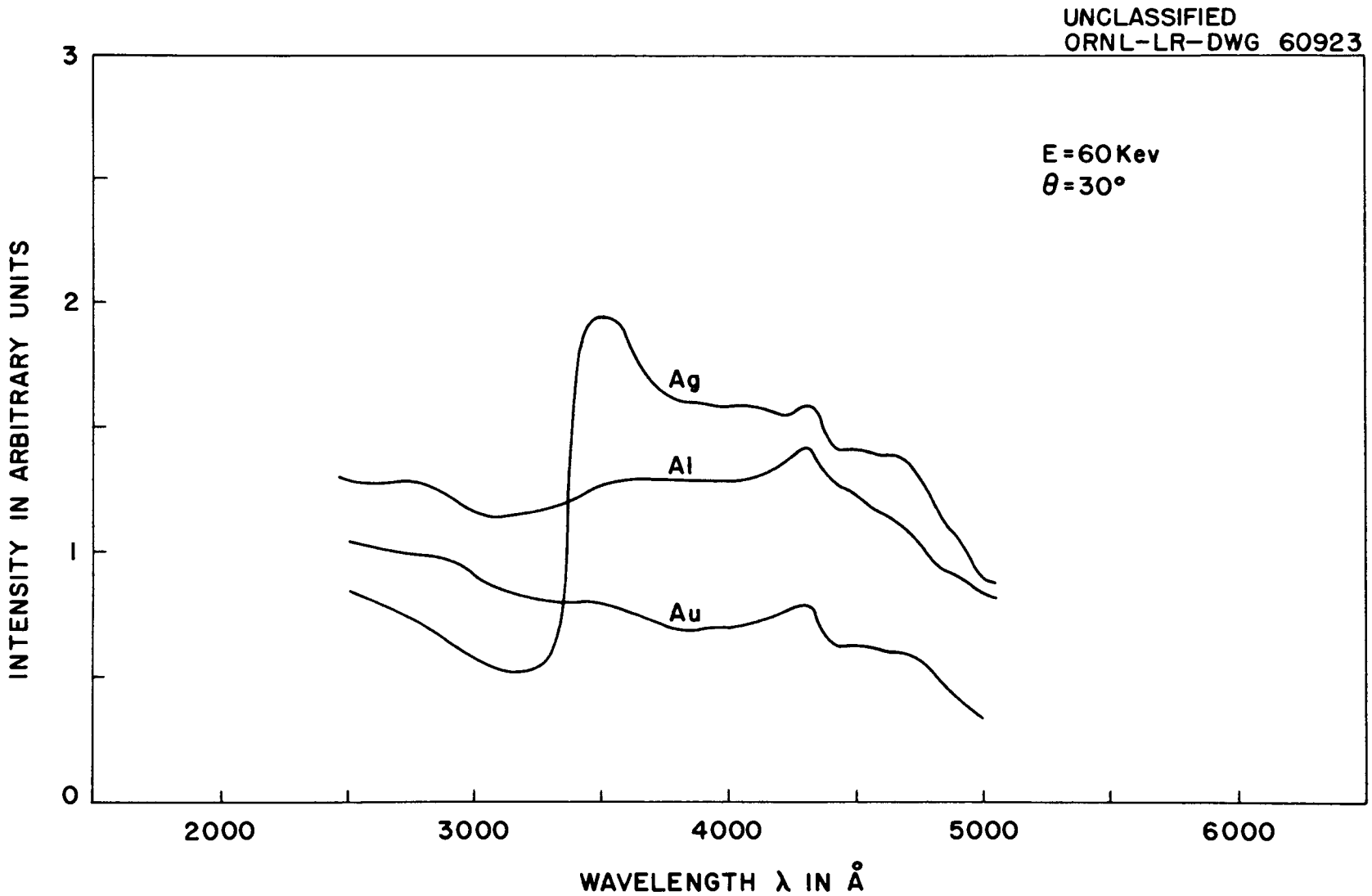

Figure 42. Spectral Distributions from Ag, Al, and Au ($\theta = 30^{\circ}$; E = 60 kev).

VII. CONCLUSIONS

Thin silver, aluminum, and gold foils were irradiated with electrons of energies between 40 kev and 115 kev and their emission spectra were recorded at various angles to the foil normal. Comparisons with the Ritchie-Eldridge and Ferrell theories revealed acceptable agreement considering the uncertainties in the experiment and in the dielectric constant. Discrepancies between the experimental results and theory indicate that bremsstrahlung may be present.

Future experiments should include irradiations of thinner silver foils and measurements of the spectrum in the region of 3260 Å where theory predicts a great increase in emission. An important need for measurements of the light from aluminum is a detector capable of measuring the intensity at wave lengths as low as 800 Å where intensity is predicted to rise sharply. Attention should be directed to the origin of the broad band which appears in both the aluminum and silver spectra.

BIBLIOGRAPHY

Adams, E. N., "Plasma Oscillations in Metals," Phys. Rev. 98, 947 (1955).

Berning, P. H., Haas, G., and Madden, R. P., "Reflectance-Increasing Coatings for the Vacuum Ultraviolet and Their Applications," J. Opt. Soc. Am. 50, 586 (1960).

Beutler, H. G., "The Theory of the Concave Grating," J. Opt. Soc. Am. 35, 311 (1945).

Bohm, D. and Pines, D., "Collective Description of Electron Interactions I. Magnetic Interactions," Phys. Rev. 92, 609 (1953).

Brown, R. W., Wessel, P., and Trounson, E. P., "Plasma Reradiation from Silver Films," Phys. Rev. Letters 5, 472 (1960).

DeVos, J. C., "A New Determination of the Emissivity of Tungsten Ribbon," Physica 20, 690 (1954).

Eldridge, H. B., "Wein's Law Black Body Tables," Oak Ridge National Laboratory, Oak Ridge, Tennessee (1961 - unpublished).

Ferrell, R. A., "Angular Dependence of the Characteristic Energy Loss of Electrons Passing Through Metal Foils," Phys. Rev. 101, 555 (1956).

Ferrell, R. A., "Characteristic Energy Loss of Electrons Passing Through Metal Foils: Dispersion Relation and Short Wave Length Cutoff for Plasma Oscillations," Phys. Rev. 107, 450 (1957).

Ferrell, R. A., "Predicted Radiation of Plasma Oscillations in Metal Films," Phys. Rev. 111, 1214 (1958).

Frank, I. M., and Ginsburg, V. L., "Radiation of a Uniformly Moving Electron Due to Its Transition from One Medium into Another," J. Exptl. Theoret. Phys. (U.S.S.R.) 16, 15 (1945).

Gluckstern, R. L., and Hull, M. H., Jr., "Polarization Dependence of Integrated Bremsstrahlung Cross Section," Phys. Rev. 90, 1030 (1953).

Gluckstern, R. L., Hull, M. H., Jr., and Breit, G., "Polarization of Bremsstrahlung Radiation," Phys. Rev. 90, 1026 (1953).

Haas, G., and Waylonis, J. E., "Optical Constants of Aluminum," from meeting of the Optical Society of America (October 13, 1960).

Holland, L., VACUUM DEPOSITION OF THIN FILMS, (John Wiley and Sons, Inc., New York, 1960).

Mohler, F. L. and Boeckner, C., "Probe Radiation from Silver," Bur. Standards J. Research G, 751 (1931).

Namioka, T., "Construction of a Grating Spectrometer," Science of Light 3, 15 (1954).

Pines, D., "Collective Description of Electron Interactions IV. Electron Interaction in Metals," Phys. Rev. 92, 625 (1954).

Pines, D., and Bohm, D., "Collective Description of Electron Interactions II. Collective vs. Individual Particle Aspects of the Interactions," Phys. Rev. 85, 338 (1952).

Powell, C. J., Robins, J. L., and Swan, J. B., "Effects of Contamination on the Characteristic Loss Spectrum of Tungsten," Phys. Rev. 110, 657 (1958).

Ritchie, R. H., "Plasma Losses by Fast Electrons in Thin Films," Phys. Rev. 106, 874 (1957).

Ritchie, R. H., "Interaction of Charged Particles with Degenerate Fermi-Dirac Electron Gas," Phys. Rev. 114, 644 (1959).

Ritchie, R. H., "Optical Emission from Irradiated Foils I.," (To be submitted for publication in Phys. Rev.).

Rutgers, G. A. W., and DeVos, J. E., "Relation Between Brightness, Temperature, True Temperature, and Colour Temperature of Tungsten, Luminance of Tungsten," Physica 20, 715 (1954).

Seya, M., "A New Mounting of Concave Grating Suitable for a Spectrometer," Science of Light 2, 8 (1952).

Steinman, Wulf, "Experimental Verification of Radiation of Plasma Oscillations in Thin Silver Films," Phys. Rev. Letters 5, 470 (1960).

Taft, E. A., and Philipp, H. R., "Optical Constants of Silver," Phys. Rev. 121, 1100 (1961).

Tolansky, S., AN INTRODUCTION TO INTERFEROMETRY, (Longman, Green, and Co., London, 1955).

Wolff, P. A., "Theory of Plasma Waves in Metals," Phys. Rev. 92, 18 (1953).

Ziemer, P. L., Johnson, R. M., and Birkhoff, R. D., "Measurement of Stopping Power of Copper by Calorimetric Methods," ORNL-2775, 1959, Oak Ridge National Laboratory, Oak Ridge, Tennessee.

ORNL-3114
UC-34 — Physics
TID-4500 (17th ed.)

INTERNAL DISTRIBUTION

1. Biology Library
2-3. Central Research Library
4. Laboratory Shift Supervisor
5. Reactor Division Library
6. ORNL — Y-12 Technical Library Document Reference Section
7-56. Laboratory Records Department
57. Laboratory Records, ORNL R.C.
58-107. E. T. Arakawa
108. R. E. Biggers
109. D. S. Billington
110-159. R. D. Birkhoff
160. J. F. Burns
161. J. H. Crawford, Jr.
162-186. A. L. Frank
187. W. R. Grimes
188. H. H. Hubbell, Jr.
189. G. S. Hurst
190. R. G. Jordan (Y-12)
191. W. H. Jordan
192. C. E. Larson
193. G. W. Leddicotte
194. K. Z. Morgan
195. J. P. Murray (K-25)
196-245. R. H. Ritchie
246. M. J. Skinner
247. J. A. Swartout
248. A. M. Weinberg
249. G. M. Fair (consultant)
250. J. C. Frye (consultant)
251. W. H. Langham (consultant)
252. E. P. Odum (consultant)
253. R. L. Platzman (consultant)
254. L. S. Taylor (consultant)

EXTERNAL DISTRIBUTION

255. H. B. Eldridge, Aerospace Corporation, 2400 El Segundo Blvd., El Segundo, California
256. Division of Research and Development, AEC, ORO
257-888. Given distribution as shown in TID-4500 (17th ed.) under Physics category (75 copies — OTS)